

Complete Vector-like Fourth Family with $U(1)'$: A Global Analysis

Junichiro Kawamura^{a,b,*}, Stuart Raby^{a,†}, and Andreas Trautner^{c,‡}

^a*Department of Physics, Ohio State University, Columbus, Ohio 43210, USA*

^b*Department of Physics, Keio University, Yokohama 223-8522, Japan*

^c*Max-Planck-Institut für Kernphysik, Saupfercheckweg 1, 69117 Heidelberg, Germany*

Abstract

In this paper we present an in-depth analysis of a recently proposed Standard Model extension with a complete fourth generation of quarks and leptons, which are vector-like with respect to the Standard Model gauge group and charged under a new spontaneously broken vector-like $U(1)'$ gauge symmetry. The model is designed to explain the known muon anomalies, i.e. the observed deviations from Standard Model predictions in the anomalous magnetic moment of the muon, Δa_μ , and in $b \rightarrow s\ell^+\ell^-$ processes. We perform a global χ^2 analysis of the data with 65 model parameters and including 98 observables. We find many points with χ^2 per degree of freedom ≤ 1 . The vector-like leptons and the new heavy Z' are typically much lighter than a TeV and would, thus, be eminently visible at the HL-LHC.

*kawamura.14@osu.edu

†raby.1@osu.edu

‡trautner@mpi-hd.mpg.de

Contents

1	Introduction	1
2	Model	1
2.1	Matter Content and Fermion Mass Matrices	1
2.2	Gauge and Yukawa Couplings	5
2.2.1	Neutral Gauge Couplings	5
2.2.2	CKM and PMNS Matrices	6
2.2.3	Yukawa Couplings	6
2.2.4	Landau Pole Constraints on the $U(1)'$ Gauge Coupling	7
3	Observables	7
3.1	Charged Leptons	7
3.1.1	Anomalous Magnetic Moment	8
3.1.2	$l_i \rightarrow l_j \nu \bar{\nu}$	13
3.1.3	$l_i \rightarrow l_j \gamma$	14
3.1.4	$l_i \rightarrow l_j l_k l_i$	15
3.2	EW Bosons	17
3.2.1	W Boson Decays	17
3.2.2	Z Decays and Asymmetry Parameters	19
3.2.3	Higgs Decays	20
3.3	Quarks	21
3.3.1	$b \rightarrow sl^+l^-$ Processes	22
3.3.2	Neutral Meson Mixing	24
3.3.3	$B_{d,s} \rightarrow \mu^+\mu^-$	29
3.3.4	$B \rightarrow K^{(*)} \nu \bar{\nu}$	31
3.3.5	Top Quark Decays	32
3.4	Z' Physics	32
3.4.1	Dimuon Signals at the LHC	32
3.4.2	Gauge Kinetic Mixing	33
3.4.3	Neutrino Trident Production	33
4	Results	34
4.1	χ^2 Fitting	34
4.2	Best Fit Points	34
4.3	Phenomenology	35
4.3.1	Z' Physics	36
4.3.2	$b \rightarrow sl^+l^-$	37
4.3.3	Standard Model Quark Sector	39
4.3.4	Charged Lepton Flavor Violation	41
4.3.5	Signals of Vector-Like Leptons	43
4.3.6	Signals of Vector-Like Quarks	45

5	Summary	46
A	Decay Width Formulas	47
A.1	Scalar Decays	47
A.2	Gauge Boson Decays	47
A.3	Fermion Decays	48
B	Analytical Analysis	48
B.1	Diagonalization of the Dirac Mass Matrices	48
B.2	EW Boson Couplings	52
B.3	Charged Leptons	52
B.4	Quarks	56
B.5	Neutrinos	58
C	Input Parameters at Best Fit Points	62
C.1	Best Fit Point A	62
C.2	Best Fit point B	63
C.3	Best Fit point C	64
C.4	Best Fit point D	65
D	Full List of Observables at Best Fit Points	66

1 Introduction

In the search for physics beyond the Standard Model (SM) one certainly looks for new particles produced at the LHC. Absent any new discoveries, one then considers experimental discrepancies with SM predictions. There will always be 2σ or 3σ discrepancies, some of which are real and some of which are just statistical fluctuations. In an attempt to distinguish these two possibilities, one might focus on a cluster of discrepancies which can all be resolved with the same new physics. This is what we have done in a previous letter [1]. We have shown that the muon anomalies associated with the anomalous magnetic moment of the muon, Δa_μ , and the angular and lepton non-universality anomalies in $b \rightarrow sl^+\ell^-$ decays can simultaneously be resolved by the addition to the SM of a complete vector-like (VL) family of quarks and leptons together with a new $U(1)'$ gauge symmetry carried only by the new VL states. VL leptons are introduced for Δa_μ in Refs. [2–5]. The $b \rightarrow sl^+\ell^-$ anomaly is addressed by introducing a Z' boson [6–9] and new particles which induce box diagram contributions [10–18]. Both anomalies can be explained simultaneously in models with VL fermions and a Z' boson [19–23].

In the present paper, we perform a global χ^2 analysis of these phenomena with the addition of all SM processes that might feel the effects of mixing between the VL family and the SM families. We find many solutions with $\chi^2/N_{\text{d.o.f.}} \leq 1$. Moreover, the model is highly testable via both direct observation of new physics at the LHC or via the improved analysis of SM processes. For example, precision measurements of $K-\bar{K}$ and $B_d-\bar{B}_d$ mixing may be sensitive to the new physics. Finally, the tight observational constraints on the $\mu \rightarrow e\gamma$ branching ratio hinders a simultaneous fit to Δa_μ and Δa_e . We can only fit one but not both, and we choose to fit the former.

The paper is organized as follows. In Section 2 we briefly review the details of the model and describe the mass mixing between the SM and VL states. In Section 3 we provide the theoretical formulae for calculating the 98 observables in our analysis. In Section 4 we present the results of the χ^2 analysis with many plots illustrating the range of VL masses and the quality of the fits. In addition we choose four “best fit points” to illustrate some of the new physics processes which are, in principle, observable at the LHC. Finally, in Section 5 we summarize our results. More details of the fits are presented in the Appendices.

2 Model

2.1 Matter Content and Fermion Mass Matrices

We study a model with a complete VL fourth family and $U(1)'$ gauge symmetry. The quantum number of all particles are listed in Tables 1 and 2. The $SU(2)_L$ doublets in the SM are defined as $q_{Li} = (u_{Li}, d_{Li})$, $l_{Li} = (\nu_{Li}, e_{Li})$, $H = (H_0, H_-)$. Here, $i = 1, 2, 3$ runs over the three SM families. The exotic doublets are $Q_L = (U'_L, D'_L)$, $L_L = (N'_L, E'_L)$, $\bar{Q}_R = (-\bar{D}'_R, \bar{U}'_R)$, $\bar{L}_R = (-\bar{E}'_R, \bar{N}'_R)$. Only the VL fermions and $U(1)'$ breaking scalar Φ are charged under the $U(1)'$ gauge symmetry. This model is trivially anomaly-free since

Table 1: Quantum numbers of SM particles. Here, $i = 1, 2, 3$ runs over the three SM families. The electromagnetic charge of a fermion f is $Q_f = T_f^3 + Y_f/2$.

	q_{Li}	\bar{u}_{Ri}	\bar{d}_{Ri}	l_{Li}	\bar{e}_{Ri}	$\bar{\nu}_{Ri}$	H
$SU(3)_C$	3	$\bar{3}$	$\bar{3}$	1	1	1	1
$SU(2)_L$	2	1	1	2	1	1	2
$U(1)_Y$	1/3	-4/3	2/3	-1	2	0	-1
$U(1)'$	0	0	0	0	0	0	0

Table 2: Quantum numbers of new fermion and scalar fields.

	Q_L	\bar{U}_R	\bar{D}_R	L_L	\bar{E}_R	\bar{N}_R	\bar{Q}_R	U_L	D_L	\bar{L}_R	E_L	N_L	ϕ	Φ
$SU(3)_C$	3	$\bar{3}$	$\bar{3}$	1	1	1	$\bar{3}$	3	3	1	1	1	1	1
$SU(2)_L$	2	1	1	2	1	1	2	1	1	2	1	1	1	1
$U(1)_Y$	1/3	-4/3	2/3	-1	2	0	-1/3	4/3	-2/3	1	-2	0	0	0
$U(1)'$	-1	1	1	-1	1	1	1	-1	-1	1	-1	-1	0	-1

the $U(1)'$ charges are vector-like. A singlet real scalar ϕ is introduced to model mass terms for the VL fermions.

In the gauge basis, the Yukawa couplings are given by

$$\mathcal{L}_{\text{Yukawa}} = \mathcal{L}_{\text{SM}} + \mathcal{L}_H + \mathcal{L}_\phi + \mathcal{L}_\Phi + \text{h.c.} , \quad (2.1)$$

with

$$\mathcal{L}_{\text{SM}} := \bar{u}_{Ri} y_{ij}^u q_{Lj} \tilde{H} + \bar{d}_{Ri} y_{ij}^d q_{Lj} H + \bar{e}_{Ri} y_{ij}^e l_{Lj} H + \bar{\nu}_{Ri} y_{ij}^n l_{Lj} \tilde{H} , \quad (2.2)$$

$$\begin{aligned} \mathcal{L}_H := & \lambda_u \bar{U}_R Q_L \tilde{H} + \lambda_d \bar{D}_R Q_L H + \lambda_e \bar{E}_R L_L H + \lambda_n \bar{N}_R L_L \tilde{H} \\ & + \lambda'_u \bar{Q}_R H U_L - \lambda'_d \bar{Q}_R \tilde{H} D_L - \lambda'_e \bar{L}_R \tilde{H} E_L + \lambda'_n \bar{L}_R H N_L , \end{aligned} \quad (2.3)$$

$$\begin{aligned} \mathcal{L}_\phi := & \phi \left(\lambda_V^Q \bar{Q}_R Q_L - \lambda_V^U \bar{U}_R U_L - \lambda_V^D \bar{D}_R D_L \right. \\ & \left. + \lambda_V^L \bar{L}_R L_L - \lambda_V^E \bar{E}_R E_L - \lambda_V^N \bar{N}_R N_L \right) , \end{aligned} \quad (2.4)$$

$$\begin{aligned} \mathcal{L}_\Phi := & \Phi \left(\lambda_i^Q \bar{Q}_R q_{Li} + \lambda_i^L \bar{L}_R l_{Li} \right) \\ & - \Phi^* \left(\lambda_i^U \bar{u}_{Ri} U_L + \lambda_i^D \bar{d}_{Ri} D_L + \lambda_i^E \bar{e}_{Ri} E_L + \lambda_i^N \bar{\nu}_{Ri} N_L \right) . \end{aligned} \quad (2.5)$$

Here, $\tilde{H} := i\sigma_2 H^* = (H_-^*, -H_0^*)$ and $i, j = 1, 2, 3$ label the SM generations.

The neutral scalar fields acquire Vacuum Expectation Values (VEVs) given by $v_H :=$

$\langle H_0 \rangle$, $v_\Phi := \langle \Phi \rangle$, $v_\phi := \langle \phi \rangle$. The 5×5 Dirac mass matrices are given by¹

$$\bar{e}_R \mathcal{M}^e e_L := \begin{pmatrix} \bar{e}_{Ri} & \bar{E}_R & \bar{E}'_R \end{pmatrix} \begin{pmatrix} y_{ij}^e v_H & 0_i & \lambda_i^E v_\Phi \\ 0_j & \lambda_e v_H & \lambda_V^E v_\phi \\ \lambda_j^L v_\Phi & \lambda_V^L v_\phi & \lambda'_e v_H \end{pmatrix} \begin{pmatrix} e_{Lj} \\ E'_L \\ E_L \end{pmatrix}, \quad (2.6)$$

$$\bar{n}_R \mathcal{M}^n n_L := \begin{pmatrix} \bar{\nu}_{Ri} & \bar{N}_R & \bar{N}'_R \end{pmatrix} \begin{pmatrix} y_{ij}^n v_H & 0_i & \lambda_i^N v_\Phi \\ 0_j & \lambda_n v_H & \lambda_V^N v_\phi \\ \lambda_j^L v_\Phi & \lambda_V^L v_\phi & \lambda'_n v_H \end{pmatrix} \begin{pmatrix} \nu_{Lj} \\ N'_L \\ N_L \end{pmatrix}, \quad (2.7)$$

$$\bar{u}_R \mathcal{M}^u u_L := \begin{pmatrix} \bar{u}_{Ri} & \bar{U}_R & \bar{U}'_R \end{pmatrix} \begin{pmatrix} y_{ij}^u v_H & 0_i & \lambda_i^U v_\Phi \\ 0_j & \lambda_u v_H & \lambda_V^U v_\phi \\ \lambda_j^Q v_\Phi & \lambda_V^Q v_\phi & \lambda'_u v_H \end{pmatrix} \begin{pmatrix} u_{Lj} \\ U'_L \\ U_L \end{pmatrix}, \quad (2.8)$$

$$\bar{d}_R \mathcal{M}^d d_L := \begin{pmatrix} \bar{d}_{Ri} & \bar{D}_R & \bar{D}'_R \end{pmatrix} \begin{pmatrix} y_{ij}^d v_H & 0_i & \lambda_i^D v_\Phi \\ 0_j & \lambda_d v_H & \lambda_V^D v_\phi \\ \lambda_j^Q v_\Phi & \lambda_V^Q v_\phi & \lambda'_d v_H \end{pmatrix} \begin{pmatrix} d_{Lj} \\ D'_L \\ D_L \end{pmatrix}. \quad (2.9)$$

For electrically charged fermions, $f = u, d, e$, the mass basis is defined as

$$\hat{f}_L := \left(U_L^f \right)^\dagger f_L, \quad \hat{f}_R := \left(U_R^f \right)^\dagger f_R, \quad (2.10)$$

where unitary matrices diagonalize the Dirac matrices as

$$\left(U_R^e \right)^\dagger \mathcal{M}^e U_L^e = \text{diag}(m_e, m_\mu, m_\tau, m_{E_1}, m_{E_2}), \quad (2.11)$$

$$\left(U_R^u \right)^\dagger \mathcal{M}^u U_L^u = \text{diag}(m_u, m_c, m_t, m_{U_1}, m_{U_2}), \quad (2.12)$$

$$\left(U_R^d \right)^\dagger \mathcal{M}^d U_L^d = \text{diag}(m_d, m_s, m_b, m_{D_1}, m_{D_2}). \quad (2.13)$$

Here, $m_{E_a}, m_{U_a}, m_{D_a}$ ($a = 1, 2$) are masses for the new charged leptons, up and down quarks, respectively. These are predominantly the VL fermions of the gauge basis.

We consider the type-I see-saw mechanism to explain the tiny neutrino masses. Since the $U(1)'$ gauge symmetry prohibits Majorana masses for the VL family, only three families of right-handed neutrinos have Majorana masses,

$$\mathcal{L}_{\text{Maj}} = -\frac{1}{2} \bar{\nu}_{Ri} M_{\text{Maj}}^{ij} \nu_{Rj}^c. \quad (2.14)$$

The Majorana masses are assumed to be $M_{\text{Maj}}^{ij} \sim 10^{14}$ GeV. The mass matrix for the neutrinos is then a 10×10 matrix,

$$\bar{\mathcal{N}}_R \mathcal{M}^N \mathcal{N}_L := \begin{pmatrix} \bar{n}_R & \bar{n}_L^c \end{pmatrix} \begin{pmatrix} \mathcal{M}^R & \mathcal{M}^n \\ (\mathcal{M}^n)^T & 0_{5 \times 5} \end{pmatrix} \begin{pmatrix} n_R^c \\ n_L \end{pmatrix}, \quad (2.15)$$

¹ Of course, for VL fermions there is always the possibility of rigid, Lagrangian-level mass terms. However, for all our purposes the effect of those terms is completely equivalent to the masses induced by the VEV of ϕ and so we do not include such terms here.

where the Dirac mass matrix \mathcal{M}^n is defined in Eq. (2.7). The 5×5 Majorana mass matrix is given by

$$\mathcal{M}^R = \begin{pmatrix} M_{\text{Maj}}^{ij} & 0_i & 0_i \\ 0_j & 0 & 0 \\ 0_j & 0 & 0 \end{pmatrix}. \quad (2.16)$$

After diagonalizing this matrix, there are three left-handed Majorana neutrinos $\hat{\nu}_{L_i}$ with mass of $\mathcal{O}(v_H^2/M_{\text{Maj}})$, and three right-handed Majorana neutrinos $\hat{\nu}_{R_i}$ with mass of $\mathcal{O}(M_{\text{Maj}})$ as in the ordinary type-I see-saw mechanism. In addition to these, there are two Dirac neutrinos N_1, N_2 with mass of $\mathcal{O}(v_\phi)$ which are predominantly the VL neutrinos of the gauge basis. Mixing between the left- and right-handed neutrinos is suppressed by the huge Majorana mass terms. An approximate mass basis is then defined as²

$$\hat{n}_L := (U_L^n)^\dagger n_L, \quad \hat{n}_R := (U_R^n)^\dagger n_R, \quad (2.17)$$

with unitary matrices U_L^n and U_R^n , given in Appendix B where we discuss the diagonalization of the neutrino mass matrix more explicitly.

There are three electrically neutral scalar fields in this model. We expand them around their VEVs as

$$H_0 = v_H + \frac{1}{\sqrt{2}}(h + ia_H), \quad \Phi = v_\Phi + \frac{1}{\sqrt{2}}(\chi + ia_\chi), \quad \text{and} \quad \phi = v_\phi + \sigma. \quad (2.18)$$

Here, h , χ , and σ are physical real scalar fields while the pseudo-scalar components a_H and a_χ are eaten by the gauge bosons. We introduce *effective* quartic couplings of the scalars χ and σ , which parametrize the scalar masses as

$$m_\chi^2 = \lambda_\chi v_\Phi^2, \quad m_\sigma^2 = \lambda_\sigma v_\phi^2. \quad (2.19)$$

In this paper, we do not specify a scalar potential in this model and treat their VEVs and the effective quartic couplings as input parameters. For an effective quartic coupling λ_χ in a perturbative regime and a sizable gauge coupling g' , the masses of χ and the Z' gauge boson should roughly be of the same order. This is important, since the Yukawa couplings of χ together with v_Φ set the scale of mass mixing between VL particles and the SM families. The fact that this mixing is necessary for an explanation of the muon anomalies means that also χ will give sizable contributions in our fits. In contrast, v_ϕ could be very large, and therefore m_σ very heavy, as long as the ϕ -Yukawa couplings are small enough to prevent a complete decoupling of the VL fermions. The scalar σ , thus, can be very heavy and its contributions irrelevant for all discussed observables. In fact, this limit resembles the case of rigid tree-level VL masses. Consistent with that, contributions from σ are always negligible at the best fit points we discuss below.

² In principle, the rotation that diagonalizes the neutrino mass matrix mixes left- and charge conjugated right-handed states. However, the effects of this mixing are suppressed by $\mathcal{O}(v_H/M_{\text{Maj}})$ and so we will neglect them here and in the following, see Appendix B for details.

2.2 Gauge and Yukawa Couplings

In the gauge basis, there are no interactions between the Z' boson and the SM fermions. In order to explain the muon anomalies, the SM families are required to mix with the VL families. Consequently, also the SM gauge couplings of quarks and leptons will receive corrections from these mixing effects. Of course, these couplings must remain consistent with all SM observables and we shall verify this. For this discussion we combine left- and right-handed fermions to Dirac fermions as

$$f := (f_L, f_R), \quad \text{where} \quad f = u, d, e, n. \quad (2.20)$$

2.2.1 Neutral Gauge Couplings

The fermion couplings to the Z' boson are given by

$$\mathcal{L}_{Z'} = g' Z'_\mu \sum_{f=u,d,e,n} \bar{f} \gamma^\mu (Q'_{f_L} P_L + Q'_{f_R} P_R) f \quad (2.21)$$

$$= Z'_\mu \sum_{f=u,d,e,n} \bar{\hat{f}} \gamma^\mu (\hat{g}_{f_L}^{Z'} P_L + \hat{g}_{f_R}^{Z'} P_R) \hat{f}, \quad (2.22)$$

where the charge matrices in the gauge basis are

$$Q'_{f_L} = Q'_{f_R} = \text{diag}(0, 0, 0, -1, -1). \quad (2.23)$$

The coupling matrices in the mass basis are

$$\hat{g}_{f_L}^{Z'} = g' (U_L^f)^\dagger Q'_{f_L} U_L^f \quad \text{and} \quad \hat{g}_{f_R}^{Z'} = g' (U_R^f)^\dagger Q'_{f_R} U_R^f. \quad (2.24)$$

The Z boson couplings are given by

$$\mathcal{L}_Z = \frac{g}{c_W} Z_\mu \sum_{f=u,d,e,n} \bar{f} \gamma^\mu \left[(T_3^f P_5 - Q_f s_W^2 \mathbb{1}_5) P_L + (T_3^f P_5 - Q_f s_W^2 \mathbb{1}_5) P_R \right] f \quad (2.25)$$

$$= Z_\mu \sum_{f=u,d,e,n} \bar{\hat{f}} \gamma^\mu (\hat{g}_{f_L}^Z P_L + \hat{g}_{f_R}^Z P_R) \hat{f}, \quad (2.26)$$

where Q_f and T_3^f are the electromagnetic charge and third component of the weak isospin for a fermion f , respectively, while $s_W(c_W)$ denotes the (co)sine of the weak mixing angle. The flavor space projectors are defined as

$$P_5 := \text{diag}(0, 0, 0, 0, 1) \quad \text{and} \quad P_{\bar{5}} := \mathbb{1}_5 - P_5 = \text{diag}(1, 1, 1, 1, 0). \quad (2.27)$$

The coupling matrices in the mass basis are given by

$$\hat{g}_{f_L}^Z = \frac{g}{c_W} \left[T_3^f (U_L^f)^\dagger P_{\bar{5}} U_L^f - Q_f s_W^2 \mathbb{1}_5 \right], \quad \hat{g}_{f_R}^Z = \frac{g}{c_W} \left[T_3^f (U_R^f)^\dagger P_5 U_R^f - Q_f s_W^2 \mathbb{1}_5 \right]. \quad (2.28)$$

In general, this model has tree-level flavor changing neutral vector currents mediated by the Z boson. However, for the SM generations these are automatically suppressed by $\mathcal{O}(m_{f_{\text{SM}}}^2/M_{F_{\text{VL}}}^2)$ coefficients which we show analytically in Appendix B. Here, $m_{f_{\text{SM}}}$ and $M_{F_{\text{VL}}}$ denote the mass of the SM fermion f_{SM} , as well as the mass of the VL fermion F_{VL} .

2.2.2 CKM and PMNS Matrices

The fermion couplings to the W boson are given by

$$\mathcal{L}_W = \frac{g}{\sqrt{2}} W_\mu^+ [\bar{u}\gamma^\mu (P_{\bar{5}} P_L + P_5 P_R) d + \bar{n}\gamma^\mu (P_{\bar{5}} P_L + P_5 P_R) e] + \text{h.c.} \quad (2.29)$$

$$= W_\mu^+ \left[\bar{\hat{u}}\gamma^\mu (\hat{g}_{qL}^W P_L + \hat{g}_{qR}^W P_R) \hat{d} + \bar{\hat{n}}\gamma^\mu (\hat{g}_{\ell L}^W P_L + \hat{g}_{\ell R}^W P_R) \hat{e} \right] + \text{h.c.} \quad (2.30)$$

In the mass basis, the coupling matrices are

$$\hat{g}_{qL}^W = \frac{g}{\sqrt{2}} (U_L^u)^\dagger P_{\bar{5}} U_L^d, \quad \hat{g}_{qR}^W = \frac{g}{\sqrt{2}} (U_R^u)^\dagger P_5 U_R^d, \quad (2.31)$$

$$\hat{g}_{\ell L}^W = \frac{g}{\sqrt{2}} (U_L^n)^\dagger P_{\bar{5}} U_L^e, \quad \hat{g}_{\ell R}^W = \frac{g}{\sqrt{2}} (U_R^n)^\dagger P_5 U_R^e. \quad (2.32)$$

The extended 5×5 CKM matrix \hat{V}_{CKM} is defined as

$$\hat{V}_{\text{CKM}} := (U_L^u)^\dagger P_{\bar{5}} U_L^d. \quad (2.33)$$

Since one of the left-handed quarks is an $SU(2)_L$ singlet this extended CKM matrix has only rank 4 and is, therefore, clearly non-unitary. Correspondingly, there exist right-handed charged current interactions which are completely absent in the SM. Also the 3×3 sub-matrix, which corresponds to the SM CKM matrix, is generally non-unitary due to mixing with the VL quarks. Again these effects are suppressed by $\mathcal{O}(m_{f\text{SM}}^2/M_{F\text{VL}}^2)$ coefficients. In addition, the right-handed current interactions to the SM quarks are also suppressed and at most $\mathcal{O}(10^{-4})$ as shown in Eq. (B.64), see Appendix B. These are negligible against experimental sensitivities.

The mixing between the SM and VL neutrinos are suppressed by the huge Majorana mass term. In Appendix B, we found that non-unitarity of the 3×3 PMNS matrix is induced by the Yukawa coupling λ_n and tiny mixing angles between the SM and VL charged leptons, that is U_{eL}^2 in Eq. (B.18). In other words, there would be non-zero mixing between the SM neutrinos and the Dirac neutrinos if $\lambda_n \sim 1$. This is an interesting possibility, but is beyond the scope of this paper. We consider a parameter space where $\lambda_n \ll 1$ and the PMNS matrix is approximately unitary. The details of neutrino mass diagonalization as well as the definition of the PMNS matrix are shown in Appendix B.

2.2.3 Yukawa Couplings

The Yukawa interactions with the real scalars are given by

$$-\mathcal{L}_{\text{Yukawa}} = \frac{1}{\sqrt{2}} \sum_{f=u,d,e,n} \bar{f}_R [hY_f^h + \chi Y_f^\chi + \sigma Y_f^\sigma] f_L + \text{h.c.} \quad (2.34)$$

$$= \frac{1}{\sqrt{2}} \sum_{S=h,\chi,\sigma} \sum_{f=u,d,e,n} S \bar{f}_R \hat{Y}_f^S f_L + \text{h.c.} \quad (2.35)$$

Here the Yukawa matrices for the fermions in the gauge basis are given by

$$Y_f^h := \frac{d\mathcal{M}^f}{dv_H}, \quad Y_f^\chi := \frac{d\mathcal{M}^f}{dv_\Phi}, \quad Y_f^\sigma := \sqrt{2} \frac{d\mathcal{M}^f}{dv_\phi}, \quad (2.36)$$

with the mass matrices of Eqs. (2.6)-(2.9). In the mass basis, these are

$$\hat{Y}_f^S = \left(U_R^f\right)^\dagger Y_f^S U_L^f, \quad \text{for } S = h, \chi, \sigma. \quad (2.37)$$

As in the Z and W boson couplings, the flavor violating couplings to the Higgs boson is automatically suppressed by $\mathcal{O}(m_{f_{\text{SM}}}^2/M_{F_{\text{VL}}}^2)$, see Appendix B.

2.2.4 Landau Pole Constraints on the $U(1)'$ Gauge Coupling

As already discussed in more detail in [1], the $U(1)'$ gauge coupling g' diverges at a Landau pole at the scale

$$\Lambda_{g'} \simeq \mu_{Z'} \exp\left(\frac{24\pi^2}{65g'(\mu_{Z'})^2}\right). \quad (2.38)$$

Here $\mu_{Z'} \sim 1 \text{ TeV}$ is the scale where we define the couplings of our model. In order for the model to be consistent up to a typical GUT scale of $\Lambda_{g'} \sim 10^{16} \text{ GeV}$, we require $g'(1 \text{ TeV}) < 0.35$ in our analysis.

3 Observables

In our model, Δa_μ is explained by chirally enhanced 1-loop corrections involving the Z' boson and VL leptons. At the same time, tree-level Z' exchange induces new contributions to $b \rightarrow s\ell^+\ell^-$. An explanation for Δa_μ requires sizable Z' couplings to muons, in agreement with those necessary to explain deviations in $b \rightarrow s\mu\mu$. The required mixing of the SM and VL fermions may, thus, induce new physics effects in various observables in both, lepton and quark sectors. We have already shown that this model can explain the muon anomalies without spoiling other observables in Ref. [1]. The purpose of the present paper is to completely map out the parameter space where muon anomalies are explained consistently with all other observables, and at the same time discuss the consequences for future experiments. In this section, we introduce the 98 observables included in our χ^2 analysis. In our analysis, 1σ uncertainties for observables which only have upper bounds are set so that 1.64σ (1.96σ) deviation gives a value of 90% (95%) C.L. limit.

3.1 Charged Leptons

Here we study the charged lepton masses, lepton decays, as well as lepton anomalous magnetic moments. Central values and uncertainties of the observables are listed in Table 3.

Table 3: Central values and uncertainties of charged lepton observables. Uncertainties stated in percent are understood as uncertainties relative to their central values.

Name	Center	Uncertainty	Remark
$m_e(m_Z)$ [MeV]	0.486576	0.01 %	Ref. [24]
$m_\mu(m_Z)$ [MeV]	102.719	0.01 %	Ref. [24]
$m_\tau(m_Z)$ [GeV]	1.74618	0.01 %	Ref. [24]
BR($\mu \rightarrow e\nu\bar{\nu}$)	1.0000	0.01 %	SM
BR($\mu \rightarrow e\gamma$)	0.	2.6×10^{-13}	Ref. [25]
BR($\mu^- \rightarrow e^- e^+ e^-$)	0.	6.1×10^{-13}	Ref. [25]
BR($\tau \rightarrow e\nu\bar{\nu}$)	0.179	0.01 %	SM
BR($\tau \rightarrow \mu\nu\bar{\nu}$)	0.174	0.01 %	SM
BR($\tau \rightarrow e\gamma$)	0.	2.0×10^{-8}	Ref. [25]
BR($\tau \rightarrow \mu\gamma$)	0.	2.7×10^{-8}	Ref. [25]
BR($\tau^- \rightarrow e^- e^+ e^-$)	0.	1.6×10^{-8}	Ref. [25]
BR($\tau^- \rightarrow e^- \mu^+ \mu^-$)	0.	1.6×10^{-8}	Ref. [25]
BR($\tau^- \rightarrow \mu^- e^+ \mu^-$)	0.	1.0×10^{-8}	Ref. [25]
BR($\tau^- \rightarrow \mu^- e^+ e^-$)	0.	1.1×10^{-8}	Ref. [25]
BR($\tau^- \rightarrow e^- \mu^+ e^-$)	0.	1.0×10^{-8}	Ref. [25]
BR($\tau^- \rightarrow \mu^- \mu^+ \mu^-$)	0.	1.3×10^{-8}	Ref. [25]
Δa_e	-8.7×10^{-13}	3.6×10^{-13}	Ref. [26]
Δa_μ	2.68×10^{-9}	0.76×10^{-9}	Ref. [25]

We fit the charged lepton masses to the values calculated from Yukawa couplings at $m_Z = 91.2$ GeV [24]. Charged lepton masses are experimentally known with accuracy much better than what makes sense to provide in our analysis. We, thus, assume 0.01% relative uncertainties for the lepton masses.

3.1.1 Anomalous Magnetic Moment

There are discrepancies between experiments and SM predictions for both, the electron and muon magnetic moment. The current size of the discrepancies are [25, 26]

$$\Delta a_e := a_e^{\text{exp}} - a_e^{\text{SM}} = (-87 \pm 36) \times 10^{-14}, \quad (3.1)$$

$$\Delta a_\mu := a_\mu^{\text{exp}} - a_\mu^{\text{SM}} = (2.68 \pm 0.76) \times 10^{-9}. \quad (3.2)$$

Simultaneous explanations for these two anomalies are studied in Refs. [26–36].

The 1-loop beyond the SM corrections involving Z' , Z and W bosons to Δa_μ are given by [4, 37]

$$\delta_{Z'} a_\mu = -\frac{m_\mu}{8\pi^2 m_{Z'}^2} \sum_{B=1}^5 \left[\left(\left| [\hat{g}_{e_L}^{Z'}]_{2B} \right|^2 + \left| [\hat{g}_{e_R}^{Z'}]_{2B} \right|^2 \right) m_\mu F_Z(x_{e_B}^{Z'}) \right. \\ \left. + \text{Re} \left([\hat{g}_{e_L}^{Z'}]_{2B} [\hat{g}_{e_R}^{Z'}]_{2B}^* \right) m_{e_B} G_Z(x_{e_B}^{Z'}) \right], \quad (3.3)$$

$$\delta_Z a_\mu = -\frac{m_\mu}{8\pi^2 m_Z^2} \sum_{b=4}^5 \left[\left(\left| [\hat{g}_{e_L}^Z]_{2b} \right|^2 + \left| [\hat{g}_{e_R}^Z]_{2b} \right|^2 \right) m_\mu F_Z(x_{e_b}^Z) \right. \\ \left. + \text{Re} \left([\hat{g}_{e_L}^Z]_{2b} [\hat{g}_{e_R}^Z]_{2b}^* \right) m_{e_b} G_Z(x_{e_b}^Z) \right], \quad (3.4)$$

$$\delta_W a_\mu = -\frac{m_\mu}{16\pi^2 m_W^2} \sum_{b=4}^5 \left[\left(\left| [\hat{g}_{\ell_L}^W]_{b2} \right|^2 + \left| [\hat{g}_{\ell_R}^W]_{b2} \right|^2 \right) m_\mu F_W(x_{n_b}^W) \right. \\ \left. + \text{Re} \left([\hat{g}_{\ell_L}^W]_{b2} [\hat{g}_{\ell_R}^W]_{b2}^* \right) m_{N_b} G_W(x_{n_b}^W) \right], \quad (3.5)$$

where $x_{e_B}^V := m_{e_B}^2/m_V^2$ ($V = Z, Z'$) and $x_{n_b}^W := m_{n_b}^2/m_W^2$. Here, $m_{e(n)_B}$ is the mass of the B -th generation charged(neutral) lepton. The flavor index $B = 1, \dots, 5$ runs over all five families, while $b = 4, 5$ runs only over the VL family. The loop functions are defined as

$$F_Z(x) = \frac{5x^4 - 14x^3 + 39x^2 - 38x - 18x^2 \ln(x) + 8}{12(1-x)^4}, \quad (3.6)$$

$$G_Z(x) = \frac{x^3 + 3x - 6x \ln(x) - 4}{2(1-x)^3}, \quad (3.7)$$

$$F_W(x) = -\frac{4x^4 - 49x^3 + 78x^2 - 43x + 18x^3 \ln(x) + 10}{6(1-x)^4}, \quad (3.8)$$

$$G_W(x) = -\frac{x^3 - 12x^2 + 15x + 6x^2 \ln(x) - 4}{(1-x)^3}. \quad (3.9)$$

The scalar 1-loop beyond the SM contributions to Δa_μ are given by [4, 37]

$$\delta_h a_\mu = -\frac{m_\mu}{32\pi^2 m_h^2} \sum_{b=4,5} \left[\left(\left| [\hat{Y}_e^h]_{2b} \right|^2 + \left| [\hat{Y}_e^h]_{b2} \right|^2 \right) m_\mu F_S(y_{e_b}^h) \right. \\ \left. + \text{Re} \left([\hat{Y}_e^h]_{2b} [\hat{Y}_e^h]_{b2} \right) m_{e_b} G_S(y_{e_b}^h) \right], \quad (3.10)$$

$$\delta_S a_\mu = -\frac{m_\mu}{32\pi^2 m_S^2} \sum_{B=1}^5 \left[\left(\left| [\hat{Y}_e^S]_{2B} \right|^2 + \left| [\hat{Y}_e^S]_{B2} \right|^2 \right) m_\mu F_S(y_{e_B}^S) \right. \\ \left. + \text{Re} \left([\hat{Y}_e^S]_{2B} [\hat{Y}_e^S]_{B2} \right) m_{e_B} G_S(y_{e_B}^S) \right], \quad (3.11)$$

where $S = \chi, \sigma$. Here, $y_{e_b}^h := m_{e_b}^2/m_h^2$ and $y_{e_B}^S := m_{e_B}^2/m_S^2$. The loop functions are defined

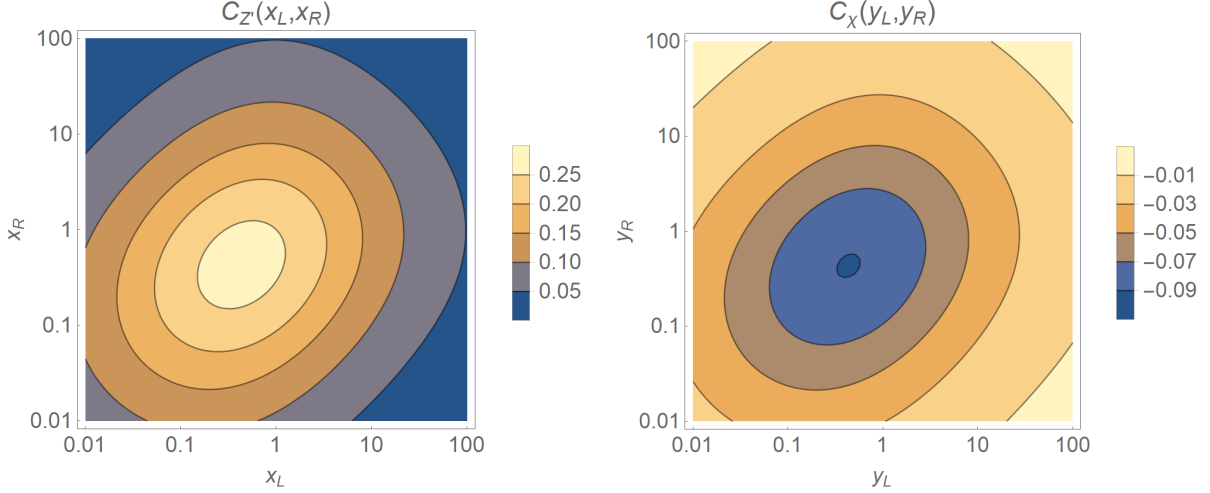


Figure 1: Contour plot of the functions $C_{Z'}(x_L, x_R)$ and $C_\chi(y_L, y_R)$ defined in Eq. (3.16).

as

$$F_S(y) = -\frac{y^3 - 6y^2 + 3y + 6y \ln(y) + 2}{6(1-y)^4}, \quad (3.12)$$

$$G_S(y) = \frac{y^2 - 4y + 2 \ln(y) + 3}{(1-y)^3}. \quad (3.13)$$

Analogous formulae for Δa_e are obtained by formally replacing $2 \rightarrow 1$ and $\mu \rightarrow e$.

We now discuss the leading contributions to Δa_μ analytically. This will be important to understand upper bounds on v_Φ and the masses of VL leptons stated below. The new physics contribution to Δa_μ is dominated by chirally enhanced effects proportional to $\lambda'_e v_H$, namely the Higgs-VEV induced mixing between left- and right-handed VL leptons. Contributions involving the SM bosons are very suppressed. The leading contribution can be estimated as

$$\Delta a_\mu \sim -\frac{m_\mu \lambda'_e v_H}{64\pi^2 v_\Phi^2} s_{2\mu_L} s_{2\mu_R} C_{LR} \sim 2.9 \times 10^{-9} \times \left(\frac{s_{2\mu_L} s_{2\mu_R} C_{LR}}{0.1} \right) \left(\frac{\lambda'_e}{-1.0} \right) \left(\frac{1 \text{ TeV}}{v_\Phi} \right)^2, \quad (3.14)$$

where $s_{2\mu_{L(R)}}$ are mixing angles between the muon and VL leptons and C_{LR} is a function of the mass ratios that we will define shortly. The mixing angles are approximately given by (see Appendix B for details)

$$s_{2\mu_L} = 2s_{\mu_L} c_{\mu_L} \sim 2 \frac{\lambda_V^L v_\phi \lambda_2^L v_\Phi}{M_{E_L} M_{E_L}}, \quad s_{2\mu_R} = 2s_{\mu_R} c_{\mu_R} \sim 2 \frac{\lambda_V^E v_\phi \lambda_2^E v_\Phi}{M_{E_R} M_{E_R}}. \quad (3.15)$$

Here, M_{E_L} and M_{E_R} the masses of the doublet- and singlet-like VL leptons which can be approximated as $M_{E_L}^2 \sim (\lambda_V^L v_\phi)^2 + (\lambda_2^L v_\Phi)^2$ and $M_{E_R}^2 \sim (\lambda_V^E v_\phi)^2 + (\lambda_2^E v_\Phi)^2$. The mixing angles are maximized at $\lambda_V^L v_\phi = \lambda_2^L v_\Phi$, and $\lambda_V^E v_\phi = \lambda_2^E v_\Phi$.

The dimensionless function C_{LR} is defined in (B.46) in Appendix B. It can be approximated as

$$C_{LR} := C_{Z'}(x_L, x_R) + C_\chi(y_L, y_R) \quad (3.16)$$

$$\approx \sqrt{x_L x_R} \frac{G_Z(x_L) - G_Z(x_R)}{x_L - x_R} + \frac{1}{2} \sqrt{y_L y_R} \frac{y_L G_S(y_L) - y_R G_S(y_R)}{y_L - y_R},$$

with $x_{L,R} := M_{E_{L,R}}^2/m_{Z'}^2$ and $y_{L,R} := M_{E_{L,R}}^2/m_\chi^2$. Figure 1 shows contour plots of the functions $C_{Z'}$ and C_χ . $C_{Z'}$ has a maximum value ~ 0.272 at $x_L = x_R \sim 0.433$. $C_{Z'}$ (C_χ) is always positive (negative) and $|C_{Z'}| > |C_\chi|$ at most parts of the parameter space. Altogether, an upper bound on Δa_μ is given by

$$\Delta a_\mu \lesssim \frac{m_\mu v_H}{64\pi^2 v_\Phi^2} C_{Z'} := \Delta a_\mu^{\max}. \quad (3.17)$$

The equality is saturated when $\lambda'_e \sim -1.0$, $s_{2\mu_L} \sim s_{2\mu_R} \sim 1$ and $C_\chi \sim 0$. Inserting the maximal value of $C_{Z'}$ one finds

$$\Delta a_\mu \lesssim 2.74 \times 10^{-9} \times \left(\frac{1.7 \text{ TeV}}{v_\Phi} \right)^2. \quad (3.18)$$

Thus $v_\Phi \lesssim 1.7 \text{ TeV}$ is required to explain Δa_μ . Moreover,

$$M_{E_L} \sim M_{E_R} \sim \sqrt{0.433} \cdot m_{Z'} \lesssim 550 \text{ GeV}, \quad (3.19)$$

is required to maximize $C_{Z'}$. We are interested in upper bounds on the lightest VL charged lepton. For a fixed lightest VL charged lepton mass, the function $C_{Z'}$ is maximized if the heavier state has the same mass, i.e. $M_{E_L} = M_{E_R} := M_E$. Then $x_L = x_R := x$, and

$$C_{Z'}(x, x) = x \frac{dG_Z(x)}{dx} = \frac{3x [x^2 + 4x - 5 - 2(2x + 1) \log x]}{2(1 - x)^4}. \quad (3.20)$$

Figure 2 shows contours of $\Delta a_\mu^{\max} = 2.68 \times 10^{-9}$ in the $(m_{Z'}, M_E)$ plane where $C_{Z'}$ is replaced by Eq. (3.20) and the gauge coupling constant g' is fixed. Different colors correspond to different values of g' . $\Delta a_\mu = 2.68 \times 10^{-9}$ can be realized only inside the contours for a given g' . We further restrict the VL masses by $M_E < \sqrt{2}v_\Phi$, because the condition $s_{2\mu_L} = s_{2\mu_R} = 1$ requires $M_{E_L} = M_{E_R} = \sqrt{2}\lambda_2^E v_\Phi \leq \sqrt{2}v_\Phi$. The last inequality comes from our requirement for perturbativity, $\lambda_2^E \leq 1$. This condition is depicted by the straight lines in Fig. 2. Altogether, the upper bound on the VL lepton mass is about 1.4 TeV where $m_{Z'} \sim 500 \text{ GeV}$ and $g' = 0.35$. Note that $m_{E_1} \sim 1.4 \text{ TeV}$ is realized only if all of the conditions are satisfied: (1) $s_{2\mu_L} \sim s_{2\mu_R} \sim 1$, (2) $\lambda'_e \sim -1.0$, (3) $C_\chi \sim 0$ (4) $m_{Z'} \sim 500 \text{ GeV}$, (5) $M_{E_L} \sim M_{E_R}$ and (6) $g' \sim 0.35$. Consequently, the upper bound is hardly ever saturated. The dashed lines in Fig. 2 show the same contour but the destructive χ contribution with $m_\chi = 100 \text{ GeV}$ is added to $C_{Z'}$. $m_\chi = 100 \text{ GeV}$ is chosen to minimize the C_χ contribution. Including the scalar contribution, the upper bound on

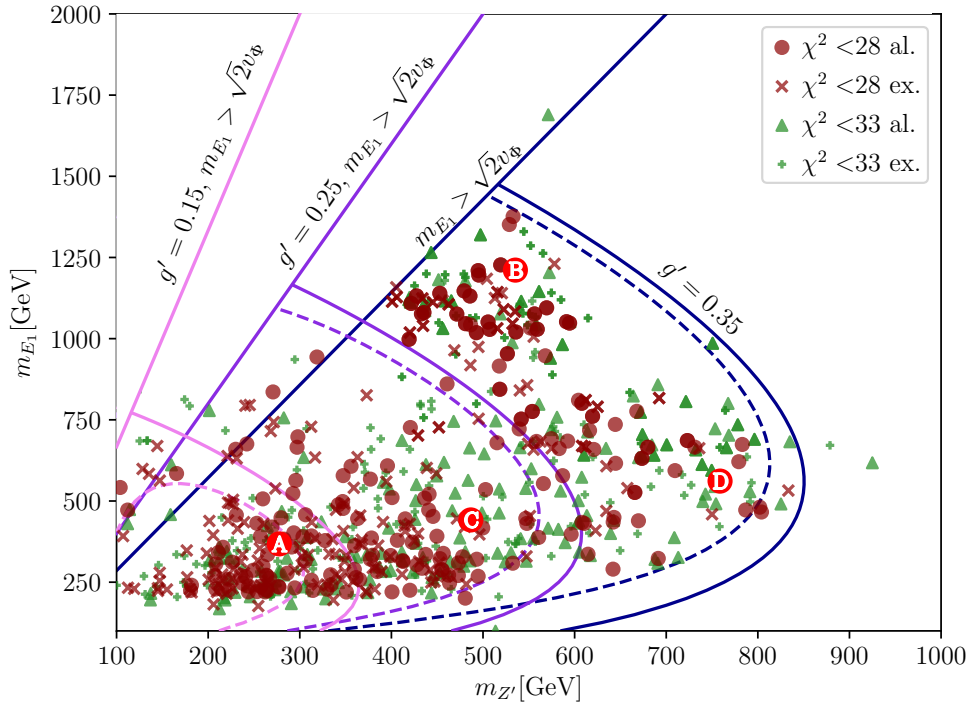


Figure 2: Contours in the $(m_{Z'}, m_E)$ plane which realize the maximal possible value of $\Delta a_\mu = 2.68 \times 10^{-9}$ for several values of g' . The solid (dashed) lines are obtained without (with) the scalar contribution C_χ , where for the purpose of the plot $m_\chi = 100$ GeV. $M_E > \sqrt{2}v_\Phi$ on the left of the straight lines. The dots and crosses represent best fit points (which in particular fit Δa_μ in the 1σ allowed region). Details will be explained in detail in Section 4. Red (green) dots have $\chi^2 < 28$ (33), while points which are excluded by other data are shown as crosses or pluses.

m_E is tightened to 1.3 TeV. Clearly the actual upper bound will be lower if some of the conditions (1)-(6) are not satisfied. The points shown in Fig. 2 are results of our fit. As anticipated, good fits are only obtained for points within the contours. The details of our analysis will be shown in the next section.

On a different note, a lighter scalar χ allows one to explain Δa_μ with smaller Z' contribution (see Figure 1), especially when the VL leptons are heavy. $y_{L,R} \ll 1$ or $y_{L,R} \gg 1$ is favored to suppress the destructive contributions from C_χ . In the phenomenologically viable parameter space, $M_{E_{L,R}} \gtrsim 250$ GeV and a lower bound on $y_{L,R}$ is

$$y_{L,R} \gtrsim 0.0625 \times \left(\frac{1 \text{ TeV}}{m_\chi} \right)^2. \quad (3.21)$$

For $y_{L,R} \sim 0.0625$ with $m_\chi = 1$ TeV, we have $C_\chi \sim -0.06$. On the other hand, $y_{L,R} \sim 100$, corresponding to $C_\chi \sim 0.004$, is possible if $m_\chi \sim 100$ GeV and $M_{E_{L,R}} \sim 1$ TeV.

Another important consequence of Δa_μ is that the Higgs Yukawa coupling λ'_e should

Table 4: Values of constants for charged lepton decays [25].

m_e [MeV]	0.5109989	Γ_e [GeV]	0
m_μ [MeV]	105.65837	Γ_μ [GeV]	2.99598×10^{-19}
m_τ [GeV]	1.77686	Γ_τ [GeV]	2.26735×10^{-12}
g	0.65290	m_W [GeV]	80.379

be ~ -1 . Of course, chiral enhancement proportional to the VL lepton mass is absent if there is no mixing between the left-handed and right-handed VL leptons. In other words, Δa_μ is enhanced by the left-right mixing induced by the Higgs VEV v_H and not directly by the VL lepton masses. Hence, Δa_μ is proportional to λ'_e . For this reason, the $U(1)'$ charge assignment in our model must not be universal for (L_L, \bar{E}_R) , but must be flipped as in Table 2. Importantly, such a charge assignment is incompatible with $SO(10)$ unification. However, it is still consistent with unification in the Pati-Salam gauge group, $SU(4) \times SU(2)_L \times SU(2)_R$.

3.1.2 $\ell_i \rightarrow \ell_j \nu \bar{\nu}$

The dominant decay modes of the charged leptons are three-body decays via a W boson. The branching fraction for a lepton ℓ_i to decay into a lighter lepton ℓ_j is given by

$$\text{BR}(\ell_i \rightarrow \ell_j \nu \bar{\nu}) = \sum_{k,l=1}^3 \frac{|\hat{g}_{\ell_L}^W]_{ki}|^2 \cdot |\hat{g}_{\ell_L}^W]_{lj}|^2}{1536\pi^3 \Gamma_{\ell_i}} \frac{m_{\ell_i}^5}{m_W^4} F_\ell \left(\frac{m_{\ell_j}^2}{m_{\ell_i}^2} \right), \quad (3.22)$$

where m_{ℓ_i} and Γ_{ℓ_i} are the mass and decay width of the lepton ℓ_i , respectively. The function F_ℓ is given by

$$F_\ell(y) = 1 - 8y + 8y^3 - y^4 - 12y^2 \log y. \quad (3.23)$$

Experimental values of the lepton masses and decay widths are listed in Table 4. For the muon decay rate, the tree-level branching fractions are multiplied by a QED correction factor $\eta_{\text{QED}} = 0.995802$ [25]. This factor is less important for tau decay. Just as for the charged lepton masses, the charged lepton decay rates are measured more precisely than the accuracy of our numerical analysis. We assume 0.01% relative uncertainties for these observables, remarking that we could always fit them by increasing the numerical accuracy of our analysis. Branching fractions could deviate from their SM predictions if the mixing between the SM families and VL family affects the W couplings. The values obtained in our model are compared with the tree-level SM values, that are given by replacing $[\hat{g}_{\ell_L}^W]_{ij} \rightarrow g [V_{\text{PMNS}}]_{ij} / \sqrt{2}$ in Eq. (3.22).

3.1.3 $\ell_i \rightarrow \ell_j \gamma$

Lepton Flavor Violating (LFV) processes are severely constrained by experiments. We follow [38] to calculate one-loop corrections including general gauge and Yukawa interactions. The Lagrangian for general gauge and Yukawa interactions is given by

$$\mathcal{L}_{\ell_i \rightarrow \ell_j \gamma} = \sum_{k=i,j} \sum_F \bar{F} \left[\sum_V V_\mu \gamma^\mu (L_k^{VF} P_L + R_k^{VF} P_R) - \sum_S S (L_k^{SF} P_L + R_k^{SF} P_R) \right] \ell_k + \text{h.c.}, \quad (3.24)$$

where ℓ_k are external charged leptons, F internal fermions, V vector bosons and S scalars. The gauge couplings in our model are identified as

$$L_k^{Z'\hat{e}A} = [\hat{g}_{eL}^{Z'}]_{Ak}, \quad L_k^{Z\hat{e}A} = [\hat{g}_{eL}^Z]_{Ak}, \quad L_k^{W\hat{n}B} = [\hat{g}_{\ell L}^W]_{kB}, \quad (3.25)$$

$$R_k^{Z'\hat{e}A} = [\hat{g}_{eR}^{Z'}]_{Ak}, \quad R_k^{Z\hat{e}A} = [\hat{g}_{eR}^Z]_{Ak}, \quad R_k^{W N_b} = [\hat{g}_{\ell R}^W]_{kb}, \quad (3.26)$$

where $A, B = 1, \dots, 5$, while $b = 4, 5$ runs only over the VL neutrinos.³ The Yukawa couplings are given by

$$L_k^{S\hat{e}A} = \frac{1}{\sqrt{2}} [\hat{Y}_e^S]_{Ak}, \quad R_k^{S\hat{e}B} = \frac{1}{\sqrt{2}} [\hat{Y}_e^S]_{kB}^*, \quad S = h, \chi, \sigma. \quad (3.27)$$

The branching fraction is then given by

$$\text{BR}(\ell_i \rightarrow \ell_j \gamma) = \frac{e^2}{16\pi\Gamma_{\ell_i}} \left(m_{\ell_i} - \frac{m_{\ell_j}^2}{m_{\ell_i}} \right)^3 (|\sigma_L|^2 + |\sigma_R|^2), \quad (3.28)$$

where

$$\begin{aligned} \sigma_L = & \sum_F \left[\rho^{WF} \bar{y}_1 + \lambda^{WF} \bar{y}_2 + v^{WF} \bar{y}_3 + \zeta^{WF} \bar{y}_4 \right. \\ & + \sum_{V=Z, Z'} (\rho^{VF} y_1 + \lambda^{VF} y_2 + v^{VF} y_3 + \zeta^{VF} y_4) \\ & \left. + \sum_{S=h, \chi, \sigma} (\rho^{SF} k_1 + \lambda^{BF} k_2 + v^{BF} k_3) \right]. \end{aligned} \quad (3.29)$$

Here, y_i , \bar{y}_i , and k_j (with $i = 1, \dots, 4$ and $j = 1, 2, 3$) are loop functions defined in Ref. [38] while combinations of couplings are defined as

$$\lambda^{BF} = (L_j^{BF})^* L_i^{BF}, \quad \rho^{BF} = (R_j^{BF})^* R_i^{BF}, \quad (3.30)$$

$$\zeta^{BF} = (L_j^{BF})^* R_i^{BF}, \quad v^{BF} = (R_j^{BF})^* L_i^{BF}, \quad (3.31)$$

³The sum for the W-boson coupling $R_k^{W N_b}$ only runs over the Dirac neutrinos because the light neutrinos are left-handed.

with $B = S, V, W$. σ_R is obtained from σ_L by formally replacing $\rho^{BF} \leftrightarrow \lambda^{BF}$ and $\zeta^{BF} \leftrightarrow \nu^{BF}$.

Just as for Δa_μ , the dominant contribution to $\ell_i \rightarrow \ell_j \gamma$ is again a chirally enhanced effect. To a good approximation, σ_L is given by

$$\sigma_L \simeq \sum_{b=4,5} \left(\frac{m_{e_b}}{m_{Z'}^2} \left[\hat{g}_{e_R}^{Z'} \right]_{jb} \left[\hat{g}_{e_L}^{Z'} \right]_{bi} G_Z(x_{e_b}^{Z'}) + \frac{m_{e_b}}{4m_\chi^2} \left[\hat{Y}_e^\chi \right]_{jb} \left[\hat{Y}_e^\chi \right]_{bi} G_S(y_{e_b}^\chi) \right), \quad (3.32)$$

where the loop functions $G_{Z,S}$ are the same as in Eqs. (3.7) and (3.13). Using the results from Appendix B, analytic expressions for the branching fractions of $\mu \rightarrow e \gamma$ and $\tau \rightarrow \mu \gamma$ are given by

$$\begin{aligned} \text{BR}(\mu \rightarrow e \gamma) &\sim \frac{\alpha_e m_\mu^3}{1024 \pi^4 \Gamma_\mu} \left(\frac{\lambda'_e v_H}{2v_\Phi^2} c_{\mu_L} c_{\mu_R} C_{LR} \right)^2 (\epsilon_{e_R}^2 s_{\mu_L}^2 + \epsilon_{e_L}^2 s_{\mu_R}^2) \\ &\sim 2.3 \times 10^{-14} \times \left(\frac{c_{\mu_L} c_{\mu_R} C_{LR}}{0.1} \right)^2 \left(\frac{\lambda'_e}{1.0} \right)^2 \left(\frac{1.0 \text{ TeV}}{v_\Phi} \right)^4 \left(\frac{\epsilon_{e_R}^2 s_{\mu_L}^2 + \epsilon_{e_L}^2 s_{\mu_R}^2}{10^{-12}} \right), \end{aligned} \quad (3.33)$$

$$\begin{aligned} \text{BR}(\tau \rightarrow \mu \gamma) &\sim \frac{\alpha_e m_\tau^3}{1024 \pi^4 \Gamma_\tau} \left(\frac{\lambda'_e v_H}{2v_\Phi^2} c_{\mu_L} c_{\mu_R} C_{LR} \right)^2 (\epsilon_{\tau_L}^2 s_{\mu_R}^2 + \epsilon_{\tau_R}^2 s_{\mu_L}^2) \\ &\sim 1.5 \times 10^{-9} \times \left(\frac{c_{\mu_L} c_{\mu_R} C_{LR}}{0.1} \right)^2 \left(\frac{\lambda'_e}{1.0} \right)^2 \left(\frac{1.0 \text{ TeV}}{v_\Phi} \right)^4 \left(\frac{\epsilon_{\tau_R}^2 s_{\mu_L}^2 + \epsilon_{\tau_L}^2 s_{\mu_R}^2}{10^{-4}} \right), \end{aligned} \quad (3.34)$$

with C_{LR} given in Eq. (3.16). Here, $\epsilon_{e_{L,R}}$ ($\epsilon_{\tau_{L,R}}$) are the mixing angles between the left- and right-handed electrons (tauons) and the VL leptons, respectively. $\epsilon_{e_{L,R}} \lesssim 10^{-6}$ and $\epsilon_{\tau_{L,R}} \lesssim 10^{-2}$ are required to suppress $\mu \rightarrow e \gamma$ and $\tau \rightarrow \mu \gamma$, respectively. Once both of these processes are suppressed, $\tau \rightarrow e \gamma$ is automatically suppressed as well.

3.1.4 $\ell_i \rightarrow \ell_j \ell_k \ell_l$

The neutral bosons also mediate LFV three-body decays, such as $\mu^- \rightarrow e^- e^+ e^-$, $\tau^- \rightarrow \mu^- \mu^+ \mu^-$ and so on. Effective interactions relevant for a decay $\ell_i^- \rightarrow \ell_j^- \ell_k^+ \ell_j^-$ are

$$\begin{aligned} \mathcal{L}_{\ell_i^- \rightarrow \ell_j^- \ell_k^+ \ell_j^-} &= B_{LL}^{ijkj} (\bar{\ell}_i P_L \ell_j) (\bar{\ell}_k P_L \ell_j) + B_{LR}^{ijkj} (\bar{\ell}_i P_L \ell_j) (\bar{\ell}_k P_R \ell_j) \\ &\quad + C_{LL}^{ijkj} (\bar{\ell}_i \gamma^\mu P_L \ell_j) (\bar{\ell}_k \gamma_\mu P_L \ell_j) + C_{LR}^{ijkj} (\bar{\ell}_i \gamma^\mu P_L \ell_j) (\bar{\ell}_k \gamma_\mu P_R \ell_j) \\ &\quad + (L \leftrightarrow R) + \text{h.c.} . \end{aligned} \quad (3.35)$$

The branching fraction is given by [39, 40]

$$\begin{aligned} \text{BR}(\ell_i^- \rightarrow \ell_j^- \ell_k^+ \ell_j^-) &= \frac{m_{\ell_i}^5}{1536 \pi^3 \Gamma_{\ell_i}} \\ &\quad \times \left[2 \left(\left| C_{LL}^{ijkj} \right|^2 + \frac{\left| B_{LL}^{ijkj} \right|^2}{16} \right) + \left| C_{LR}^{ijkj} - \frac{1}{2} B_{RL}^{ijkj} \right|^2 + (L \leftrightarrow R) \right], \end{aligned} \quad (3.36)$$

where masses of daughter leptons are neglected. Interactions relevant for $\ell_i^- \rightarrow \ell_j^- \ell_j^+ \ell_k^-$, $k \neq j$ (see Table 3) are given by

$$\begin{aligned} \mathcal{L}_{\ell_i^- \rightarrow \ell_j^- \ell_j^+ \ell_k^-} = & B_{LL}^{ikjj} (\bar{\ell}_i P_L \ell_k) (\bar{\ell}_j P_L \ell_j) + B_{LL}^{ijjk} (\bar{\ell}_i P_L \ell_j) (\bar{\ell}_j P_L \ell_k) \\ & + B_{LR}^{ikjj} (\bar{\ell}_i P_L \ell_k) (\bar{\ell}_j P_R \ell_j) + B_{LR}^{ijjk} (\bar{\ell}_i P_L \ell_j) (\bar{\ell}_j P_R \ell_k) \\ & + C_{LL}^{ikjj} (\bar{\ell}_i \gamma^\mu P_L \ell_k) (\bar{\ell}_j \gamma_\mu P_L \ell_j) + C_{LL}^{ijjk} (\bar{\ell}_i \gamma^\mu P_L \ell_j) (\bar{\ell}_j \gamma_\mu P_L \ell_k) \\ & + C_{LR}^{ikjj} (\bar{\ell}_i \gamma^\mu P_L \ell_k) (\bar{\ell}_j \gamma_\mu P_R \ell_j) + C_{LR}^{ijjk} (\bar{\ell}_i \gamma^\mu P_L \ell_j) (\bar{\ell}_j \gamma_\mu P_R \ell_k) \\ & + (L \leftrightarrow R) + \text{h.c.} . \end{aligned} \quad (3.37)$$

The branching fraction is given by [41]

$$\begin{aligned} \text{BR}(\ell_i^- \rightarrow \ell_j^- \ell_j^+ \ell_k^-) = & \frac{m_{\ell_i}^5}{1536\pi^3\Gamma_{\ell_i}} \left[\left| C_{LL}^{ikjj} + C_{LL}^{ijjk} \right|^2 + \left| C_{LR}^{ijjk} - \frac{1}{2} B_{RL}^{ikjj} \right|^2 + \left| C_{LR}^{ikjj} - \frac{1}{2} B_{RL}^{ijjk} \right|^2 \right. \\ & \left. + \frac{1}{4} \left(\left| B_{LL}^{ikjj} \right|^2 + \left| B_{LL}^{ijjk} \right|^2 + \text{Re} \left(B_{LL}^{ijjk} B_{LL}^{ikjj*} \right) \right) \right] + (L \leftrightarrow R). \end{aligned} \quad (3.38)$$

In this model, the Wilson coefficients are given by

$$\begin{aligned} B_{LL}^{ijkl} = & - \sum_{S=h,\chi,\sigma} \frac{1}{2m_S^2} [\hat{Y}_e^S]_{ij} [\hat{Y}_e^S]_{kl}, \quad B_{LR}^{ijkl} = - \sum_{S=h,\chi,\sigma} \frac{1}{2m_S^2} [\hat{Y}_e^S]_{ij} [\hat{Y}_e^S]_{lk}^*, \quad (3.39) \\ B_{RL}^{ijkl} = & - \sum_{S=h,\chi,\sigma} \frac{1}{2m_S^2} [\hat{Y}_e^S]_{ji}^* [\hat{Y}_e^S]_{kl}, \quad B_{RR}^{ijkl} = - \sum_{S=h,\chi,\sigma} \frac{1}{2m_S^2} [\hat{Y}_e^S]_{ji}^* [\hat{Y}_e^S]_{lk}^*, \\ C_{XY}^{ijkl} = & \sum_{V=Z,Z'} \frac{1}{m_V^2} [\hat{g}_{eX}^V]_{ij} [\hat{g}_{eY}^V]_{kl}, \end{aligned}$$

where $X, Y = L, R$.

These LFV three body decays are dominated by Z' boson exchange. Using the result in Appendix B, the Z' contributions to $\mu^- \rightarrow e^- e^+ e^-$ and $\tau^- \rightarrow \mu^- \mu^+ \mu^-$ are estimated as

$$\text{BR}(\mu^- \rightarrow e^- e^+ e^-) \sim \frac{m_\mu^5}{1536\pi^3\Gamma_\mu} \frac{s_\mu^2 \epsilon_e^6}{2v_\Phi^4} = 2.3 \times 10^{-40} \times \left(\frac{s_\mu}{1/\sqrt{2}} \right)^2 \left(\frac{\epsilon_e}{10^{-6}} \right)^6 \left(\frac{1.0 \text{ TeV}}{v_\Phi} \right)^4, \quad (3.40)$$

$$\text{BR}(\tau^- \rightarrow \mu^- \mu^+ \mu^-) \sim \frac{m_\tau^5}{1536\pi^3\Gamma_\tau} \frac{s_\mu^6 \epsilon_\tau^2}{2v_\Phi^4} = 1.0 \times 10^{-9} \times \left(\frac{s_\mu}{1/\sqrt{2}} \right)^6 \left(\frac{\epsilon_\tau}{10^{-2}} \right)^2 \left(\frac{1.0 \text{ TeV}}{v_\Phi} \right)^4, \quad (3.41)$$

where s_μ , ϵ_e , and ϵ_τ are the maximum values of $s_{\mu L,R}$, $\epsilon_{e L,R}$ and $\epsilon_{\tau L,R}$, respectively. $\text{BR}(\mu \rightarrow 3e)$ is strongly suppressed by ϵ_e^6 and will be much smaller than $\text{BR}(\mu \rightarrow e\gamma)$. On the other hand, $\text{BR}(\tau \rightarrow 3\mu)$ scales as ϵ_τ^2 , and therefore in the same way as $\text{BR}(\tau \rightarrow \mu\gamma)$. $\text{BR}(\tau \rightarrow 3\mu) \gtrsim \text{BR}(\tau \rightarrow \mu\gamma)$ is expected because the former is proportional to an absolute sum of different chirality structures, while the latter is dominated by the left-right mixing effect. All other τ decays are suppressed by additional factors of ϵ_e .

Table 5: Values of constants for EW boson sector. Masses and widths are from Ref. [25].

m_W [GeV]	80.379 ± 0.012	Γ_W [GeV]	2.085 ± 0.042
m_Z [GeV]	91.1876 ± 0.0021	Γ_Z [GeV]	2.4952 ± 0.0023
m_h [GeV]	125.18 ± 0.16	Γ_h [MeV]	4.07 ± 0.16
$g(m_Z)$ [24]	0.65184 ± 0.00018	$\alpha_s(m_Z)$	0.1181 ± 0.0011
s_W^2 [25]	0.22343 ± 0.00007	\bar{s}_ℓ^2 [25]	0.23154 ± 0.00003

3.2 EW Bosons

The fermion couplings to the SM bosons, namely Higgs, W and Z bosons, are also modified by the mixing to VL fermions. This might affect their decays. For instance, LFV Higgs boson decays are predicted in models with VL leptons studied in Refs. [4, 20, 42]. All observables here are calculated at tree-level, except for $h \rightarrow \gamma\gamma$. All formulae that we use to compute two-body decays are summarized in Appendix A. Table 5 summarizes experimentally determined values of constants used in the EW boson observables. Experimental central values and uncertainties of the relevant observables are summarized in Table 6.

3.2.1 W Boson Decays

There is a right-handed charged current coupling to the W boson which is absent in the SM. Furthermore, the non-unitarity of the CKM and PMNS matrices can affect the W boson couplings. These will alter W boson decays.

The branching fractions for W boson decays are given by

$$\text{BR}(W^+ \rightarrow e_i^+ \nu) = \frac{m_W}{48\pi\Gamma_W} (1 - x_{e_i}^W)^2 (2 + x_{e_i}^W) \sum_{k=1}^3 |[\hat{g}_{\ell_L}^W]_{ki}|^2, \quad (3.42)$$

$$\begin{aligned} \text{BR}(W^+ \rightarrow u_i \bar{d}_j) &= \frac{m_W}{8\pi\Gamma_W} \lambda(x_{u_i}^W, x_{d_j}^W) \left[\left(|[\hat{g}_{qL}^W]_{ij}|^2 + |[\hat{g}_{qR}^W]_{ij}|^2 \right) \right. \\ &\quad \left. \times \left(1 - \frac{x_{u_i}^W + x_{d_j}^W}{2} - \frac{(x_{u_i}^W - x_{d_j}^W)^2}{2} \right) + 6 \text{Re} \left([\hat{g}_{qL}^W]_{ij} [\hat{g}_{qR}^W]_{ij} \right) \sqrt{x_{u_i}^W x_{d_j}^W} \right], \end{aligned} \quad (3.43)$$

where $x_{f_i}^W := m_{f_i}^2/m_W^2$ ($f = e, u, d$). The function λ is defined in Eq. (A.3).

SM predictions for these decays are calculated by replacing

$$[\hat{g}_{\ell_L}^W]_{ij} \rightarrow \frac{g}{\sqrt{2}} [V_{\text{PMNS}}]_{ij}, \quad [\hat{g}_{qL}^W]_{ij} \rightarrow \frac{g}{\sqrt{2}} [V_{\text{CKM}}]_{ij}, \quad \hat{g}_{qR}^W \rightarrow 0. \quad (3.44)$$

Here, experimental absolute values of the PMNS and CKM matrix elements are used. For the leptonic decays, radiative corrections and experimental uncertainties are small. We

Table 6: Central values and uncertainty of the observables for EW gauge bosons.

Name	Exp.	Unc.	Remark
$\text{BR}(W^+ \rightarrow e^+\nu)$	0.1086	0.1 %	SM
$\text{BR}(W^+ \rightarrow \mu^+\nu)$	0.1086	0.1 %	SM
$\text{BR}(W^+ \rightarrow \tau^+\nu)$	0.1085	0.1 %	SM
$\text{BR}(W^+ \rightarrow \text{had})$	0.6656	3.76 %	SM
$\text{BR}(W^+ \rightarrow c\bar{s})$	0.3239	10 %	SM
$\text{BR}(Z \rightarrow e^+e^-)$	0.03333	0.187 %	SM
$\text{BR}(Z \rightarrow \mu^+\mu^-)$	0.03333	0.187 %	SM
$\text{BR}(Z \rightarrow \tau^+\tau^-)$	0.03326	0.187 %	SM
$\text{BR}(Z \rightarrow \text{had})$	0.6766	3.76 %	SM
$\text{BR}(Z \rightarrow (u\bar{u} + c\bar{c}))/2$	0.1157	3.76 %	SM
$\text{BR}(Z \rightarrow (d\bar{d} + s\bar{s} + b\bar{b}))/3$	0.1483	3.76 %	SM
$\text{BR}(Z \rightarrow c\bar{c})$	0.1157	3.76 %	SM
$\text{BR}(Z \rightarrow b\bar{b})$	0.1479	3.76 %	SM
$\text{BR}(Z \rightarrow e\mu)$	0.0	3.8×10^{-7}	Ref. [25]
$\text{BR}(Z \rightarrow e\tau)$	0.0	5.0×10^{-6}	Ref. [25]
$\text{BR}(Z \rightarrow \mu\tau)$	0.0	6.1×10^{-6}	Ref. [25]
A_e	0.1469	1 %	SM
A_μ	0.1469	10 %	SM
A_τ	0.1469	1 %	SM
A_s	0.9406	10 %	SM
A_c	0.6949	1 %	SM
A_b	0.9406	1 %	SM
$\mu_{\mu\mu}$	0.0	1.3	Ref. [25]
$\mu_{\tau\tau}$	1.12	0.23	Ref. [25]
μ_{bb}	0.95	0.22	Ref. [25]
$\mu_{\gamma\gamma}$	1.16	0.18	Ref. [25]
$\text{BR}(h \rightarrow ee)$	0.0	9.7×10^{-4}	Ref. [25]
$\text{BR}(h \rightarrow e\mu)$	0.0	1.8×10^{-4}	Ref. [25]
$\text{BR}(h \rightarrow e\tau)$	0.0	3.1×10^{-3}	Ref. [25]
$\text{BR}(h \rightarrow \mu\tau)$	0.0	1.3×10^{-3}	Ref. [25]

use a 0.1% relative uncertainty for these decays. For the hadronic decay modes, QCD corrections may change the values by a factor proportional to $\alpha_s/\pi \sim 0.038$. We use a relative uncertainty of 3.8% for the total hadronic branching fraction, while we use a 10% relative uncertainty for $W \rightarrow cs$ because experimental uncertainties here are still large.

3.2.2 Z Decays and Asymmetry Parameters

The Z boson couplings are, in general, changed by the mixing effects. This can affect the branching fractions and asymmetry parameters of Z decays. The Z boson couplings depend on the weak mixing angle θ_W . For the lepton couplings, we use the effective angle $\bar{s}_\ell = 0.23154$ including radiative corrections, while the tree-level value $s_W = 0.22343$ is used for the quark couplings [25]. Using the effective angle is necessary to reproduce the observed values of $A_{\ell=e,\mu,\tau}$.

The branching fractions for flavor conserving decays are given by

$$\text{BR}(Z \rightarrow f_i \bar{f}_i) = \frac{N_c^f m_Z}{24\pi\Gamma_Z} \sqrt{1 - 4x_{f_i}^Z} \left[\left(\left| [\hat{g}_{f_L}^Z]_{ii} \right|^2 + \left| [\hat{g}_{f_R}^Z]_{ii} \right|^2 \right) (1 - x_{f_i}^Z) + 6x_{f_i}^Z \text{Re} \left([\hat{g}_{f_L}^Z]_{ii}^* [\hat{g}_{f_R}^Z]_{ii} \right) \right], \quad (3.45)$$

where N_c^f is a color factor and $x_{f_i}^Z := m_{f_i}^2/m_Z^2$ for a fermion f_i . Those for flavor violating decays are given by

$$\text{BR}(Z \rightarrow f_i^\pm f_j^\mp) = \frac{N_c^f m_Z}{12\pi\Gamma_Z} \lambda(x_{f_i}^Z, x_{f_j}^Z) \left[\left(\left| [\hat{g}_{f_L}^Z]_{ij} \right|^2 + \left| [\hat{g}_{f_R}^Z]_{ij} \right|^2 \right) \times \left(1 - \frac{x_{f_i}^Z + x_{f_j}^Z}{2} - \frac{(x_{f_i}^Z - x_{f_j}^Z)^2}{2} \right) + 6\sqrt{x_{f_i}^Z x_{f_j}^Z} \text{Re} \left([\hat{g}_{f_L}^Z]_{ij}^* [\hat{g}_{f_R}^Z]_{ij} \right) \right]. \quad (3.46)$$

For $\text{BR}(Z \rightarrow \text{had})$, the experimental value of a four-body decay $\text{BR}(Z \rightarrow b\bar{b}b\bar{b}) = 0.00036$ [25] is added to the sum of two-body decays to quarks. The Z -pole asymmetry parameters are defined as

$$A_{f_i} := \frac{2g_{V_{f_i}} g_{A_{f_i}}}{g_{V_{f_i}}^2 + g_{A_{f_i}}^2}, \quad (3.47)$$

where $f_i = e, \mu, \tau, s, c, b$, and (axial-)vector couplings are obtained as

$$g_{V_{f_i}} = [\hat{g}_{f_L}^Z + \hat{g}_{f_R}^Z]_{ii}, \quad g_{A_{f_i}} = [\hat{g}_{f_L}^Z - \hat{g}_{f_R}^Z]_{ii}. \quad (3.48)$$

SM predictions for these observables are obtained by formally replacing $P_5, P_5 \rightarrow \mathbb{1}_3, 0_3$ in Eq. (2.28). The leading QED and QCD corrections to these decays are proportional to $3\alpha_e/4\pi \sim 0.0019$ and $\alpha_s/\pi \sim 0.038$ for leptonic or hadronic decays, respectively. We, therefore, use a 0.19% (3.8%) relative uncertainty on the leptonic (hadronic) decays. The relative uncertainties for the asymmetry parameters are taken as 1% for A_e, A_τ, A_c, A_b , and

10% for A_μ and A_s , consistent with their experimental uncertainties. The uncertainties for flavor violating decays are determined from their experimental upper bounds.

Let us illustrate how the SM boson couplings, in general, are very close to their SM values. We show this analytically in Appendix B. In general, one finds the mixing to be suppressed by $\sim \epsilon_{f_{\text{SM}}}^2 m_{f_{\text{SM}}}^2 / M_{\text{FVL}}^2$. Considering, for example, the left-handed $Z - \mu\tau$ coupling we find that it can be estimated as

$$[\hat{g}_{eL}^Z]_{23} \sim \frac{g}{2c_W} s_{\mu L} \epsilon_{\tau L} \frac{m_\mu m_\tau}{M_{E_L}^2} \sim 2.0 \times 10^{-9} \times \left(\frac{s_{\mu L}}{1/\sqrt{2}} \right) \left(\frac{\epsilon_{\tau L}}{0.01} \right) \left(\frac{500 \text{ GeV}}{M_{E_L}} \right)^2. \quad (3.49)$$

Corrections for lighter flavors are even more suppressed.

3.2.3 Higgs Decays

The Higgs boson couplings to SM fermions can, in general, depart from their SM predictions due to misalignment of the Yukawa couplings and mass matrices. We have studied the signal strengths for the measured decay modes to $\mu\mu$, $\tau\tau$, bb , and $\gamma\gamma$ final states as well as the branching fractions for the unobserved decays ee , $e\mu$, $e\tau$, and $\mu\tau$. Central values and uncertainties are set to their experimentally observed values. Decay widths for flavor conserving decays are given by

$$\Gamma(h \rightarrow f_i \bar{f}_i) = \frac{m_h}{16\pi} \sqrt{1 - 4x_{f_i}^h} \left[\left| [\hat{Y}_f^h]_{ii} \right|^2 - 4x_{f_i}^h \left(\text{Re} [\hat{Y}_f^h]_{ii} \right)^2 \right], \quad (3.50)$$

and those for flavor violating decays are

$$\begin{aligned} \Gamma(h \rightarrow f_i^\pm f_j^\mp) &= \frac{m_h}{16\pi} \lambda(x_{f_i}^h, x_{f_j}^h) \\ &\times \left[\left(\left| [\hat{Y}_f^h]_{ij} \right|^2 + \left| [\hat{Y}_f^h]_{ji} \right|^2 \right) (1 - x_{f_i}^h - x_{f_j}^h) - 4 \text{Re} \left([\hat{Y}_f^h]_{ij} [\hat{Y}_f^h]_{ji} \right) \sqrt{x_{f_i}^h x_{f_j}^h} \right], \end{aligned} \quad (3.51)$$

where $x_{f_i}^h := m_{f_i}^2 / m_h^2$.

In addition to the tree-level decays, the VL families may significantly contribute to the loop-induced decay, $h \rightarrow \gamma\gamma$ and $h \rightarrow gg$. The decay width for $h \rightarrow \gamma\gamma$ is given by [43]

$$\Gamma(h \rightarrow \gamma\gamma) = \frac{G_F \alpha_e^2 m_H^3}{128 \sqrt{2} \pi^3} \left| A_1^H(\tau_W) + \sum_{f_A} N_c^f Q_f^2 \left(\frac{y_{f_A} v_H}{m_{f_A}} \right) A_{1/2}^H(\tau_{f_A}) \right|^2, \quad (3.52)$$

where $\tau_I = m_H^2 / (4m_I^2)$ with $I = f_A, W$. Here, f_A runs over all the fermions in this model and $A = 1, \dots, 5$ is a flavor index. N_c^f is the number of color degrees of freedom and $y_{f_A} := [\hat{Y}_f^h]_{AA}$ is a diagonal Yukawa coupling constant of the Higgs boson to a fermion f_A . The form factors are given by

$$A_{1/2}^H(\tau) = \frac{2}{\tau^2} [\tau + (\tau - 1)f(\tau)], \quad A_1^H(\tau) = -\frac{1}{\tau^2} [2\tau^2 + 3\tau + 3(2\tau - 1)f(\tau)], \quad (3.53)$$

where

$$f(\tau) = \begin{cases} \arcsin^2 \sqrt{\tau} & \tau \leq 1, \\ -\frac{1}{4} \left[\log \frac{1 + \sqrt{1 - \tau^{-1}}}{1 - \sqrt{1 - \tau^{-1}}} - i\pi \right]^2 & \tau > 1. \end{cases} \quad (3.54)$$

Similarly, the decay width of $h \rightarrow gg$ is given by [43]

$$\Gamma(h \rightarrow gg) = \frac{G_F \alpha_s^2 m_H^3}{36 \sqrt{2} \pi^3} \left| \frac{3}{4} \sum_{q_A} \left(\frac{y_{q_A} v_H}{m_{q_A}} \right) A_{1/2}^H(\tau_{q_A}) \right|^2, \quad (3.55)$$

where q_A only runs over the quarks.

Naively, one expects the size of VL fermion contributions to these one-loop decays to be suppressed by the squared ratio of $SU(2) \times U(1)$ breaking mass to VL mass, i.e. by a factor $(\lambda'_f v_H)^2 / M_{F_{VL}}^2$. This is exactly what we find. Using the result of Appendix B, contributions from VL fermions F_L, F_R are given by

$$\begin{aligned} \sum_{f=F_L, F_R} \left(\frac{y_f v_H}{m_f} \right) A_{1/2}^H(\tau_f) &\sim (\lambda'_f v_H)^2 \frac{A_{1/2}^H(\tau_{F_L}) - A_{1/2}^H(\tau_{F_R})}{\tilde{M}_{F_L}^2 - \tilde{M}_{F_R}^2} \sim -\frac{7}{90} \frac{m_H^2 (\lambda'_f v_H)^2}{M_{F_L}^2 M_{F_R}^2} \\ &\sim -5.9 \times 10^{-4} \times \left(\frac{\lambda'_f}{1.0} \right)^2 \left(\frac{500 \text{ GeV}}{\sqrt{M_{F_L} M_{F_R}}} \right)^4, \end{aligned} \quad (3.56)$$

where $\tilde{M}_{F_{L(R)}}$ is the approximated mass of VL fermion $F_{L(R)}$ defined in Eq. (B.9). Here, $\lambda'_f v_H \ll M_{F_{L,R}}$ and $\lambda_f \ll \lambda'_f$ have been assumed. For the last equality in the first line, we use the series expansion $A_{1/2}^H(\tau) \approx 4/3 + 14/45 \tau$ around $\tau \approx 0$. A possible cancellation between the two VL fermions gives an extra suppression. Altogether, we confirm that the VL fermions only give very small corrections to these decay rates. Especially VL quarks will be heavy, and their effects therefore particularly suppressed. Thus, there is no meaningful constraint arising from $h \rightarrow gg$ for our analysis, and also the Higgs boson production rate is unchanged with respect to the SM.

The signal strengths of the Higgs boson are defined as

$$\mu_{XX} := \frac{\sigma^{\text{prod}} \cdot \text{BR}(h \rightarrow XX)}{\sigma_{\text{SM}}^{\text{prod}} \cdot \text{BR}(h \rightarrow XX)_{\text{SM}}} \simeq \frac{\text{BR}(h \rightarrow XX)}{\text{BR}(h \rightarrow XX)_{\text{SM}}}, \quad X = \mu, \tau, \gamma, b. \quad (3.57)$$

3.3 Quarks

We study the SM quark masses, 9 absolute values of the CKM matrix elements and 3 CP phases α, β, γ . The Wilson coefficients relevant to the $b \rightarrow s \ell^+ \ell^-$ processes are fitted to explain the anomalies. The new physics contributions will also affect neutral meson mixing, namely $K-\bar{K}$, $B_d-\bar{B}_d$, $B_s-\bar{B}_s$ and $D-\bar{D}$ mixing, (semi-)leptonic decays of B mesons and top quark decays. Central values and uncertainties for quark masses and the CKM elements are listed in Table 7. Values for the other observables are listed in Table 8. We do not assume unitarity of the CKM matrix for our analysis and our parameters are fit directly to the values determined by experimental measurements.

Table 7: Central values and uncertainties of quark masses and CKM mixing parameters.

Name	Exp.	Unc.	Remark
$m_u(m_Z)$ [MeV]	1.29	0.39	Ref. [24]
$m_c(m_Z)$ [MeV]	627	19.	Ref. [24]
$m_t(m_Z)$ [GeV]	171.7	1.5	Ref. [24]
$m_d(m_Z)$ [MeV]	2.75	0.29	Ref. [24]
$m_s(m_Z)$ [MeV]	54.3	2.9	Ref. [24]
$m_b(m_Z)$ [GeV]	2.853	0.026	Ref. [24]
$ V_{ud} $	0.97420	0.00021	Ref. [25]
$ V_{us} $	0.2243	0.0005	Ref. [25]
$ V_{ub} $	0.00394	0.00036	Ref. [25]
$ V_{cd} $	0.218	0.004	Ref. [25]
$ V_{cs} $	0.997	0.017	Ref. [25]
$ V_{cb} $	0.0422	0.0008	Ref. [25]
$ V_{td} $	0.0081	0.0005	Ref. [25]
$ V_{ts} $	0.0394	0.0023	Ref. [25]
$ V_{tb} $	1.019	0.025	Ref. [25]
α [rad]	1.475	0.097	Ref. [25]
$\sin 2\beta$	0.691	0.017	Ref. [25]
γ [rad]	1.283	0.081	Ref. [25]

3.3.1 $b \rightarrow s\ell^+\ell^-$ Processes

The relevant effective Hamiltonian for $b \rightarrow s\ell^+\ell^-$ is given by [50, 51],

$$\mathcal{H}_{\text{eff}}^\ell = -\frac{4G_F}{\sqrt{2}} \frac{\alpha}{4\pi} V_{tb}V_{ts}^* \sum_{a=9,10} \left(C_a^\ell \mathcal{O}_a^\ell + C_a^{\prime\ell} \mathcal{O}_a^{\prime\ell} \right), \quad (3.58)$$

where

$$\mathcal{O}_9^\ell = [\bar{s}\gamma^\mu P_L b] [\bar{\ell}\gamma_\mu \ell], \quad \mathcal{O}_{10}^\ell = [\bar{s}\gamma^\mu P_L b] [\bar{\ell}\gamma_\mu \gamma_5 \ell], \quad (3.59)$$

$$\mathcal{O}_9^{\prime\ell} = [\bar{s}\gamma^\mu P_R b] [\bar{\ell}\gamma_\mu \ell], \quad \mathcal{O}_{10}^{\prime\ell} = [\bar{s}\gamma^\mu P_R b] [\bar{\ell}\gamma_\mu \gamma_5 \ell]. \quad (3.60)$$

Here, $\ell = e, \mu, \tau$. The Wilson coefficients induced by Z' exchange are given by

$$C_9^\ell = -\frac{\sqrt{2}}{4G_F} \frac{4\pi}{\alpha_e} \frac{1}{V_{tb}V_{ts}^*} \frac{1}{2m_{Z'}^2} \cdot \left[\hat{g}_{dL}^{Z'} \right]_{23} \left[\hat{g}_{eR}^{Z'} + \hat{g}_{eL}^{Z'} \right]_{ii}, \quad (3.61)$$

Table 8: Values of observables of the quark sector. Theoretical uncertainties are included for ΔM_K , ΔM_d , ΔM_s and ϵ_K . Values for $C_{9,10}^{(\prime),e,\mu}$ are discussed in the text.

Name	Exp.	Unc.	Remark
ΔM_K [ps ⁻¹]	0.005293	0.0022	Ref. [25]
$ \epsilon_K \times 10^3$	2.228	0.21	Ref. [25]
ΔM_d [ps ⁻¹]	0.5065	0.081	Ref. [25]
$S_{\psi K_S}$	0.695	0.019	Ref. [44]
ΔM_s [ps ⁻¹]	17.757	2.5	Ref. [25]
$S_{\psi\phi}$	0.021	0.031	Ref. [44]
$ \Delta^{\text{NP}} x_D $ [%]	0.0	0.5	Ref. [25]
$R_K^{\nu\bar{\nu}}$	1.0	2.6	Ref. [45]
$R_{K^*}^{\nu\bar{\nu}}$	1.0	2.7	Ref. [46]
$R_{B_d \rightarrow \mu\mu}$	1.5	1.4	Refs. [25, 47]
$R_{B_s \rightarrow \mu\mu}$	0.75	0.16	Refs. [25, 48]
Γ_t [GeV]	1.41	0.17	Ref. [25]
BR($t \rightarrow Zq$)	0.0	2.6×10^{-4}	Ref. [25]
BR($t \rightarrow hu$)	0.0	9.7×10^{-4}	Ref. [25]
BR($t \rightarrow hc$)	0.0	8.2×10^{-4}	Ref. [25]
BR($B_s \rightarrow K\tau\tau$)	0.0	1.4×10^{-3}	Ref. [49]

$$C_{10}^{\prime\ell} = -\frac{\sqrt{2}}{4G_F} \frac{4\pi}{\alpha_e} \frac{1}{V_{tb}V_{ts}^*} \frac{1}{2m_{Z'}^2} \cdot \left[\hat{g}_{dL}^{Z'} \right]_{23} \left[\hat{g}_{eR}^{Z'} - \hat{g}_{eL}^{Z'} \right]_{ii}, \quad (3.62)$$

$$C_9^{\prime\ell} = -\frac{\sqrt{2}}{4G_F} \frac{4\pi}{\alpha_e} \frac{1}{V_{tb}V_{ts}^*} \frac{1}{2m_{Z'}^2} \cdot \left[\hat{g}_{dR}^{Z'} \right]_{23} \left[\hat{g}_{eR}^{Z'} + \hat{g}_{eL}^{Z'} \right]_{ii}, \quad (3.63)$$

$$C_{10}^{\prime\ell} = -\frac{\sqrt{2}}{4G_F} \frac{4\pi}{\alpha_e} \frac{1}{V_{tb}V_{ts}^*} \frac{1}{2m_{Z'}^2} \cdot \left[\hat{g}_{dR}^{Z'} \right]_{23} \left[\hat{g}_{eR}^{Z'} - \hat{g}_{eL}^{Z'} \right]_{ii}, \quad (3.64)$$

where $i = 1, 2, 3$ for $\ell = e, \mu, \tau$, respectively.

In Ref. [52]⁴, one or two of the Wilson coefficients are fitted to the latest data for $R_{K^{(*)}}$ and $b \rightarrow s\ell^+\ell^-$ decay observables, while all the other Wilson coefficients are assumed to vanish. There are three scenarios in the one-dimensional analysis that have pulls larger than 5σ with respect to the SM prediction:

$$(I) \quad \text{Re } C_9^\mu = -0.95 \pm 0.15, \quad (3.65)$$

$$(II) \quad \text{Re } C_{10}^\mu = 0.73 \pm 0.14, \quad (3.66)$$

⁴See for the similar analyses before Moriond 2019 [53–61] and after Moriond 2019 [52, 62–68]

$$(III) \quad \text{Re } C_9^\mu = -\text{Re } C_{10}^\mu = -0.53 \pm 0.09. \quad (3.67)$$

For the two-dimensional analysis there are two patterns that have pulls larger than 6σ with respect to the SM prediction:

$$(IV) \quad \text{Re } C_9^\mu = -0.7 \pm 0.3, \quad \text{Re } C_{10}^\mu = 0.4 \pm 0.25, \quad (3.68)$$

$$(V) \quad \text{Re } C_9^\mu = -1.04 \pm 0.24, \quad \text{Re } C_9^{\prime\mu} = 0.48 \pm 0.30. \quad (3.69)$$

In our analysis, we attempt to fit $C_{9,10}^{(\prime)\ell=e,\mu}$ to one of these 5 patterns. The central values and uncertainties of the other coefficients are assumed to be 0.0 ± 0.1 . We also include imaginary parts, and try to fit them to 0.0 ± 0.1 . We remark here that non-zero imaginary parts are actually favored by the analysis of Ref. [61], however, we do not consider this possibility in the present paper.

C_9^μ is sizable in most of the above preferred patterns of Wilson coefficients. The Z' contribution to C_9^μ can be estimated as

$$C_9^\mu \sim -1.0 \times \left(\frac{0.3}{g'}\right) \left(\frac{1 \text{ TeV}}{v_\Phi}\right)^2 \left(\frac{s_{\mu_L}^2 + s_{\mu_R}^2}{1.0}\right) \left(\frac{[\hat{g}_{d_L}^{Z'}]_{23}}{0.001}\right), \quad (3.70)$$

where we note that $(s_{\mu_L}^2 + s_{\mu_R}^2) \sim 1$ is required by a successful explanation of Δa_μ . Therefore, the $b \rightarrow s\ell^+\ell^-$ anomalies can be explained with small, $\mathcal{O}(10^{-3})$, couplings of the SM quarks to the Z' boson.

The Wilson coefficients with $\ell = \tau$ contribute to the semi-leptonic decays $B_s \rightarrow K^{(*)}\tau\bar{\tau}$ and $B_s \rightarrow \phi\tau\bar{\tau}$. Branching fractions for these decays as a function of the Wilson coefficients are calculated in Ref. [69].

3.3.2 Neutral Meson Mixing

The neutral bosons, Z' , χ and σ , give contributions to neutral meson mixing. We neglect contributions from the Z boson and the Higgs boson, since the flavor violating couplings are expected to be small, as discussed above and shown in Appendix B. We study $K-\bar{K}$, $B_d-\bar{B}_d$, $B_s-\bar{B}_s$ and $D-\bar{D}$ mixing [70–75].

The relevant effective Hamiltonian is given by

$$\mathcal{H}_{\text{eff}}^{\Delta F=2} = \sum_{i,a} C_i^a Q_i^a, \quad (3.71)$$

where $(i, a) = (1, \text{VLL}), (1, \text{VRR}), (1, \text{LR}), (2, \text{LR}), (1, \text{SLL}), (2, \text{SLL}), (1, \text{SRR}), (2, \text{SRR})$. The four-fermi operators are defined as

$$Q_1^{\text{VLL}} = (\bar{F}^\alpha \gamma_\mu P_L f^\alpha) (\bar{F}^\beta \gamma^\mu P_L f^\beta), \quad Q_1^{\text{VRR}} = (\bar{F}^\alpha \gamma_\mu P_R f^\alpha) (\bar{F}^\beta \gamma^\mu P_R f^\beta), \quad (3.72)$$

$$Q_1^{\text{LR}} = (\bar{F}^\alpha \gamma_\mu P_L f^\alpha) (\bar{F}^\beta \gamma^\mu P_R f^\beta), \quad Q_2^{\text{LR}} = (\bar{F}^\alpha P_L f^\alpha) (\bar{F}^\beta P_R f^\beta), \quad (3.73)$$

$$Q_1^{\text{SLL}} = (\bar{F}^\alpha P_L f^\alpha) (\bar{F}^\beta P_L f^\beta), \quad Q_1^{\text{SRR}} = (\bar{F}^\alpha P_R f^\alpha) (\bar{F}^\beta P_R f^\beta), \quad (3.74)$$

$$Q_2^{\text{SLL}} = (\bar{F}^\alpha \sigma_{\mu\nu} P_L f^\alpha) (\bar{F}^\beta \sigma^{\mu\nu} P_L f^\beta), \quad Q_2^{\text{SRR}} = (\bar{F}^\alpha \sigma_{\mu\nu} P_R f^\alpha) (\bar{F}^\beta \sigma^{\mu\nu} P_R f^\beta), \quad (3.75)$$

where α, β are the color indices and $\sigma_{\mu\nu} = [\gamma_\mu, \gamma_\nu]/2$. Here, $(F, f) = (s, d), (b, d), (b, s), (c, u)$ for $K-\bar{K}, B_d-\bar{B}_d, B_s-\bar{B}_s$ and $D-\bar{D}$ mixing, respectively.

The Wilson coefficients including $\mathcal{O}(\alpha_s)$ corrections are given by [76]

$$C_1^{\text{VLL}}(\mu) = \left[1 + \frac{\alpha_s}{4\pi} \left(-2 \log \frac{m_{Z'}^2}{\mu^2} + \frac{11}{3} \right) \right] \frac{g_L^{Z'} g_L^{Z'}}{2m_{Z'}^2}, \quad (3.76)$$

$$C_1^{\text{LR}}(\mu) = \left[1 + \frac{\alpha_s}{4\pi} \left(-\log \frac{m_{Z'}^2}{\mu^2} - \frac{1}{6} \right) \right] \frac{g_L^{Z'} g_R^{Z'}}{m_{Z'}^2} - \left(-\frac{3\alpha_s}{2 \cdot 4\pi} \right) \sum_{S=\chi, \sigma} \frac{y_L^S y_R^S}{2m_S^2}, \quad (3.77)$$

$$C_2^{\text{LR}}(\mu) = \frac{\alpha_s}{4\pi} \left(-6 \log \frac{m_{Z'}^2}{\mu^2} - 1 \right) \frac{g_L^{Z'} g_R^{Z'}}{m_{Z'}^2} - \left(1 - \frac{\alpha_s}{4\pi} \right) \sum_{S=\chi, \sigma} \frac{y_L^S y_R^S}{2m_S^2}, \quad (3.78)$$

$$C_1^{\text{SLL}}(\mu) = - \sum_{S=\chi, \sigma} \left[1 + \frac{\alpha_s}{4\pi} \left(-3 \log \frac{m_S^2}{\mu^2} + \frac{9}{2} \right) \right] \frac{y_L^S y_L^S}{4m_S^2}, \quad (3.79)$$

$$C_2^{\text{SLL}}(\mu) = - \sum_{S=\chi, \sigma} \frac{\alpha_s}{4\pi} \left(-\frac{1}{12} \log \frac{m_S^2}{\mu^2} + \frac{1}{8} \right) \frac{y_L^S y_L^S}{4m_S^2}, \quad (3.80)$$

where μ is the $\overline{\text{MS}}$ -scheme renormalization scale. The gauge couplings $g_{L,R}^{Z'}$ and Yukawa couplings $y_{L,R}^S$ are given by

$$g_L^{Z'} = [\hat{g}_{dL}^{Z'}]_{ij}, \quad g_R^{Z'} = [\hat{g}_{dR}^{Z'}]_{ij}, \quad y_L^S = [\hat{Y}_d^S]_{ij}, \quad y_R^S = [\hat{Y}_d^S]_{ji}^*. \quad (3.81)$$

where the flavor indices are $(i, j) = (2, 1), (3, 1), (3, 2)$ for $K-\bar{K}, B_d-\bar{B}_d$, or $B_s-\bar{B}_s$ mixing, respectively. For $D-\bar{D}$ mixing,

$$g_L^{Z'} = [\hat{g}_{uL}^{Z'}]_{21}, \quad g_R^{Z'} = [\hat{g}_{uR}^{Z'}]_{21}, \quad y_L^S = [\hat{Y}_u^S]_{21}, \quad y_R^S = [\hat{Y}_u^S]_{12}^*. \quad (3.82)$$

The right-right Wilson coefficients ($C_1^{\text{VRR}}, C_1^{\text{SRR}}, C_2^{\text{SRR}}$) are obtained by formally replacing $L \rightarrow R$ in the above expressions. The off-diagonal mixing matrix element in the respective meson's mass matrix is given by

$$(M_{12}(M))^* = (M_{12}^{\text{SM}}(M))^* + \frac{1}{2m_M} \sum_{i,a} C_i^a \langle \bar{M} | Q_i^a | M \rangle, \quad \text{for } M = K, B_d, B_s, D. \quad (3.83)$$

Here, m_M is the mass of the meson M . Values of the operators

$$O_i^a := \langle \bar{M} | Q_i^a(\mu_B) | M \rangle / (2m_M) \quad (3.84)$$

at $\mu_B = 1$ TeV according to our own evaluation are listed in Table 9. For this we have used input values of meson masses, decay constants and quark masses which are listed in Table 10. Values of hadronic matrix elements are taken from the results of the respective lattice collaborations. We refer to Ref. [77] for hadronic matrix elements of $K-\bar{K}$ and $f_{B_q}^2 \hat{B}_{B_q}$. Those for $f_{B_q}^2 B_{B_q}^{(2-5)}$ and $B_D^{(1-5)}$ are taken from Refs. [78, 79] and Ref. [80],

Table 9: Numerical values of the operators $O_i^a := \langle \bar{M} | Q_i^a | M \rangle / (2m_M)$ at $\mu_B = 1$ TeV. The corresponding right-right operators have the same values as the LL operators.

	$O_1^{VLL}(\mu_B)$	$O_1^{LR}(\mu_B)$	$O_2^{LR}(\mu_B)$	$O_1^{SLL}(\mu_B)$	$O_2^{SLL}(\mu_B)$
$K-\bar{K}$	0.00159	-0.159	0.261	-0.0761	-0.132
$B_d-\bar{B}_d$	0.0465	-0.186	0.241	-0.0909	-0.167
$B_s-\bar{B}_s$	0.0701	-0.264	0.338	-0.136	-0.252
$D-\bar{D}$	0.0162	-0.157	0.227	-0.0845	-0.152

respectively. The QCD running between the respective lattice scales and $\mu = 1$ TeV has been calculated based on the anomalous dimensions shown in Ref. [81].

SM contributions to $K-\bar{K}$, $B_q-\bar{B}_q$ ($q = d, s$) mixing are given by

$$(M_{12}^{\text{SM}}(K))^* = \frac{G_F^2}{12\pi^2} m_W^2 m_K f_K^2 \hat{B}_K \times \left[(\lambda_c^K)^2 S_0(x_c) \eta_1 + (\lambda_t^K)^2 S_0(x_t) \eta_2 + 2\lambda_c^K \lambda_t^K S_0(x_c, x_t) \eta_3 \right], \quad (3.85)$$

$$(M_{12}^{\text{SM}}(B_q))^* = \frac{G_F^2}{12\pi^2} m_W^2 (\lambda_t^{B_q})^2 S_0(x_t) \eta_B m_{B_q} f_{B_q}^2 \hat{B}_{B_q}, \quad (3.86)$$

with $\lambda_q^K := V_{qs}^* V_{qd}$, $\lambda_t^{B_q} := V_{tb}^* V_{tq}$, as well as $x_t := m_t^2/m_W^2$ and $x_c := m_c^2/m_W^2$. Here, V is the 3×3 CKM matrix of the SM families. The Inami-Lim functions are given by

$$S_0(x) = \frac{4x - 11x^2 + x^3}{4(1-x)^2} - \frac{3x^3 \log x}{2(1-x)^3}, \quad (3.87)$$

$$S_0(x_c, x_t) \simeq x_c \left[\log \frac{x_t}{x_c} - \frac{3x_t}{4(1-x_t)} - \frac{3x_t^2 \log x_t}{4(1-x_t)^2} \right]. \quad (3.88)$$

Short distance corrections are quantified by $\eta_{1,2,3}$ and η_B . Values for all relevant factors and their respective references are listed in Table 10. The relevant observables are defined as

$$\Delta M_K = 2 \operatorname{Re}(M_{12}(K)), \quad \epsilon_K = \frac{\kappa_\epsilon e^{i\phi_\epsilon}}{\sqrt{2} (\Delta M_K)_{\text{exp}}} \operatorname{Im}(M_{12}(K)), \quad (3.89)$$

$$\Delta M_d = 2 |M_{12}(B_d)|, \quad S_{\psi K_s} = \sin(\operatorname{Arg}(M_{12}(B_d))), \quad (3.90)$$

$$\Delta M_s = 2 |M_{12}(B_s)|, \quad S_{\psi\phi} = -\sin(\operatorname{Arg}(M_{12}(B_s))), \quad (3.91)$$

$$x_D = \left| \frac{2M_{12}(D)}{\Gamma_D} \right|. \quad (3.92)$$

Values of κ_ϵ and ϕ_ϵ are stated in Table 10. $(\Delta M_K)_{\text{exp}}$ is the experimentally determined value of the Kaon mass splitting and Γ_D is the experimentally determined decay width of the D_0 meson; both are taken from the PDG [25].

Table 10: Values of constants used in our numerical analysis.

m_K [25]	497.611 ± 0.013 MeV	f_K [82]	156.3 ± 0.9 MeV
\hat{B}_K [77]	0.733 ± 0.040	η_1 [83]	1.87 ± 0.76
η_2 [84]	0.5765 ± 0.0065	η_3 [85]	0.496 ± 0.047
$m_s(2 \text{ GeV})$ [25]	93.8 ± 2.4 MeV	$m_d(2 \text{ GeV})$ [25]	4.70 ± 0.20 MeV
κ_ϵ [86, 87]	0.94 ± 0.02	ϕ_ϵ [86, 87]	$(43.51 \pm 0.05)^\circ$
m_{B_d} [25]	5.27963 ± 0.00015 GeV	m_{B_s} [25]	5.36689 ± 0.00019 GeV
$f_{B_d} \sqrt{\hat{B}_{B_d}}$ [77]	0.225 ± 0.009 GeV	$f_{B_s} \sqrt{\hat{B}_{B_s}}$ [77]	0.274 ± 0.008 GeV
η_B [84, 88]	0.55 ± 0.01	$m_b(m_b)$ [25]	4.18 ± 0.03 GeV
$m_c(m_c)$ [25]	1.28 ± 0.025 GeV	$m_t(m_t)$ [79, 89]	163.53 ± 0.83 GeV
m_D [25]	1.86483 ± 0.00005 GeV	f_D [77]	212.0 ± 0.7 MeV
τ_D [25]	0.4101 ± 0.0015 ps	$m_c(3 \text{ GeV})$ [77]	0.988 ± 0.007 GeV
$m_u(2 \text{ GeV})$ [25]	2.15 ± 0.15 MeV		

The experiments measure the mass differences and ϵ_K precisely. On the other hand, there are large theoretical uncertainties to estimate the SM contributions for these observables originating from the determination of the bag parameter, QCD factors and the CKM matrix elements. For K - \bar{K} mixing, uncertainties come from $\eta_1, f_K, \hat{B}_K, \kappa_\epsilon$ and the CKM elements. The uncertainty of ΔM_K is dominated by the NLO factor η_1 , while for ϵ_K it is dominated by the CKM elements. With the Wolfenstein parametrization, ϵ_K is approximately proportional to A^4 . Hence, we include the uncertainty from $A = 0.836 \pm 0.015$ [25] as the CKM uncertainty together with those from $f_K^2 \hat{B}_K$ and κ_ϵ . The relative uncertainties are estimated as 41% and 9.3% for ΔM_K and ϵ_K , respectively.

For the mass differences $\Delta M_{B_q} \equiv \Delta M_q$, we include the uncertainties originating from $\eta_B, f_{B_q}^2 \hat{B}_{B_q}$ and the absolute values of the CKM matrix elements. Note that unlike the analyses in Refs [75, 90], we cannot reduce the uncertainties by assuming exact unitarity of the CKM matrix, because the unitarity of CKM matrix is not guaranteed in our model. Altogether, the relative uncertainties are estimated as 16% and 14% for ΔM_d and ΔM_s , respectively. For the CP asymmetry parameters $S_{\psi K_S}$ and $S_{\psi\phi}$, we require our model to fit them within their experimental uncertainties.

For D - \bar{D} mixing there is a large theoretical uncertainty from long-distance effects. The observed value is $x_D = 0.32$ (14)% [44]. We simply require that the new physics contribution to x_D should be less or equal than the size of the observed value, that is $|\Delta^{\text{NP}} x_D| := |2M_{12}^{\text{NP}}(D)/\Gamma_D| = 0.0 \pm 0.5\%$.

It is convenient to express the size of new physics contributions relative to the SM,

$$R_{\Delta M_K} := \frac{M_{12}(K) - M_{12}^{\text{SM}}(K)}{\text{Re}(M_{12}^{\text{SM}}(K))}, \quad R_{\epsilon_K} := \frac{M_{12}(K) - M_{12}^{\text{SM}}(K)}{\text{Im}(M_{12}^{\text{SM}}(K))}, \quad (3.93)$$

$$R_{\Delta M_d} := \frac{M_{12}(B_d) - M_{12}^{\text{SM}}(B_d)}{|M_{12}^{\text{SM}}(B_d)|}, \quad R_{\Delta M_s} := \frac{M_{12}(B_s) - M_{12}^{\text{SM}}(B_s)}{|M_{12}^{\text{SM}}(B_s)|}, \quad (3.94)$$

and these are given by

$$R_{\Delta M_K} \times 10^{-3} \approx 0.053 \cdot (r_{VLL}^K + r_{VRR}^K) - 10.6 \cdot r_{VLR}^K \quad (3.95)$$

$$+ \sum_S (1.27 (r_{SLL}^K + r_{SRR}^K) - 8.70 \cdot r_{SLR}^K),$$

$$R_{\epsilon_K} \times 10^{-3} \approx 6.94 \cdot (r_{VLL}^K + r_{VRR}^K) - 1380 \cdot r_{VLR}^K \quad (3.96)$$

$$+ \sum_S (166 \cdot (r_{SLL}^K + r_{SRR}^K) - 1140 \cdot r_{SLR}^K),$$

$$R_{\Delta M_d} \approx 11.5 \cdot (r_{VLL}^{B_d} + r_{VRR}^{B_d}) - 91.5 \cdot r_{VLR}^{B_d} \quad (3.97)$$

$$+ \sum_S (11.2 (r_{SLL}^{B_d} + r_{SRR}^{B_d}) - 59.2 \cdot r_{SLR}^{B_d}),$$

$$R_{\Delta M_s} \approx 0.538 (r_{VLL}^{B_s} + r_{VRR}^{B_s}) - 4.05 \cdot r_{VLR}^{B_s} \quad (3.98)$$

$$+ \sum_S (0.522 (r_{SLL}^{B_s} + r_{SRR}^{B_s}) - 2.59 \cdot r_{SLR}^{B_s}).$$

Here,

$$r_{VXY}^M := \left[\hat{g}_{dX}^{Z'} \right]_{Ff} \left[\hat{g}_{dY}^{Z'} \right]_{Ff} \left(\frac{10^5 \text{ GeV}}{m_{Z'}} \right)^2, \quad (3.99)$$

$$r_{SXY}^M := \left[\hat{Y}_{dX}^S \right]_{Ff} \left[\hat{Y}_{dY}^S \right]_{Ff} \left(\frac{10^5 \text{ GeV}}{m_S} \right)^2, \quad (3.100)$$

with $X, Y = L, R$ and $(F, f) = (2, 1), (3, 1), (3, 2)$ for $M = K, B_d, B_s$, respectively, and we identify $\hat{Y}_{dL} \equiv \hat{Y}_d$ and $\hat{Y}_{dR} \equiv \hat{Y}_d^\dagger$ (and similarly for the up sector). The numerical coefficients are obtained by using the values listed in Table 9 and neglecting the $\mathcal{O}(\alpha_s)$ corrections in Eqs. (3.76)-(3.80). The SM contributions are calculated with the unitary CKM matrix fitted to the experimental values [25]. The coefficients for the lighter mesons tend to be larger because the SM contributions are smaller. Left-right contributions are enhanced, especially r_{VLR}^K , by the large hadronic matrix element itself and the enhancement by the running effects [81], see Table 9.

Similarly, $\Delta^{\text{NP}} x_D$ is given by

$$\Delta^{\text{NP}} x_D = |1.01 (r_{VLL}^D + r_{VRR}^D) - 19.5 r_{VLR}^D + 2.63 (r_{SLL}^D + r_{SRR}^D) - 14.1 r_{SLR}^D|, \quad (3.101)$$

with

$$r_{VXY}^D := \left[\hat{g}_{uX}^{Z'} \right]_{21} \left[\hat{g}_{uY}^{Z'} \right]_{21} \left(\frac{10^5 \text{ GeV}}{m_{Z'}} \right)^2, \quad (3.102)$$

$$r_{SXY}^D := \left[\hat{Y}_{uX}^S \right]_{21} \left[\hat{Y}_{uY}^S \right]_{21} \left(\frac{10^5 \text{ GeV}}{m_S} \right)^2. \quad (3.103)$$

We now comment on the box-diagram contributions involving W bosons and up-type quarks which are the dominant contribution in the SM. In general, the unitarity of the CKM matrix is violated by the mixing with the $SU(2)_L$ singlet VL quark. The GIM mechanism may, in principle, become invalid in our model. The mass independent contributions is proportional to a sum over the five internal quarks,

$$\sum_{A=1}^5 \left[\hat{V}_{\text{CKM}}^\dagger \right]_{iA} \left[\hat{V}_{\text{CKM}} \right]_{Aj} = \left[(U_L^d)^\dagger P_{\bar{5}} U_L^u \cdot (U_L^u)^\dagger P_{\bar{5}} U_L^d \right]_{ij} = \left[(U_L^d)^\dagger P_{\bar{5}} U_L^d \right]_{ij}. \quad (3.104)$$

This has the same structure as the weak-isospin part of the Z boson couplings. Using the analytical expressions of Appendix B, the size of flavor violating contribution is estimated as

$$\begin{aligned} \left[(U_L^d)^\dagger P_{\bar{5}} U_L^d \right]_{ij} - \delta_{ij} &\sim \epsilon_{D_i} \epsilon_{D_j} \frac{m_{d_i} m_{d_j}}{M_{D_{\text{VL}}}^2} \\ &\lesssim 1.6 \times 10^{-11} \left(\frac{\sqrt{\epsilon_{D_i} \epsilon_{D_j}}}{10^{-2}} \right)^2 \left(\frac{\sqrt{m_{d_i} m_{d_j}}}{0.6 \text{ GeV}} \right)^2 \left(\frac{1.5 \text{ TeV}}{M_{D_{\text{VL}}}} \right)^2, \end{aligned} \quad (3.105)$$

where ϵ_{D_i} is a mixing angle between the singlet VL quark D_R and the SM down quark d_i , and $M_{D_{\text{VL}}}$ is a typical VL down quark mass. In addition, there can be an, in principle, important contribution which is enhanced by the heavy VL quark mass. Using Eq. (B.65), the dominant contribution is estimated as

$$\begin{aligned} \sum_{b=4,5} \left(\left[\hat{V}_{\text{CKM}}^\dagger \right]_{ib} \left[\hat{V}_{\text{CKM}} \right]_{bj} \right)^2 S_0 \left(\frac{m_{ub}^2}{m_W^2} \right) &\sim \frac{M_{U_R}^2}{4m_W^2} \left(\epsilon_{U_3}^2 \frac{m_t^2}{M_{U_R}^2} V_{ti}^* V_{tj} \right)^2 \\ &\sim 2.5 \times 10^{-9} \times \left(\frac{\epsilon_{U_3}}{0.1} \right)^4 \left(\frac{V_{ti}^* V_{tj}}{0.04} \right)^2 \left(\frac{1.5 \text{ TeV}}{M_{U_R}} \right)^2, \end{aligned} \quad (3.106)$$

where ϵ_{U_i} is defined in the same way as ϵ_{D_i} . For B_s - \bar{B}_s mixing, $(i, j) = (3, 2)$, this should be compared with the top loop contribution $(\lambda_t^{B_s})^2 S_0(x_t) \sim 0.004$ and is, thus, much smaller than the SM contribution. The same suppression happens for the other meson mixing. Thus, the violation of the GIM mechanism is extremely small.

3.3.3 $B_{d,s} \rightarrow \mu^+ \mu^-$

The new bosons, in general, induce new physics contributions to $B_q \rightarrow \mu^+ \mu^-$ ($q = d, s$). We refer to Ref. [48]. The relevant effective interactions are

$$-\mathcal{L}_{B_q \rightarrow \mu\mu} = C_{AA}^V (\bar{q} \gamma^\mu \gamma_5 b) (\bar{\mu} \gamma_\mu \gamma_5 \mu) + C_{PS}^S (\bar{q} \gamma_5 b) (\bar{\mu} \mu) + C_{PP}^S (\bar{q} \gamma_5 b) (\bar{\mu} \gamma_5 \mu). \quad (3.107)$$

In this model, the coefficients are given by

$$C_{AA}^V = C_{\text{SM}}(B_q) + \frac{1}{m_{Z'}^2} \left([\hat{g}_{eR}^{Z'}]_{22} - [\hat{g}_{eL}^{Z'}]_{22} \right) \left([\hat{g}_{dL}^{Z'}]_{i3} - [\hat{g}_{dR}^{Z'}]_{i3} \right), \quad (3.108)$$

$$C_{PS}^S = \sum_{S=\chi,\sigma} \frac{1}{m_S^2} \cdot \text{Re} \left([\hat{\lambda}_e^S]_{22} \right) \left([\hat{\lambda}_d^S]_{i3} - [\hat{\lambda}_d^S]_{3i}^* \right), \quad (3.109)$$

$$C_{PP}^S = - \sum_{S=\chi,\sigma} \frac{i}{m_S^2} \cdot \text{Im} \left([\hat{\lambda}_e^S]_{22} \right) \left([\hat{\lambda}_d^S]_{i3} - [\hat{\lambda}_d^S]_{3i}^* \right), \quad (3.110)$$

where $i = 1, 2$ for $q = d, s$, respectively. The SM contribution in C_{AA}^V is given by

$$C_{\text{SM}}(B_q) = 4 \frac{G_F}{\sqrt{2}} \frac{\alpha}{2\pi \sin^2 \theta_W} V_{tq}^* V_{tb} \eta_Y Y_0(x_t), \quad (3.111)$$

where $\eta_Y = 1.012$ quantifies QCD corrections [91, 92] and the loop function is given by

$$Y_0(x_t) = \frac{x_t}{8} \left[\frac{x_t - 4}{x_t - 1} + \frac{3x_t}{(x_t - 1)^2} \log x_t \right], \quad x_t = \frac{m_t^2}{m_W^2}. \quad (3.112)$$

The decay width of $B_q \rightarrow \mu^+ \mu^-$ is proportional to

$$|P_q|^2 + |S_q|^2 := \left| \frac{C_{AA}^V}{C_{\text{SM}}(B_q)} - \frac{m_{B_q}^2}{2m_\mu(m_q + m_b)} \frac{C_{PP}^S}{C_{\text{SM}}(B_q)} \right|^2 + \left| \sqrt{1 - \frac{4m_\mu^2}{m_{B_q}^2}} \frac{m_{B_q}^2}{2m_\mu(m_q + m_b)} \frac{C_{PS}^S}{C_{\text{SM}}(B_q)} \right|^2. \quad (3.113)$$

We define the ratios of branching fractions of our model to the SM,

$$R_{B_d \rightarrow \mu\mu}^{\text{th}} := \frac{\text{BR}(B_d \rightarrow \mu^+ \mu^-)}{\text{BR}(B_d \rightarrow \mu^+ \mu^-)_{\text{SM}}} = |P_d|^2 + |S_d|^2, \quad (3.114)$$

$$R_{B_s \rightarrow \mu\mu}^{\text{th}} := \frac{\overline{\text{BR}}(B_s \rightarrow \mu^+ \mu^-)}{\overline{\text{BR}}(B_s \rightarrow \mu^+ \mu^-)_{\text{SM}}} = \frac{1 + A_{\Delta\Gamma} y_s}{1 + y_s} (|P_s|^2 + |S_s|^2). \quad (3.115)$$

Mind the bars: In the B_s - \overline{B}_s system, the measured width difference between light and heavy mass eigenstates, $y_s := \Delta\Gamma_{B_s} / (2\Gamma_{B_s}) = 0.065 \pm 0.005$ [44], is not negligible [93, 94]. The experimentally determined value for the branching ratio, therefore, corresponds to the time-integrated value

$$\overline{\text{BR}}(B_s \rightarrow \mu^+ \mu^-) = \frac{1 + A_{\Delta\Gamma} y_s}{1 - y_s^2} \cdot \text{BR}(B_s \rightarrow \mu^+ \mu^-), \quad (3.116)$$

where the mass-eigenstate rate asymmetry $A_{\Delta\Gamma}$ is given by [95, 96]

$$A_{\Delta\Gamma} = \frac{|P_s|^2 \cos(2\phi_P - \phi_s^{\text{NP}}) - |S_s|^2 \cos(2\phi_S - \phi_s^{\text{NP}})}{|S_s|^2 + |P_s|^2}. \quad (3.117)$$

Here, $P_s = |P_s| e^{i\phi_P}$, $S_s = |S_s| e^{i\phi_S}$ and ϕ_s^{NP} relates to $S_{\psi\phi}$, defined in Eq. (3.89), as

$$S_{\psi\phi} = \sin(2\beta_s - \phi_s^{\text{NP}}), \quad \text{where} \quad V_{ts} = -|V_{ts}| e^{i\beta_s}, \quad (3.118)$$

in the standard phase convention of the CKM matrix. $A_{\Delta\Gamma} = 1$ in the SM.

The SM predictions are [47, 48],

$$\text{BR}(B_d \rightarrow \mu^+ \mu^-)_{\text{SM}} = (1.06 \pm 0.09) \times 10^{-10}, \quad (3.119)$$

$$\overline{\text{BR}}(B_s \rightarrow \mu^+ \mu^-)_{\text{SM}} = (3.60 \pm 0.18) \times 10^{-9}. \quad (3.120)$$

The experimental values are [25],

$$\text{BR}(B_d \rightarrow \mu^+ \mu^-)_{\text{exp}} = (1.6 \pm 1.5) \times 10^{-10}, \quad (3.121)$$

$$\overline{\text{BR}}(B_s \rightarrow \mu^+ \mu^-)_{\text{exp}} = (2.7 \pm 0.55) \times 10^{-9}. \quad (3.122)$$

Altogether, the values of the ratios are given by

$$R_{B_d \rightarrow \mu\mu}^{\text{exp}} := \frac{\text{BR}(B_d \rightarrow \mu^+ \mu^-)_{\text{exp}}}{\text{BR}(B_d \rightarrow \mu^+ \mu^-)_{\text{SM}}} = 1.5 \pm 1.4, \quad (3.123)$$

$$R_{B_s \rightarrow \mu\mu}^{\text{exp}} := \frac{\overline{\text{BR}}(B_s \rightarrow \mu^+ \mu^-)_{\text{exp}}}{\overline{\text{BR}}(B_s \rightarrow \mu^+ \mu^-)_{\text{SM}}} = 0.75 \pm 0.16. \quad (3.124)$$

The current data for $\overline{\text{BR}}(B_s \rightarrow \mu^+ \mu^-)$ has a slight tension with the SM prediction. We note that $\text{BR}(B_s \rightarrow \mu^+ \mu^-)$ is included in the analysis of Ref. [52], where due to the tension a larger C_{10}^μ is favored. Nonetheless, we additionally include $\text{BR}(B_s \rightarrow \mu^+ \mu^-)$ individually in our χ^2 analysis in order to take into account scalar contributions which were not included in [52].

3.3.4 $B \rightarrow K^{(*)} \nu \bar{\nu}$

The Z' boson typically affects $B \rightarrow K^{(*)} \nu \bar{\nu}$. We consider the observables given by [97–99],

$$R_K^{\nu\bar{\nu}} := \frac{1}{3} \sum_{i,j=1,2,3} [1 - 2\eta_{ij}] \epsilon_{ij}^2, \quad R_{K^*}^{\nu\bar{\nu}} := \frac{1}{3} \sum_{i,j=1,2,3} [1 + 1.31\eta_{ij}] \epsilon_{ij}^2, \quad (3.125)$$

where

$$\epsilon_{ij}^2 := \frac{|X_L^{ij}(B_s)|^2 + |X_R^{ij}(B_s)|^2}{|\eta_X X_0(x_t)|^2}, \quad \eta_{ij} := -\frac{\text{Re}(X_L^{ij}(B_s) X_R^{ij*}(B_s))}{|X_L^{ij}(B_s)|^2 + |X_R^{ij}(B_s)|^2}. \quad (3.126)$$

Here, $i, j = 1, 2, 3$ run over the three neutrino flavor. In this model, X_L^{ij}, X_R^{ij} are given by

$$X_L^{ij}(B_s) = \eta_X X_0(x_t) \delta_{ij} + \frac{[\hat{g}_{\nu L}^{Z'}]_{ij}}{g_{\text{SM}}^2 m_{Z'}^2} \frac{[\hat{g}_{dL}^{Z'}]_{23}}{V_{ts}^* V_{tb}}, \quad X_R^{ij}(B_s) = \frac{[\hat{g}_{\nu L}^{Z'}]_{ij}}{g_{\text{SM}}^2 m_{Z'}^2} \frac{[\hat{g}_{dR}^{Z'}]_{23}}{V_{ts}^* V_{tb}}. \quad (3.127)$$

The first term in $X_L^{ij}(B_s)$ is the SM contribution. The loop function is defined as

$$X_0(x_t) = \frac{x_t}{8} \left[\frac{x_t + 2}{x_t - 1} + \frac{3x_t - 6}{(x_t - 1)^2} \log x_t \right], \quad x_t = \frac{m_t^2}{m_W^2}. \quad (3.128)$$

$\eta_X = 0.994$ is the QCD factor [91, 92]. The experimental limits are [45, 46],

$$R_K^{\nu\bar{\nu}} < 4.3, \quad R_{K^*}^{\nu\bar{\nu}} < 4.4 \quad (3.129)$$

at 90% C.L [97].

3.3.5 Top Quark Decays

The mixing with the VL quarks may affect top quark decays. We study the dominant top quark decay $t \rightarrow W^+ b$ and the flavor violating decays $t \rightarrow Zq$ and $t \rightarrow hq$ ($q = u, c$). The partial decay width and the branching fractions for the flavor violating decays are,

$$\Gamma(t \rightarrow W^+ b) = \frac{m_t}{32\pi} \lambda(y_b^t, z_W^t) \left[\left(|\hat{g}_{uL}^W]_{33}|^2 + |\hat{g}_{uR}^W]_{33}|^2 \right) \times \left(\frac{(1 - y_b^t)^2}{z_W^t} + 1 + y_b^t - 2z_W^t \right) - 3\sqrt{y_b^t} \operatorname{Re} \left([\hat{g}_{uL}^W]_{33} \cdot [\hat{g}_{uR}^W]_{33} \right) \right], \quad (3.130)$$

$$\operatorname{BR}(t \rightarrow Zq_i) = \frac{m_t}{32\pi\Gamma_t} \frac{1 + 2z_Z^t}{z_Z^t} (1 - z_Z^t)^2 \left(|\hat{g}_{uL}^Z]_{i3}|^2 + |\hat{g}_{uR}^Z]_{i3}|^2 \right), \quad (3.131)$$

$$\operatorname{BR}(t \rightarrow hq_i) = \frac{m_t}{64\pi\Gamma_t} (1 - z_h^t)^2 \left(|\hat{Y}_u]_{i3}|^2 + |\hat{Y}_u]_{3i}|^2 \right), \quad (3.132)$$

where $x_B^t := m_B^2/m_t^2$ ($B = h, Z, W$) and $y_b^t := m_b^2/m_t^2$. Here, the light quark masses are neglected. $\Gamma(t \rightarrow W^+ b)$ is compared with the total decay width of the top quark. The other modes, CKM suppressed and flavor violating decays, are neglected to calculate the total decay width of top quark, i.e we use the approximation $\Gamma_t \approx \Gamma(t \rightarrow W^+ b)$. Uncertainties for the flavor violating decays are determined from the experimental upper limits [25].

3.4 Z' Physics

We now study potential signals of the Z' gauge boson at the LHC, in gauge kinetic mixing, and in neutrino trident production. In general, there are exclusion regions from all these observables. Note that we do not include these observables in our χ^2 analysis, but only check a posteriori whether the respective constraints are fulfilled.

3.4.1 Dimuon Signals at the LHC

In the present model, the Z' gauge boson should be lighter than about 800 GeV to explain Δa_μ . The most relevant Z' -related process at the LHC is resonant dimuon production,

$$pp \rightarrow Z' \rightarrow \mu^+ \mu^-. \quad (3.133)$$

Δa_μ requires sizable couplings to muons, while small couplings to the SM quarks are enough to explain $b \rightarrow s\ell^+\ell^-$ anomalies. Hence, the Z' boson will dominantly decay to muons and muon neutrinos, and its production cross section will be suppressed by the small couplings to the SM quarks. General LHC limits on Z' bosons responsible for $b \rightarrow s\ell^+\ell^-$ anomalies are studied in Refs. [100, 101]. Exclusion bounds are given in Ref. [102] based on 139 fb^{-1} of data. We have calculated the fiducial cross section, using the definition and cuts of Ref. [102], with `MadGraph5_2_6_5` [103] based on an `UFO` [104] model file generated with `FeynRules_2_3_32` [103, 105].

3.4.2 Gauge Kinetic Mixing

We assume that the gauge kinetic mixing between the $U(1)_Y$ and $U(1)'$ gauge boson is absent at tree-level. At the one-loop level mixing is unavoidable and the corresponding Z - Z' mixing parameter ϵ is estimated as

$$\epsilon \simeq \frac{g_Y g'}{6\pi^2} \log \left(\frac{m_E^2}{m_L^2} \frac{m_Q^2 m_D^2}{m_U^4} \right), \quad (3.134)$$

where $m_F \sim \lambda_V^F v_\phi$ for $F = E, L, Q, U, D$ and g_Y is the $U(1)_Y$ gauge coupling constant. Current experimental limits are summarized in Ref. [106]. Values of $\epsilon \sim 0.05$ are not excluded provided that the Z' is heavier than a few 100 GeV.

3.4.3 Neutrino Trident Production

The Z' contributes to muon-neutrino induced muon pair production off a nucleus $\nu_\mu N \rightarrow \nu_\mu \mu^+ \mu^- N$, the so-called neutrino trident process [6, 107–111]. The cross section for this process at the CCFR experiment is estimated as [111] (see also [112] for a complete SM computation)

$$R_{\text{CCFR}} := \frac{\sigma_{\text{CCFR}}}{\sigma_{\text{CCFR}}^{\text{SM}}} \simeq \frac{(1 + 4s_W^2 + \Delta g_{\mu\mu\mu\mu}^V)^2 + 1.13(1 - \Delta g_{\mu\mu\mu\mu}^A)^2}{(1 + 4s_W^2)^2 + 1.13}. \quad (3.135)$$

The experimentally observed rate is $\sigma_{\text{CCFR}}/\sigma_{\text{CCFR}}^{\text{SM}} = 0.82 \pm 0.28$ at 95% C.L. The relevant effective interactions are

$$\mathcal{H}_{\text{eff}} = \frac{G_F}{\sqrt{2}} \left[g_{\mu\mu\mu\mu}^V (\bar{\nu}_\mu \gamma_\alpha P_L \nu_\mu) (\bar{\mu} \gamma^\alpha \mu) + g_{\mu\mu\mu\mu}^A (\bar{\nu}_\mu \gamma_\beta P_L \nu_\mu) (\bar{\mu} \gamma^\beta \gamma_5 \mu) \right], \quad (3.136)$$

where the neutrinos are taken as flavor states. In our model, the coupling constants are given by

$$g_{\mu\mu\mu\mu}^V = 1 + 4s_W^2 + \Delta g_{\mu\mu\mu\mu}^V \quad \text{and} \quad g_{\mu\mu\mu\mu}^A = -1 + \Delta g_{\mu\mu\mu\mu}^A, \quad (3.137)$$

with Z' boson contributions given by

$$\Delta g_{\mu\mu\mu\mu}^{V,A} = \frac{\sqrt{2}}{G_F \cdot 2m_{Z'}^2} \left[\hat{g}_{e_L}^{Z'} \right]_{\nu_\mu \nu_\mu} \left(\left[\hat{g}_{e_R}^{Z'} \right]_{22} \pm \left[\hat{g}_{e_L}^{Z'} \right]_{22} \right). \quad (3.138)$$

Here, $[\hat{g}_{e_L}^{Z'}]_{\nu_\mu\nu_\mu}$ is given by

$$[\hat{g}_{e_L}^{Z'}]_{\nu_\mu\nu_\mu} = g' [U_{e_L}^\dagger Q'_{n_L} U_{e_L}]_{22}, \quad (3.139)$$

and we have used $s_W^2 = 0.23129$ specifically for this process as in Ref. [111]. This constraint is relevant only for light Z' 's and becomes unimportant for $m_{Z'} \gtrsim 200$ GeV.

4 Results

4.1 χ^2 Fitting

We search for parameters that can explain both Δa_μ and $b \rightarrow s\ell^+\ell^-$ anomalies consistently with the other observables. For this, we attempt to minimize the χ^2 function,

$$\chi^2(x) := \sum_I \frac{(y_I(x) - y_I^0)^2}{\sigma_I^2}, \quad (4.1)$$

where x is a parameter space point, $y_I(x)$ is the value of an observable I with central value y_I^0 and uncertainty σ_I . Altogether, we include 98 observables with central values and uncertainties listed in Tables 3, 6, 7 and 8. Values for $C_{9,10}^{(\prime)e,\mu}$ have been stated in Section 3.3.1. We use exact numerical evaluation to compute the observables, not the analytic expressions that we have only used to illustrate the general features of the model. In our analysis there are 65 free model parameters. Five of these are in the bosonic sector, namely

$$m_{Z'}, v_\phi, g', \lambda_\chi, \lambda_\sigma, \quad (4.2)$$

which are the Z' mass, the VEV of ϕ , the $U(1)'$ gauge coupling constant, and the effective quartic couplings of the scalars Φ and ϕ . All other parameters are Yukawa coupling constants appearing in Eqs. (2.2)-(2.5). Generally, we assume that the Yukawa coupling constants are real, except for the couplings $y_{13}^{u,d}, y_{31}^{u,d}$ which are taken to be complex in order to explain the complex phases in the CKM matrix. The Yukawa couplings involving the right-handed neutrinos with heavy Majorana masses, that is λ_i^N and y_{ij}^n , are not included in our χ^2 analysis as none of our 98 observables is sensitive to them. As discussed in Section 2.2.4, $g' < 0.35$ is imposed, such that the gauge coupling stays perturbative up to $\sim 10^{16}$ GeV. We restrict all Yukawa and effective quartic coupling constants to be smaller than unity and impose $v_\phi \leq 5.0$ TeV.

4.2 Best Fit Points

We find a landscape of good fit points in similar phenomenological regions. We will focus our discussion on the four best fit points A, B, C and D with $\chi^2 = 22.6, 25.0, 23.3$ and 23.8 (for $N_{\text{d.o.f.}} = 98 - 65 = 33$ degrees of freedom), respectively. All four best fit points

Table 11: Values of χ^2 , selected input parameters and observables for Z' physics at the best fit points A, B, C and D. The degree of freedom in our analysis is $N_{\text{obs}} - N_{\text{inp}} = 98 - 65 = 33$.

Parameters	Point A	Point B	Point C	Point D
χ^2	22.6	25.0	23.3	23.8
g'	0.250	0.340	0.323	0.349
(v_Φ, v_ϕ) [TeV]	(0.785, 4.08)	(1.11, 3.12)	(1.07, 4.98)	(1.54, 4.82)
$m_{Z'}$ [GeV]	277.6	535.3	486.7	758.7
$\sigma_{\text{fid}}(pp \rightarrow Z' \rightarrow \mu^+ \mu^-)$ [fb]	0.618	0.245	0.126	0.069
$\epsilon_{Z-Z'} \times 10^3$	-1.33	3.15	1.62	-0.365
R_{CCFR}	1.019	1.010	1.028	1.008

are selected from points with the charged VL lepton heavier than 250 GeV and the fiducial cross section $\sigma_{\text{fid}}(pp \rightarrow Z' \rightarrow \mu^+ \mu^-)$ smaller than the latest experimental limit. Point A is the global best fit point under these conditions. The point B is the best fit point of points with $m_{E_1} > 1.2$ TeV. This point has slightly larger χ^2 value than the other three best fit points (see Table 12), mainly because $R_{B_s \rightarrow \mu\mu}^{\text{th}} \sim 0.9$ due to the smaller $\text{Re}C_{10}^\mu$. The points C and D are the best fit points under the conditions $m_\chi > 750$ GeV and $m_{Z'} > 750$ GeV, respectively.

The values of selected input parameters and observables are listed in Tables 11 and 12. All input parameters are shown in Appendix C and complete lists of all observables at the best fit points are listed in Appendix D. Masses and predicted dominant decay modes of new particles are summarized in Tables 18, 19, 20 and 21. The decay widths are calculated based on the formulae in Appendix A.

4.3 Phenomenology

We now discuss some global features of our model. Figure 3 shows fit points with $\chi^2 < 33 = N_{\text{d.o.f.}}$. The red circles (green triangles) have $\chi^2 < 28$ (33). Points which are excluded by Z' physics, namely LHC searches and/or neutrino trident production, are denoted by red crosses (green pluses) with the same color coding as above. The Z - Z' mixing parameter ϵ is always less than or equal $\mathcal{O}(10^{-3})$ and, thus, much smaller than the experimental limit. All subsequent plots show *the same* model parameter points as Figure 3.

The blue solid (dashed) line in Figure 3 corresponds to $v_\Phi = 1.7$ (2.0) TeV. Consistent with our analytical analysis of Δa_μ in Section 3.1.1, c.f. especially Eq. (3.18), there is no point with $\chi^2 < 28$ (33) whenever $v_\Phi > 1.7$ (2.0) TeV. This results in an upper bound on the Z' mass: $m_{Z'} \lesssim 840$ GeV for $g' < 0.35$. We note that in Fig. 3 allowed and excluded points co-exist for similar values of $m_{Z'}$ and g' . This is because in this plane one does

Table 12: Values of selected observables at the best fit points A, B, C and D. The last column shows experimental central values and their uncertainties. The upper limits on the LFV decays are 90% C.L. limits.

Observables	Point A	Point B	Point C	Point D	Exp.
$\Delta a_\mu \times 10^9$	2.62	2.52	2.52	2.45	2.68 ± 0.76
$\text{BR}(\mu \rightarrow e\gamma) \times 10^{13}$	0.147	1.597	0.061	0.822	< 4.2
$\text{BR}(\tau \rightarrow \mu\gamma) \times 10^8$	3.34×10^{-4}	3.62×10^{-4}	3.27×10^{-6}	8.45×10^{-7}	< 4.4
$\text{BR}(\tau \rightarrow \mu\mu\mu) \times 10^8$	6.96×10^{-3}	4.77×10^{-4}	6.55×10^{-5}	4.36×10^{-7}	< 2.1
$\text{Re } C_9^\mu$	-0.548	-0.806	-0.838	-0.808	-0.7 ± 0.3
$\text{Re } C_{10}^\mu$	0.370	0.252	0.347	0.322	0.4 ± 0.2
$\Delta M_d [\text{ps}^{-1}]$	0.561	0.610	0.598	0.590	0.506 ± 0.081
$\Delta M_s [\text{ps}^{-1}]$	19.6	19.8	19.4	20.0	17.76 ± 2.5
$S_{\psi K_s}$	0.697	0.696	0.692	0.695	0.695 ± 0.019
$S_{\psi\phi}$	0.0366	0.0374	0.0373	0.0379	0.021 ± 0.031
$R_{B_s \rightarrow \mu\mu}^{\text{th}}$	0.841	0.890	0.850	0.861	0.75 ± 0.16

not resolve the different textures for Yukawa couplings, which can lead to vastly different phenomenology of Z' physics. For example, ΔC_9^μ requires $[\hat{g}_{d_L}^{Z'}]_{23} \sim 0.001$, but this would not exclude $\mathcal{O}(1)$ values of $[\hat{g}_{d_L}^{Z'}]_{22}$ or $[\hat{g}_{d_L}^{Z'}]_{33}$ which have dramatic consequences for Z' direct production as we will discuss now.

4.3.1 Z' Physics

Figure 4 shows the good fit points in the $(m_{Z'}, \sigma_{\text{fid}}(pp \rightarrow Z' \rightarrow \mu\mu))$ plane, where we use the definition and cuts for the fiducial cross section σ_{fid} of Ref. [102]. The blue solid line is the 95% C.L. limit from the ATLAS analysis [102]. Since the limit is given only for $m_{Z'} > 250$ GeV, we use an extrapolation down to lower masses shown by the dashed blue line. As a rough estimate for the sensitivity to be expected at the HL-LHC we can scale the limit on the cross section by $\sqrt{139/3000}$, the square root of the expected ratio of integrated luminosities. This sensitivity is shown as a purple, dot-dashed line in Fig. 4.

A small flavor violating coupling to Z' , $[\hat{g}_{d_L}^{Z'}]_{23} \sim 10^{-3}$ is enough to explain the $b \rightarrow s\ell^+\ell^-$ anomalies. A diagonal coupling of Z' to bottom quarks or to the light quarks could be sizable without changing other flavor violating observables. However, fitting the observed CKM matrix sets limits on the size of such couplings. Therefore, a good fit prefers small diagonal couplings to quarks. In agreement with that, our best fit points predict fiducial cross section roughly about an order of magnitude smaller than the current limits. We stress that the LHC limits were not part of the fit and only checked subsequently on good fit points.

Since Δa_μ requires sizable Z' coupling to muons, a sizable muon neutrino coupling

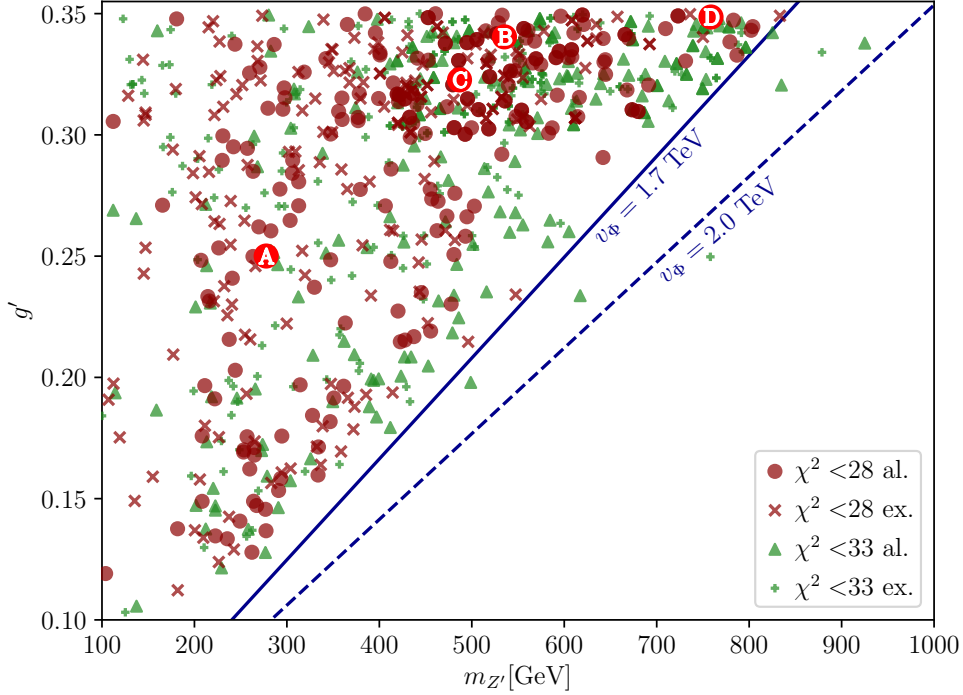


Figure 3: Good fit points in the $(m_{Z'}, g')$ plane. The red (green) dots represent $\chi^2 < 28$ (33), where points which are already excluded by direct Z' searches or neutrino trident production are shown with crosses or pluses. The blue solid (dashed) line shows the maximally allowed values of v_Φ to give an explanation of Δa_μ .

is also predicted. Our model, therefore, is sensitive to the neutrino trident process if $v_\Phi \lesssim 350$ GeV. Focusing on this mass range in Fig. 4, we see that there are a handful of points which are excluded exclusively by the trident constraints and not by LHC searches. On a different note, the one-loop induced gauge kinetic mixing for all points is $\mathcal{O}(10^{-3})$ or less, much smaller than the current limits.

4.3.2 $b \rightarrow sl^+\ell^-$

All the best fit points A-D are fitted to pattern (IV) (“ C_9 and C_{10} ”, cf. eq. (3.68)). There are also a lot of points which are fitted to pattern (I) (“ C_9 only”, eq. (3.65)). We show our good fit points the $(\text{Re } C_9^\mu, \text{Re } C_{10}^\mu)$ plane in the left panel of Fig. 5. Points with pattern (IV) tend to have smaller χ^2 because of the tension in $R_{B_s \rightarrow \mu\mu}$ which favors non zero C_{10} . The other patterns (II) (“ C_{10} only”), (III) (“ $C_9 = -C_{10}$ ”), and (V) (“ C_9 and C_9' ”), are hardly compatible with other observables and we will now discuss this in some detail. Making use of the analytic discussion in Appendix B, the Z' couplings to muons can be expressed as

$$\left[\hat{g}_{eL}^{Z'} \right]_{22} \sim -g' s_{\mu L}^2, \quad \left[\hat{g}_{eR}^{Z'} \right]_{22} \sim -g' s_{\mu R}^2. \quad (4.3)$$

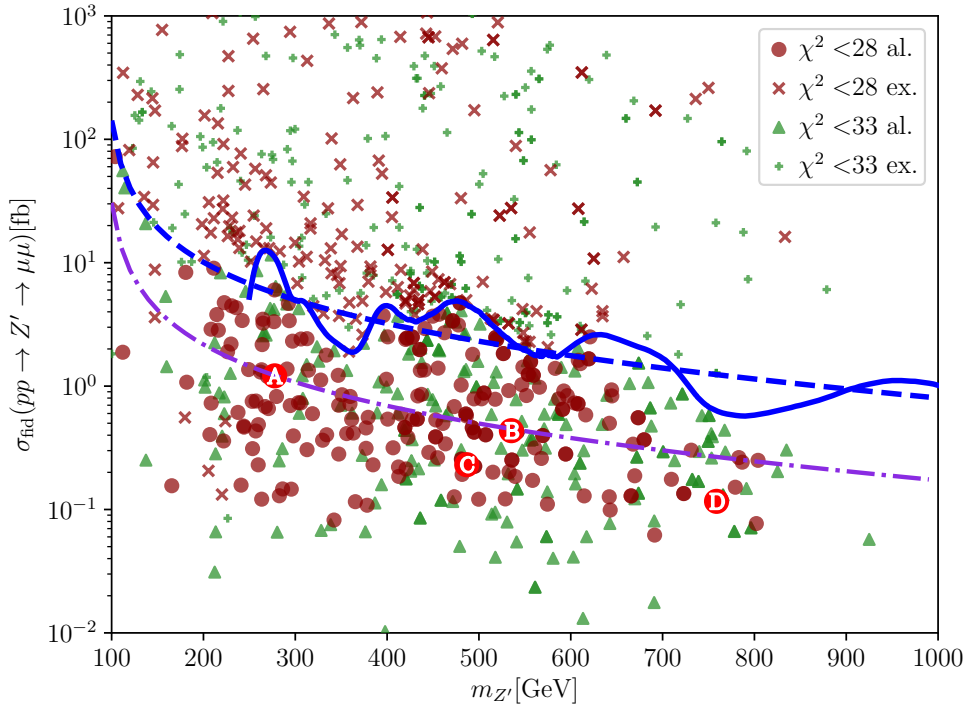


Figure 4: Good fit points in the $(m_{Z'}, \sigma_{\text{fid}}(pp \rightarrow Z' \rightarrow \mu\mu))$ plane. The color coding is the same as in Fig. 3. The solid blue line is the 95% C.L. exclusion limit from ATLAS [102]. The blue dashed line extrapolates this line to test the points with $m_{Z'} < 250$ GeV. As purple dot-dashed line we show a rough estimate of the future sensitivity to be expected after HL-LHC. Excluded points below the blue line are not excluded by LHC direct searches but by neutrino trident production.

Hence, the ratio C_{10}^μ/C_9^μ is given by

$$\frac{C_{10}^\mu}{C_9^\mu} \sim \frac{s_{\mu_R}^2 - s_{\mu_L}^2}{s_{\mu_R}^2 + s_{\mu_L}^2}. \quad (4.4)$$

This indicates $|C_{10}^\mu/C_9^\mu| \leq 1$, and that pattern (II) (“ C_{10} only”) can never be realized. pattern (III) is $C_9^\mu \approx -C_{10}^\mu$, implying $s_{\mu_R}^2 \ll 1$. However, as $\Delta a_\mu \propto s_{\mu_L} s_{\mu_R}/v_\Phi^2$ (cf. Eqs. (3.14), (3.15)) it would be suppressed in this case unless the suppression is compensated by a small $v_\Phi \lesssim 500$ GeV. We show this on the right panel of Fig. 5, where one can clearly see that there are no good points with $\text{Re}(C_{10}^\mu/C_9^\mu) \lesssim -0.8$ for $v_\Phi \gtrsim 1.0$ TeV. Finally, pattern (V) is incompatible with neutral meson mixing: As can be seen from Eqs. (3.95), mixed LR contributions of Z' exchange are enhanced by large negative coefficients. Since pattern (V) requires that $[\hat{g}_{d_L}^{Z'}]_{23}$ and $[\hat{g}_{d_R}^{Z'}]_{23}$ have opposite signs, their LR contribution to meson mixing adds constructively with the SM. As the SM prediction for ΔM_s is already larger than the experimentally measured value, Z' couplings compatible with pattern (V) would only ever increase the tension with experiment. This could be overcome if there were

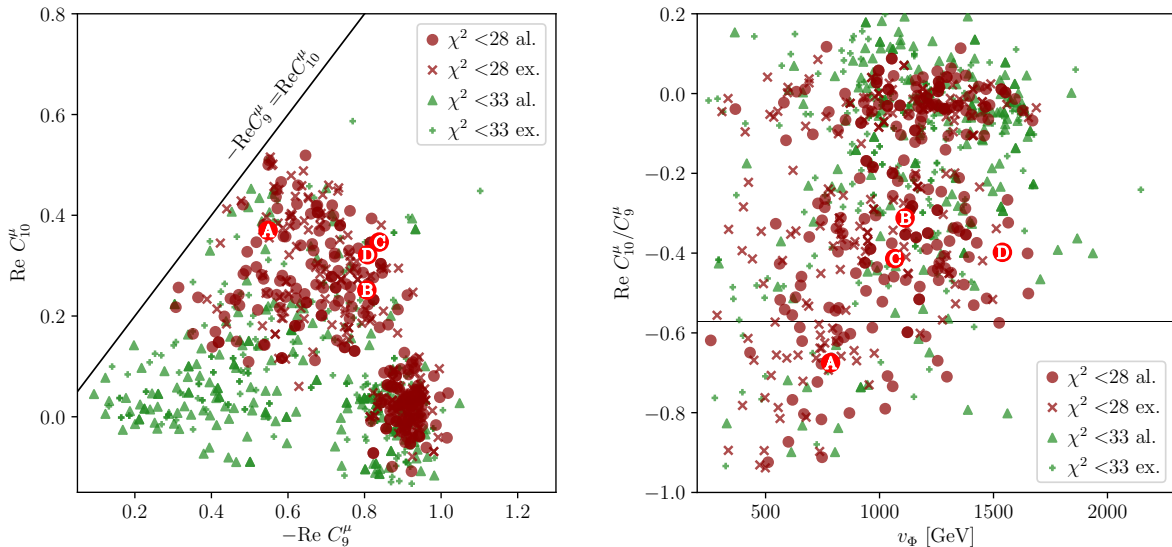


Figure 5: Good fit points in the $(-\text{Re} C_9^{\mu}, \text{Re} C_{10}^{\mu})$ and $(v_{\Phi}, \text{Re}(C_{10}^{\mu}/C_9^{\mu}))$ planes. The color coding is the same as in Fig. 3. The black line in the right plot correspond to pattern (IV) of Eq. (3.68).

sizable negative contributions from the scalar exchange, however, the scalar couplings in our model are always suppressed as shown in Appendix B.

4.3.3 Standard Model Quark Sector

We fit our model parameters to match the quark masses, absolute values of the CKM matrix elements, and relative physical phases α , β and γ . We do not assume unitarity of the CKM matrix and fit our parameters directly to the experimentally determined absolute values and angles. In addition, we require our model to fit the Wilson coefficients of $b \rightarrow s \ell^+ \ell^-$ processes such that the anomalies are matched. Furthermore, we fit to CP-even and CP-odd observables in $K-\bar{K}$, $B_d-\bar{B}_d$, $B_s-\bar{B}_s$ and $D-\bar{D}$ mixing as well as $R_{K^{(*)}}^{\nu\bar{\nu}}$, $R_{B_{d(s)} \rightarrow \mu\mu}$, $\text{BR}(B_s \rightarrow K\tau\tau)$ and top quark decays. Of course, to some extent this approach consists of a “double fitting” as CKM angles and phases are themselves extracted also from some of these observables under the assumption of the SM. However, our approach should be valid here as NP contributions to the relevant observables are typically less than $\mathcal{O}(10\%)$.

Our best fit values for CKM matrix elements and angles, relative to the SM extraction, are shown in Fig. 6. The brown lines and yellow bands show central values and their uncertainties as obtained in a global fit to the SM [25]. It is an important non-trivial crosscheck of our fitting procedure that we reproduce the SM best-fit values for most elements. In general, our results are consistent with the SM as most of the values agree within their 1σ region. However, some elements, namely $|V_{cb}|$, $|V_{td}|$ and $|V_{ts}|$ show consistent deviations from the SM extraction. Perhaps these deviations could be tested by

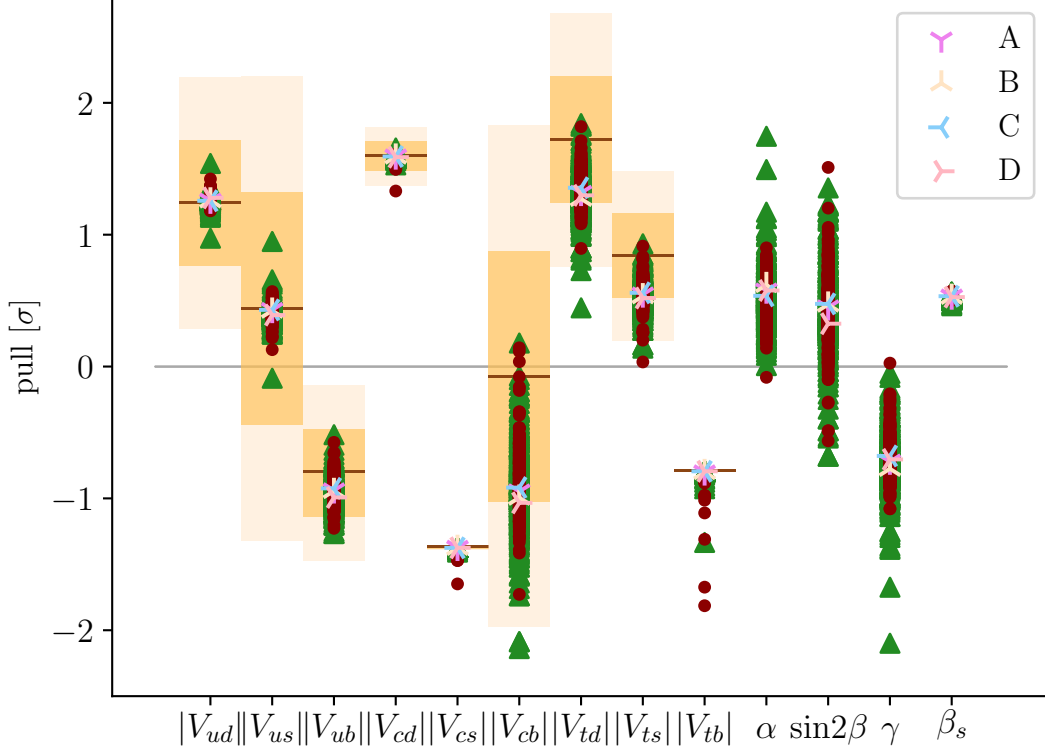


Figure 6: Pulls of good fit points of our model with respect to experimental determinations of absolute values and physical relative phases of CKM matrix elements. The color coding for the red and green points is the same as in Fig. 3. The brown lines and dark (lighter) yellow bands are the central values and 1σ (2σ) ranges of CKM elements as determined in a global SM fit taken from [25].

future experiments, which would be especially interesting if they are correlated with other observables. In Fig. 7 we show the good fit points in the $(\Delta M_d, \Delta M_s)$ plane compared to experimental measurements and SM prediction with and without the assumption of CKM unitarity. Uncertainties of the SM predictions are shown in the figure. As discussed Section 3.3.2, the relative uncertainties for ΔM_d and ΔM_s are estimated as 16% and 14% without assuming unitarity of the CKM matrix. These uncertainties reduce to 9.8% and 7.1% if CKM unitarity is assumed [25].

Although there are sizable Z' contributions these are still small compared with the uncertainties originating from the CKM elements without assuming unitarity. The CP asymmetry parameters $S_{\psi_{K_s}}$ and $S_{\psi_{\phi}}$ are well fit to the experimental values, cf. their values at the best fit points in Table 12 and experimental values in Table 8.

The right panel of Fig. 7 shows the good fit points in the $(\Delta M_K, \epsilon_K)$ plane. Similar

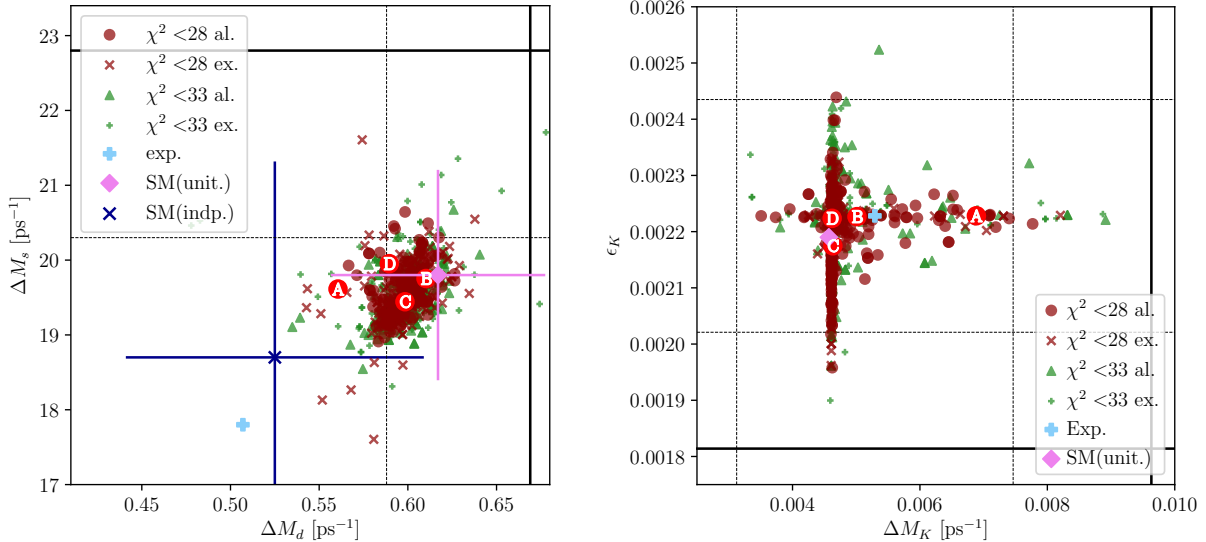


Figure 7: Good fit points in the $(\Delta M_d, \Delta M_s)$ (left) and $(\Delta M_K, \epsilon_K)$ plane (right). The color coding is the same as in Fig. 3. Black thin-dashed (thick) lines show 1σ (2σ) deviations from the experimental values. The experimental central values are shown as light-blue plus. SM predictions with (without) assuming CKM unitarity are shown as a purple diamond (dark-blue x in the left panel).

to $B-\bar{B}$ mixing, the Z' contributions are smaller than the uncertainties from the CKM values and QCD corrections.

There may be a sizable contribution from Z' exchange to $D-\bar{D}$ mixing as well. However, theoretical errors here are too large to hope for a discrimination of SM and NP effects. Also the effects in top quark decays, including flavor violating ones, are too small to be tested by experiment.

Potentially, there are also contributions from the new scalar fields. However, as shown in Appendix B, the Yukawa coupling of the new scalars to the SM fermions first arise at the second order of the small mixing angles. Therefore, scalar contributions are very suppressed for $B_s \rightarrow \mu\mu$. The ratio $R_{B_s \rightarrow \mu\mu}$ is predominantly determined by C_{10}^μ where a larger C_{10}^μ relaxes the tension between measurements and the SM prediction, see Table 12. Finally, $\text{BR}(B_s \rightarrow K\tau\tau)$ is generally not much affected as the Z' coupling to τ 's can be suppressed. At all the best fit points, $R_{K^{(*)}}^{\nu\nu} \lesssim 1.06$ which is a deviation much smaller than the experimental sensitivities.

4.3.4 Charged Lepton Flavor Violation

We now discuss predictions for charged LFV in this model. While we have included the experimental upper bounds on charged LFV in the fit, it still is interesting to see the size and spread of LFV obtained in this model. Figure 8 shows the best fit points in the $(\text{BR}(\mu \rightarrow e\gamma), \text{BR}(\mu \rightarrow eee))$ and $(\text{BR}(\tau \rightarrow \mu\gamma), \text{BR}(\tau \rightarrow \mu\mu\mu))$ planes, respectively. For

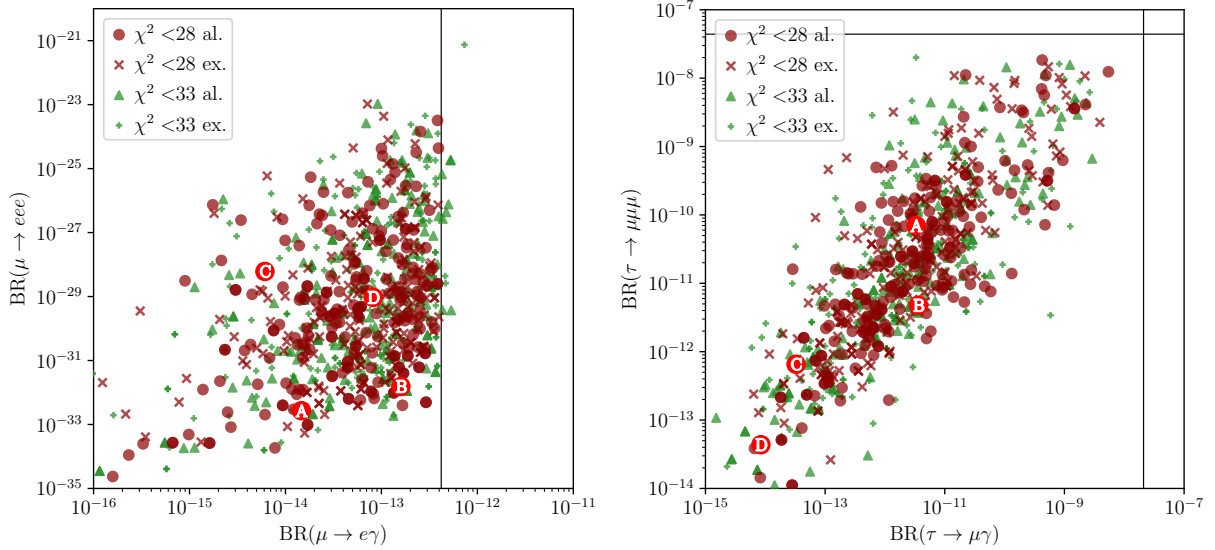


Figure 8: Predictions of the best fit points for $\text{BR}(\mu \rightarrow e\gamma)$, $\text{BR}(\mu \rightarrow eee)$, $\text{BR}(\tau \rightarrow \mu\gamma)$, as well as $\text{BR}(\tau \rightarrow \mu\mu\mu)$ and their correlations. The color coding is the same as in Fig. 3. The black lines are the current experimental 90% C.L. exclusion limits.

LFV muon decays, $\text{BR}(\mu \rightarrow e\gamma)$ is much larger than $\text{BR}(\mu \rightarrow eee)$. As already discussed in Section 3.1.3 and 3.1.4 this can be understood analytically. While the former decay is quadratically proportional to the tiny mixing angle ϵ_e between electron and VL leptons, the latter decay scales with ϵ_e^6 . Thus, our model predicts $\text{BR}(\mu \rightarrow e\gamma) \gg \text{BR}(\mu \rightarrow eee)$.

For LFV τ decays, in contrast, $\text{BR}(\tau \rightarrow \mu\mu\mu)$ is roughly of the same order of magnitude as $\text{BR}(\tau \rightarrow \mu\gamma)$. This can be understood because both of them are scaling as ϵ_τ^2 , where ϵ_τ is the small mixing angle between τ and the VL leptons. All the other LFV tau decays are suppressed by additional powers of ϵ_τ and/or ϵ_e .

We see that especially for $\mu \rightarrow e\gamma$ there are many best fit points close to the current upper limit. This limit will be significantly improved to $< 6 \times 10^{-14}$ by the upcoming MEG II experiment [113]. Similarly an improvement on the upper limit of $\text{BR}(\tau \rightarrow \mu\gamma)$ by up to two orders of magnitude is expected from Belle II [114]. Nonetheless, we find good fit points that extend into regions which will not be probed by upcoming experiments. We therefore conclude that while a future excess in the charged LFV channels $\mu \rightarrow e\gamma$ and/or $\tau \rightarrow \mu\gamma$ could consistently be explained in our model, those observables will not be the first to exclude this model.

Regarding charged LFV decays of SM bosons at tree level, we find that the respective branching fractions are more than several orders of magnitude smaller than the current bounds. In fact, the couplings of SM bosons to SM fermions are very close to their SM values which we have already discussed in Section 3.2 based on our analytical treatment shown in Appendix B.

4.3.5 Signals of Vector-Like Leptons

Finally, let us investigate collider signatures of VL fermions. As discussed in Section 3.1.1, the VL lepton mass is constrained to explain the muon anomalous magnetic moment, and $\Delta a_\mu = 2.68 \times 10^{-9}$ can be realized only within the parameter space shown in Fig. 2. In the same figure we show the masses of the lightest VL lepton m_{E_1} and $m_{Z'}$ for our best fit points. Most points have $m_{E_1} \lesssim 800$ GeV and the points with $m_{E_1} > 800$ GeV are found only where $m_{Z'} \sim 500$ GeV as expected from our analytical discussion illustrated by the contours in Fig. 2. In the upper panels of Fig. 9 we show the distribution of the heavier VL lepton masses m_{E_2} with respect to $m_{Z'}$ (left) and with respect to the lighter VL lepton m_{E_1} (right). The black thick, thin, and dashed lines show mass splittings $\Delta m_E := m_{E_2} - m_{E_1} = 0, 174,$ and $2 \cdot 174$ GeV, respectively. The mass splitting is bounded by $\sim \lambda'_e v_H$, and it is typically not very large, since the loop function $C_{Z'}$ contributing to Δa_μ , defined in Eq. (3.16), is maximized when the masses are degenerate. Consequently, the heavier VL lepton E_2 is typically not much heavier than about 1.5 TeV. According to Ref. [115], the production cross section of a doublet VL lepton with mass 1.5 TeV is about $\mathcal{O}(0.1)$ fb which corresponds to about 30 (300) total events at the end of LHC (HL-LHC). Therefore, the HL-LHC could exclude the whole parameter space compatible with Δa_μ if the signals for VL leptons are very clean.

In the present model, high-multiplicity muon signals are expected from the production and decay of VL leptons. The decay modes crucially depend on the masses of the Z' and χ bosons. We show the dominant two-body decay modes and their branching fractions at our best fit points in Tables 18-21 in Appendix D. If either of the following final states is kinematically allowed, the lightest VL lepton decays dominantly to

$$E_1 \rightarrow Z' + \mu, \quad \text{and/or} \quad E_1 \rightarrow \chi + \mu. \quad (4.5)$$

For illustration, the lower left panel in Fig. 9 shows the sum of $\text{BR}(E_1 \rightarrow Z' \mu) + \text{BR}(E_1 \rightarrow \chi \mu)$ in dependence of m_{E_1} for our good fit points, cf. also Tables 18-21. Often either χ or Z' is lighter than the VL leptons, as is the case for the best fit points A, B, and D. This comes about because a light scalar χ is favored to suppress its destructive contribution to Δa_μ , while the Z' mass is controlled by the overall scale v_Φ which is rarely above ~ 1 TeV.

On the contrary, if $m_{E_1} < m_{Z'}, m_\chi$ (as in our best fit point C), E_1 decays predominantly to a SM boson and a muon or neutrino,

$$E_1 \rightarrow h/Z + \mu, \quad \text{and/or} \quad E_1 \rightarrow W + \nu_\mu. \quad (4.6)$$

The detailed ratio of these branching fractions depends on the mixing between the singlet-like and doublet-like VL states.

The final states in Eq. (4.6) have been studied as a signature of VL leptons in several papers [115–121]. However, there is no study by LHC experiments of VL leptons decaying to a muon based on LHC Run-2 data. A dedicated analysis of the experimental data shows that a singlet-like VL lepton at the point C with mass above 200 GeV can not be excluded [117].

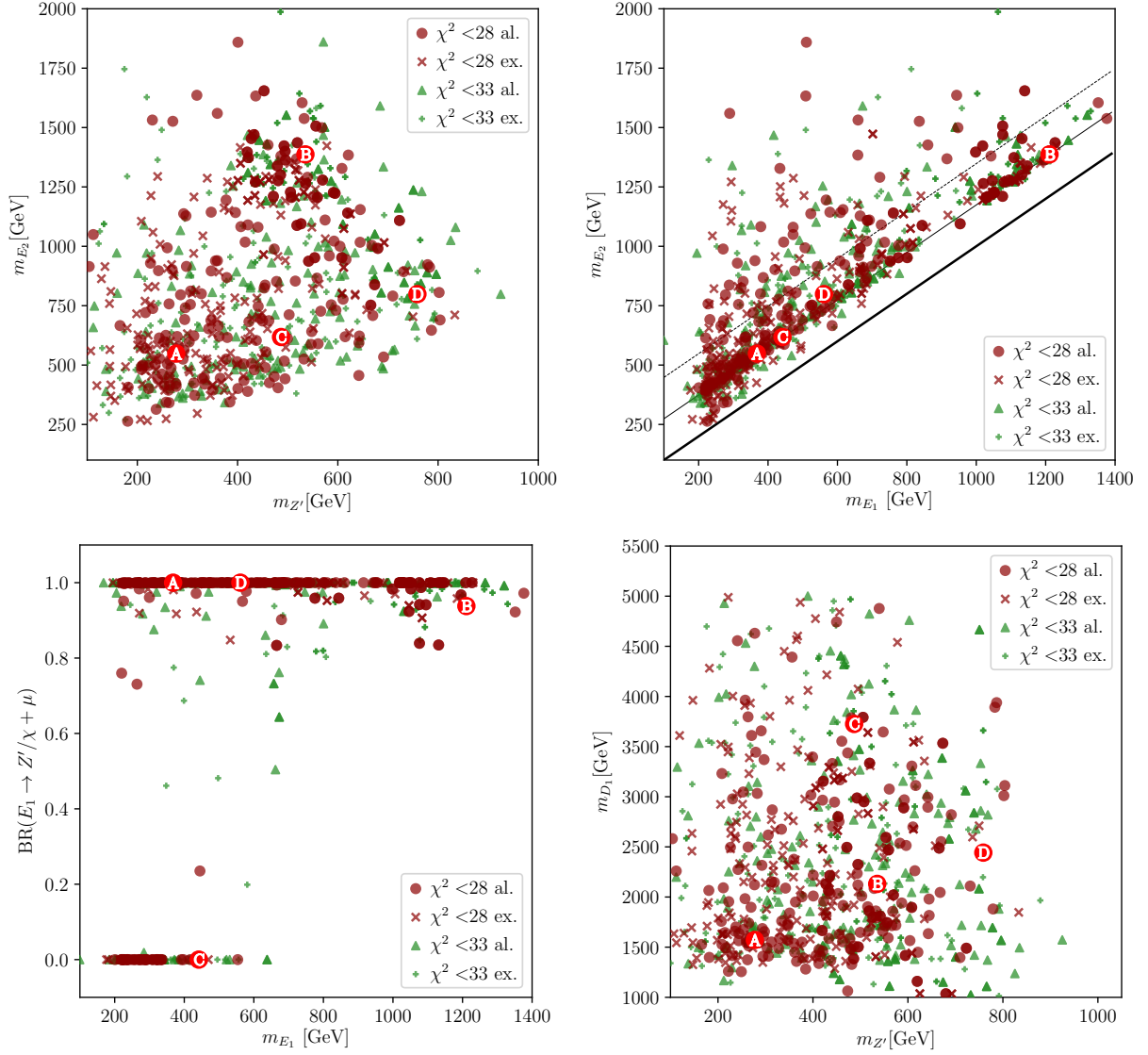


Figure 9: Good fit points and their predicted values of the observables, $m_{Z'}$, m_{E_1} , m_{E_2} , m_{D_1} , and $BR(E_1 \rightarrow Z'/\chi + \mu)$. The color coding is the same as in Fig. 3.

The final states in Eq. (4.5) have not been considered so far; they give rise to characteristic multi-lepton final states. This comes about because the Z' boson predominantly decays to a pair of muons or muon neutrinos, cf. Tables 18-21. The scalar χ couples to SM fermions through the tiny Yukawa couplings induced by mixing effects, $\sim \epsilon_{f_{\text{SM}}} m_{f_{\text{SM}}}/M_{F_{\text{VL}}}$. However, at most points χ has a large coupling to muons because of the large mixing. In addition, couplings to third generation quarks could also be large due to an enhancement by their heavy masses. This is the case at our best fit point D, cf. Table 21. The sizable branching fractions of the exotic boson to pairs of muons provide clean resonance signals,

$$Z' \rightarrow \mu^+ \mu^- \quad \text{and} \quad \chi \rightarrow \mu^+ \mu^-. \quad (4.7)$$

Therefore, processes with dramatic multi-resonant multi-lepton final states, such as

$$pp \rightarrow E_1^+ E_1^- \rightarrow \mu^+ (\mu^+ \mu^-)_B + \mu^- (\mu^+ \mu^-)_B, \quad B = \chi, Z' \quad (4.8)$$

are expected from the VL lepton production. Here, $(\mu^+ \mu^-)_B$ is a pair of muons with a resonant feature at the invariant mass $m_{\mu\mu}^2 \sim m_B^2$. At point D, the doublet-like VL neutrino also decays to the exotic scalar and signals such as

$$pp \rightarrow E_1 N_1 \rightarrow \mu (\mu^+ \mu^-)_B + \nu (\mu^+ \mu^-)_B, \quad (4.9)$$

are expected. This signal is expected if the lightest VL lepton is doublet-like.

The heavier VL lepton decays in a more complicated way. It will predominantly decay to the lighter VL lepton under the emission of a SM boson, since there is sizable mixing between the VL leptons in order to enhance the left-right effects to Δa_μ . The most dramatic case may be

$$E_2 \rightarrow E_1 Z \rightarrow \mu (\mu^+ \mu^-)_{Z'} + (\ell^+ \ell^-)_Z, \quad (4.10)$$

which results in five SM leptons from one VL lepton. A pair of VL leptons, thus, could produce up to ten leptons per event. Although it may be difficult to reconstruct all of them, such high-multiplicity lepton signals provide a very distinctive event topology.

4.3.6 Signals of Vector-Like Quarks

The lower right panel of Fig. 9 shows the good fit points in the $(m_{Z'}, m_{D_1})$ plane. Unlike for the VL leptons, there is no stringent upper limit on the VL quark masses. This is because small Z' couplings to the SM quarks are enough to explain the $b \rightarrow s \ell^+ \ell^-$ anomalies. Moreover, the mixing itself is given by $\lambda_i^Q v_\Phi / \lambda_V^Q v_\phi$ and is independent of the Higgs VEV. The VL quarks can be within the reach of current and future collider experiments if they are light. For instance, point A has a singlet-like VL quark with mass ~ 1.6 TeV. Since $v_\Phi < 1.7$ TeV is required, VL quark decays to Z' or χ is always kinematically allowed. As for the VL leptons, dramatic signals involving Z' or χ , e.g.

$$pp \rightarrow QQ \rightarrow \text{jet} (\mu^+ \mu^-)_{Z'} + \text{jet} (\mu^+ \mu^-)_{Z'}, \quad (4.11)$$

are expected. These high-multiplicity leptons with resonant features in association with jets provide another distinctive signal of this model.

5 Summary

We have presented an extension of the Standard Model with the addition of a vector-like family of quarks and leptons which also carry a new $U(1)'$ charge. The model is constructed to address the known experimental anomalies associated with muons, i.e. the anomalous magnetic moment of the muon and the decays $b \rightarrow s\ell^+\ell^-$. SM quarks and leptons feel the new Z' gauge interactions only via mass mixing with the VL family. The model contains two additional SM singlet scalars, one that is used to model the masses of the VL family and another one that mixes the VL family with the SM states and obtains a VEV that spontaneously breaks the $U(1)'$ symmetry. We performed a global χ^2 analysis of the data, with 65 arbitrary model parameters and taking into account 98 observables. We have found many model points which satisfy $\chi^2/N_{\text{d.o.f.}} \leq 1$. We cannot simultaneously fit the anomalous magnetic moment of the electron and muon, because the theory is severely constrained by the experimental upper bound on $\text{BR}(\mu \rightarrow e\gamma)$.⁵ We, therefore, decided to only fit Δa_μ . All good fit points have $\text{BR}(\mu \rightarrow e\gamma) > 10^{-16}$ and $\text{BR}(\tau \rightarrow \mu\gamma) > 10^{-15}$ with the latter being strongly correlated with $\text{BR}(\tau \rightarrow 3\mu)$. Roughly half of our best fit points have $\text{BR}(\mu \rightarrow e\gamma)$ in a range that is accessible by upcoming experiments. However, note that this is not a necessity of the model, i.e. $\text{BR}(\mu \rightarrow e\gamma)$ could always be suppressed by tuning $\epsilon_{e_{L,R}}$ to zero without affecting the explanation of the anomalies or SM predictions.

With regards to $b \rightarrow s\ell^+\ell^-$ decay processes, we fit the Wilson coefficients for new physics contributions as discussed in Ref. [52]. Only two of the five possible good fit points of this analysis can be fit in our model. The flavor violating decays of SM bosons, i.e. Higgs, W and Z are severely suppressed in our model. The vector-like quark induced coupling to Z' also gives sizable contributions to neutral meson mixing, particularly $K-\bar{K}$, $B_{d,s}-\bar{B}_{d,s}$, and $D-\bar{D}$ mixing. The best-fit values for many CKM elements in our model consistently deviate from their experimental central values at the level of $1-2\sigma$ (as they do also in the Standard Model). Hence, more accurate constraints of CKM non-unitarity and more precise measurements of CKM elements would be very welcome to further test the model.

In order to understand the predictions for new physics we have presented four “best fit points” - A, B, C, and D with the masses of the new particles and their decay rates given in Tables 18, 19, 20 and 21, respectively. Many more details are given in the Appendices. The fit values for some selected observables are given in Table 12. Although the Z' mass is typically significantly less than a TeV and it decays with a significant branching fraction to $\mu^+\mu^-$, we find many points not excluded by recent ATLAS searches for a dimuon resonance. We are also constrained by neutrino trident processes. The VL leptons are typically light, while the VL quarks are significantly heavier with mass of order a few TeV. Since the lightest VL leptons at best fit points, A, C and D, have mass between 300 - 600 GeV, these states may be accessible even at the LHC, and even more so at the HL-LHC. They typically result in multi-muon production channels as discussed in Section 4.3.5.

This model is a prototype which highlights that fixing anomalies with consistent mod-

⁵During the completion of our work, Ref. [36] appeared on the arXiv which reaches the same conclusion for a model with Z' and VL leptons (see also the somewhat related discussion in [28]).

els, while maintaining the successful Standard Model predictions, comes at a price: The model appears eminently testable and, therefore, can be excluded in many complementary ways.

Acknowledgments

We thank R. Dermisek for useful discussions. The work of J.K. and S.R. is supported in part by the Department of Energy (DOE) under Award No. DE-SC0011726. The work of J.K. is supported in part by the Grant-in-Aid for Scientific Research from the Ministry of Education, Science, Sports and Culture (MEXT), Japan No. 18K13534. The work of A.T. was partly supported by a postdoc fellowship of the German Academic Exchange Service (DAAD). A.T. is grateful to the Physics Department of Ohio State University and Centro de Física Teórica de Partículas (CFTP) at Instituto Superior Técnico, Lisbon for hospitality during parts of this work.

A Decay Width Formulas

Widths of two-body decays with both left-handed and right-handed interactions are summarized in this Appendix.

A.1 Scalar Decays

With the Yukawa interactions of a real scalar field ϕ and two fermions f_1, f_2 ,

$$\mathcal{L}_{\phi \rightarrow f_1 \bar{f}_2} = -\phi (y_L \bar{f}_1 P_L f_2 + y_R \bar{f}_1 P_R f_2), \quad (\text{A.1})$$

the partial width of ϕ is given by

$$\Gamma(\phi \rightarrow f_1 \bar{f}_2) = \frac{m_\phi}{16\pi} \lambda(x_1, x_2) [(|y_L|^2 + |y_R|^2)(1 - x_1 - x_2) - \text{Re}(y_L y_R^*) 4\sqrt{x_1 x_2}], \quad (\text{A.2})$$

where $x_i = m_{f_i}/m_\phi^2$ and

$$\lambda(x_1, x_2) := \sqrt{1 - 2(x_1 + x_2) + (x_1 - x_2)^2}. \quad (\text{A.3})$$

A.2 Gauge Boson Decays

Gauge interactions of a vector field V , two fermions f_1, f_2 ,

$$\mathcal{L}_{V \rightarrow f_1 \bar{f}_2} = V_\mu (g_L \bar{f}_1 \gamma^\mu P_L f_2 + g_R \bar{f}_1 \gamma^\mu P_R f_2). \quad (\text{A.4})$$

give the partial width,

$$\Gamma(V \rightarrow f_1 \bar{f}_2) = \frac{m_V}{24\pi} \lambda(x_1, x_2) \left[(|g_L^2| + |g_R^2|) \left(1 - \frac{x_1 + x_2}{2} - \frac{(x_1 - x_2)^2}{2} \right) + \text{Re}(g_L g_R^*) 6\sqrt{x_1 x_2} \right], \quad (\text{A.5})$$

where $x_i = m_{f_i}/m_V^2$.

A.3 Fermion Decays

If $m_{f_2} > m_{f_1} + m_\phi$, a fermion f_2 can decay as $f_2 \rightarrow f_1 \phi$ through the Yukawa interaction in Eq. (A.1). The partial width is given by

$$\Gamma(f_2 \rightarrow f_1 \phi) = \frac{m_{f_2}}{32\pi} \lambda(y, z) [(|y_L^2| + |y_R^2|) (1 - y - z) + \text{Re}(y_L y_R^*) 4\sqrt{y}], \quad (\text{A.6})$$

where $y = m_{f_1}^2/m_{f_2}^2$ and $z = m_\phi^2/m_{f_2}^2$.

The gauge interactions in Eq. (A.4) induce a decay $f_2 \rightarrow f_1 V$, if $m_{f_2} > m_{f_1} + m_V$. The partial width is given by

$$\Gamma(f_2 \rightarrow f_1 V) = \frac{m_{f_2}^3}{32\pi m_V^2} \lambda(y, z) \left[(|g_L^2| + |g_R^2|) \{(1 - y)^2 + z(1 + y) - 2z^2\} - \text{Re}(g_L g_R^*) 3z\sqrt{y} \right], \quad (\text{A.7})$$

where $y = m_{f_1}^2/m_{f_2}^2$ and $z = m_V^2/m_{f_2}^2$.

B Analytical Analysis

Many analytical formulae used in the main text are derived in this Appendix.

B.1 Diagonalization of the Dirac Mass Matrices

The 5×5 Dirac mass matrices are given by

$$\bar{f}_R \mathcal{M}^f f_L = \begin{pmatrix} \bar{f}_{Ri} & \bar{F}_R & \bar{F}'_R \end{pmatrix} \begin{pmatrix} y_{ij}^f v_H & 0 & \lambda_i^R v_\Phi \\ 0 & \lambda_f v_H & \lambda_V^R v_\phi \\ \lambda_j^L v_\Phi & \lambda_V^L v_\phi & \lambda_f' v_H \end{pmatrix} \begin{pmatrix} f_{Lj} \\ F'_L \\ F_L \end{pmatrix}, \quad (\text{B.1})$$

where $(f, F, L, R) = (e, E, L, E), (u, U, Q, U), (d, D, Q, D)$ for charged leptons, up or down quarks, respectively, see Eqs. (2.6)-(2.9). We are interested in the case $v_H \ll \lambda^{L,R} v_\phi$, in

which case the VL fermions are heavy enough to be consistent with LHC limits. We diagonalize all the Dirac mass matrices perturbatively in v_H/v_ϕ . At leading order, i.e. v_H , the mass matrices are block diagonalized by the unitary matrices,

$$U_{f_L}^0 = \begin{pmatrix} \mathbf{z}_{L_j}^f & \mathbf{n}_L^f & \mathbf{0} \\ 0_j & 0 & 1 \end{pmatrix}, \quad U_{f_R}^0 = \begin{pmatrix} \mathbf{z}_{R_j}^f & \mathbf{n}_R^f & \mathbf{0} \\ 0_j & 0 & 1 \end{pmatrix}. \quad (\text{B.2})$$

Here, the four-component vectors obey the following conditions,

$$\mathbf{n}_L^f = \frac{1}{M_{F_L}} \begin{pmatrix} \lambda_i^L v_\Phi \\ \lambda_V^L v_\phi \end{pmatrix}^*, \quad \mathbf{n}_R^f = \frac{1}{M_{F_R}} \begin{pmatrix} \lambda_i^R v_\Phi \\ \lambda_V^R v_\phi \end{pmatrix}, \quad (\text{B.3})$$

$$\left(\mathbf{z}_{L_i}^f\right)^\dagger \mathbf{n}_L^f = \left(\mathbf{z}_{R_i}^f\right)^\dagger \mathbf{n}_R^f = 0, \quad \left(\mathbf{z}_{L_i}^f\right)^\dagger \mathbf{z}_{L_j}^f = \left(\mathbf{z}_{R_i}^f\right)^\dagger \mathbf{z}_{R_j}^f = \delta_{ij}, \quad (\text{B.4})$$

where

$$M_{F_L} = \sqrt{\sum_{i=1}^3 |\lambda_i^L v_\Phi|^2 + |\lambda_V^L v_\phi|^2}, \quad M_{F_R} = \sqrt{\sum_{i=1}^3 |\lambda_i^R v_\Phi|^2 + |\lambda_V^R v_\phi|^2}. \quad (\text{B.5})$$

The vectors $\mathbf{z}_{L_i}, \mathbf{z}_{R_i}$ can be any four-component vectors which satisfy Eq. (B.4). Another set of $\mathbf{z}'_{L_i} = [u_L]_{ij} \mathbf{z}_{L_j}, \mathbf{z}'_{R_i} = [u_R]_{ij} \mathbf{z}_{R_j}$, with arbitrary unitary matrices u_L, u_R also satisfy the conditions Eq. (B.4). We define these vectors such that the upper-left 3×3 block is diagonalized by using this degree of freedom.

Rotating the mass matrix by these unitary matrices while keeping $\mathcal{O}(v_H)$ elements we obtain

$$\begin{aligned} \tilde{\mathcal{M}}^f &:= (U_{f_R}^0)^\dagger \mathcal{M}^f U_{f_L}^0 \\ &= \begin{pmatrix} \left(\mathbf{z}_{R_i}^f\right)^\dagger \hat{m}_f \mathbf{z}_{L_j}^f & \left(\mathbf{z}_{R_i}^f\right)^\dagger \hat{m}_f \mathbf{n}_L^f & 0_i \\ \left(\mathbf{n}_R^f\right)^\dagger \hat{m}_f \mathbf{z}_{L_j}^f & \left(\mathbf{n}_R^f\right)^\dagger \hat{m}_f \mathbf{z}_{L_j}^f & M_{F_R} \\ 0_j & M_{F_L} & \lambda'_f v_H \end{pmatrix} := \begin{pmatrix} \tilde{y}_i^f \delta_{ij} v_H & \tilde{y}_{R_i}^f v_H & 0_i \\ \tilde{y}_{L_j}^f v_H & \tilde{\lambda}_f v_H & M_{F_R} \\ 0_j & M_{F_L} & \lambda'_f v_H \end{pmatrix}, \end{aligned} \quad (\text{B.6})$$

where the 4×4 matrix \hat{m}_f is defined as

$$\hat{m}_f := \begin{pmatrix} y_{ij}^f & 0_i \\ 0_j & \lambda_f \end{pmatrix} v_H. \quad (\text{B.7})$$

The matrix $\tilde{\mathcal{M}}^f$ is $3 \oplus 2$ block diagonal, except $\tilde{y}_{L_i, R_j}^f v_H$. The mixing effects induced by these elements are $\mathcal{O}(\tilde{y}_{L_i, R_j}^f v_H / M_{F_{L,R}})$, suppressed by Yukawa couplings and VL fermion masses.

Next, we diagonalize the lower-right block. We are interested in parameters where $M_{E_{L,R}} \gtrsim 250$ GeV and $M_{Q_{L,R}} \gtrsim 1.5$ TeV to be consistent with LHC searches. The VL

quarks are substantially heavier than v_H , while the VL leptons are at a few hundred GeV with a Yukawa coupling $\lambda'_e \sim \mathcal{O}(1)$ as required in order to explain Δa_μ . Fortunately, the other Yukawa couplings are small enough due to the small charged leptons masses. Keeping $\lambda'_e v_H$, the next order of unitary matrices is parametrized as

$$U_{f_R}^1 = \begin{pmatrix} \delta_{ij} & 0_i & 0_i \\ 0_j & s_{\theta_R} & c_{\theta_R} \\ 0_j & c_{\theta_R} & -s_{\theta_R} \end{pmatrix}, \quad U_{f_L}^1 = \begin{pmatrix} \delta_{ij} & 0_i & 0_i \\ 0_j & c_{\theta_L} & -s_{\theta_L} \\ 0_j & s_{\theta_L} & c_{\theta_L} \end{pmatrix}, \quad (\text{B.8})$$

with angles $\theta_{L,R}$ that satisfy

$$\begin{pmatrix} s_{\theta_R} & c_{\theta_R} \\ c_{\theta_R} & -s_{\theta_R} \end{pmatrix} \begin{pmatrix} \tilde{\lambda}_f v_H & M_{F_R} \\ M_{F_L} & \lambda'_f v_H \end{pmatrix} \begin{pmatrix} c_{\theta_L} & -s_{\theta_L} \\ s_{\theta_L} & c_{\theta_L} \end{pmatrix} =: \text{diag}(\tilde{M}_{F_L}, \tilde{M}_{F_R}). \quad (\text{B.9})$$

The rotated mass matrix is

$$(U_{f_R}^1)^\dagger \tilde{\mathcal{M}}^f U_{f_L}^1 = \begin{pmatrix} m_{f_i} \delta_{ij} & c_{\theta_L} \tilde{y}_{R_i}^f v_H & -s_{\theta_L} \tilde{y}_{R_i}^f v_H \\ s_{\theta_R} \tilde{y}_{L_j}^f v_H & \tilde{M}_{F_L} & 0 \\ c_{\theta_R} \tilde{y}_{L_j}^f v_H & 0 & \tilde{M}_{F_R} \end{pmatrix}. \quad (\text{B.10})$$

We now give approximate forms for angles $\theta_{L,R}$ and masses $\tilde{M}_{F_{L,R}}$. Here, we neglect $\lambda_f v_H$. If $\lambda'_f v_H \ll |M_{F_L} - M_{F_R}|$, the mixing angles and masses are approximately given by

$$\begin{aligned} c_{\theta_{L,R}} &= 1 + \mathcal{O}(\delta_{f_{L,R}}^2), & \tilde{M}_{F_{L,R}} &= M_{F_{L,R}} + \mathcal{O}(\delta_{f_{L,R}} \lambda'_f v_H), \\ s_{\theta_{L,R}} &= \delta_{f_{L,R}} + \mathcal{O}(\delta_{f_{L,R}}^2), \end{aligned} \quad (\text{B.11})$$

with an expansion parameter defined as

$$\delta_{f_{L,R}} = \frac{\lambda'_f v_H M_{F_{L,R}}}{M_{F_L}^2 - M_{F_R}^2}. \quad (\text{B.12})$$

Clearly, this approximation becomes inaccurate if the VL fermions are nearly mass-degenerate. For the nearly mass-degenerate case one can proceed as follows. We introduce three mass parameters,

$$M_F := \frac{M_{F_L} + M_{F_R}}{2}, \quad \Delta_F := \frac{M_{F_L} - M_{F_R}}{2}, \quad \mu_F := \sqrt{\Delta_F^2 + \frac{(\lambda' v_H)^2}{4}}. \quad (\text{B.13})$$

If $|\lambda'_f v_H|, |\Delta_F| \ll M_F$, the masses are given by

$$\tilde{M}_{F_L} = M_F + \mu_F + \mathcal{O}\left(\frac{(\lambda' v_H)^2}{M_F}\right), \quad \tilde{M}_{F_R} = M_F - \mu_F + \mathcal{O}\left(\frac{(\lambda' v_H)^2}{M_F}\right). \quad (\text{B.14})$$

The mixing angles are given by

$$c_{\theta_L} = \frac{1}{\sqrt{2}} \left(\alpha_F - \frac{\lambda'_f v_H}{4M_F} \beta_F \right), \quad s_{\theta_L} = \frac{1}{\sqrt{2}} \left(\beta_F + \frac{\lambda'_f v_H}{4M_F} \alpha_F \right), \quad (\text{B.15})$$

$$c_{\theta_R} = \frac{1}{\sqrt{2}} \left(\alpha_F + \frac{\lambda'_f v_H}{4M_F} \beta_F \right), \quad s_{\theta_R} = \frac{1}{\sqrt{2}} \left(\beta_F - \frac{\lambda'_f v_H}{4M_F} \alpha_F \right), \quad (\text{B.16})$$

where

$$\alpha_F := \frac{1}{\sqrt{2}} \left(\sqrt{1 + \frac{\lambda'_f v_H}{2\mu_F}} + \sqrt{1 - \frac{\lambda'_f v_H}{2\mu_F}} \right), \quad \beta_F := \frac{1}{\sqrt{2}} \left(\sqrt{1 + \frac{\lambda'_f v_H}{2\mu_F}} - \sqrt{1 - \frac{\lambda'_f v_H}{2\mu_F}} \right). \quad (\text{B.17})$$

Here, higher orders of $\lambda' v_H/M_F$ and Δ_F/M_F are neglected.

We now proceed to further diagonalize Eq. (B.10). At the first order in $\tilde{y}_{L,R}^f v_H/\tilde{M}_{F_{L,R}}$, Eq. (B.10) is diagonalized by unitary matrices,

$$U_{f_R}^2 = \begin{pmatrix} \delta_{ij} & c_{\theta_L} \tilde{y}_{R_i}^f v_H/\tilde{M}_{F_L} & -s_{\theta_L} \tilde{y}_{R_i}^f v_H/\tilde{M}_{F_R} \\ -c_{\theta_L} \tilde{y}_{R_j}^{f*} v_H/\tilde{M}_{F_L} & 1 & 0 \\ s_{\theta_L} \tilde{y}_{R_j}^{f*} v_H/\tilde{M}_{F_R} & 0 & 1 \end{pmatrix}, \quad (\text{B.18})$$

$$U_{f_L}^2 = \begin{pmatrix} \delta_{ij} & s_{\theta_R} \tilde{y}_{L_i}^f v_H/\tilde{M}_{F_L} & c_{\theta_R} \tilde{y}_{L_i}^f v_H/\tilde{M}_{F_R} \\ -s_{\theta_R} \tilde{y}_{L_j}^{f*} v_H/\tilde{M}_{F_L} & 1 & 0 \\ -c_{\theta_R} \tilde{y}_{L_j}^{f*} v_H/\tilde{M}_{F_R} & 0 & 1 \end{pmatrix}. \quad (\text{B.19})$$

Multiplying these unitary matrices one finds

$$(U_{f_R}^2)^\dagger (U_{f_R}^1)^\dagger \tilde{\mathcal{M}}^f U_{f_L}^1 U_{f_L}^2 = \text{diag} \left(m_{f_i} \delta_{ij}, \tilde{M}_{F_L}, \tilde{M}_{F_R} \right) + \mathcal{O} \left(\frac{\left(\tilde{y}_{L,R}^f v_H \right)^2}{\tilde{M}_{F_{L,R}}} \right). \quad (\text{B.20})$$

The second-order corrections to the upper-left block are given by

$$\Delta m_{ij}^f := \tilde{y}_{R_i}^f \tilde{y}_{L_j}^f \frac{v_H^2}{\tilde{M}_{F_L} \tilde{M}_{F_R}} \left(\tilde{M}_{F_L} c_{\theta_R} s_{\theta_L} - \tilde{M}_{F_R} c_{\theta_L} s_{\theta_R} \right) \sim \tilde{y}_{R_i}^f \tilde{y}_{L_j}^f \frac{\lambda'_f v_H^3}{\tilde{M}_{F_L} \tilde{M}_{F_R}}. \quad (\text{B.21})$$

Here, it does not matter whether Eq. (B.11) or Eq. (B.15) is used in the second equality; both give the same result at this accuracy. These corrections are negligibly small in the relevant parameter space. Altogether, the approximate mass basis \hat{f}_L, \hat{f}_R is defined as

$$\hat{f}_L := (U_{f_L})^\dagger f_L := (U_{f_L}^2)^\dagger (U_{f_L}^1)^\dagger (U_{f_L}^0)^\dagger f_L, \quad (\text{B.22})$$

$$\hat{f}_R := (U_{f_R})^\dagger f_R := (U_{f_R}^2)^\dagger (U_{f_R}^1)^\dagger (U_{f_R}^0)^\dagger f_R. \quad (\text{B.23})$$

B.2 EW Boson Couplings

Couplings of the fermions to SM bosons are completely SM-like at the leading order. The leading order unitary matrices of Eq. (B.2) transforms the $SU(2)_L$ gauge couplings as

$$(U_{f_L}^1)^\dagger (U_{f_L}^0)^\dagger P_5 U_{f_L}^0 U_{f_L}^0 = V_{ij} \oplus \begin{pmatrix} c_{\theta_L} c_{\theta'_L} & -c_{\theta_L} s_{\theta'_L} \\ -s_{\theta_L} c_{\theta'_L} & s_{\theta_L} s_{\theta'_L} \end{pmatrix}, \quad (\text{B.24})$$

$$(U_{f_R}^1)^\dagger (U_{f_R}^0)^\dagger P_5 U_{f_R}^0 U_{f_R}^0 = 0_{3 \times 3} \oplus \begin{pmatrix} c_{\theta_R} c_{\theta'_R} & -c_{\theta_R} s_{\theta'_R} \\ -s_{\theta_R} c_{\theta'_R} & s_{\theta_R} s_{\theta'_R} \end{pmatrix}. \quad (\text{B.25})$$

Here, V_{ij} is a 3×3 unitary matrix, which is an identity matrix for the Z boson couplings where $f = f'$. Since $U_{f_{L,R}}^1$ do not affect SM fermion couplings, only the mixing via $U_{f_{L,R}}^2$ induces flavor violating couplings of SM generations. Their size is estimated as

$$\left[(U_{f_L}^1)^\dagger P_5 U_{f_L}^0 \right]_{ij} = V_{ij} + \mathcal{O} \left(\frac{\tilde{y}_{L_i} \tilde{y}_{L_j} v_H^2}{M_{F_{\text{VL}}}^2} \right), \quad \left[(U_{f_L}^1)^\dagger P_5 U_{f_L}^0 \right]_{ib} = \mathcal{O} \left(\frac{\tilde{y}_{L_i} v_H}{M_{F_{\text{VL}}}} \right), \quad (\text{B.26})$$

$$\left[(U_{f_R}^1)^\dagger P_5 U_{f_R}^0 \right]_{ij} = \mathcal{O} \left(\frac{\tilde{y}_{R_i} \tilde{y}_{R_j} v_H^2}{M_{F_{\text{VL}}}^2} \right), \quad \left[(U_{f_R}^1)^\dagger P_5 U_{f_R}^0 \right]_{ib} = \mathcal{O} \left(\frac{\tilde{y}_{R_i} v_H}{M_{F_{\text{VL}}}} \right), \quad (\text{B.27})$$

where $\tilde{y}_{L(R)_i} \sim \max(\tilde{y}_{L(R)_i}^f, \tilde{y}_{L(R)_i}^{f'})$ and $M_{F_{\text{VL}}}$ is the typical scale of VL fermions.

The Higgs boson couplings are aligned with the mass matrix by the rotation via $U_{f_{L,R}}^0$,

$$(U_{f_R}^0)^\dagger Y_f^h U_{f_L}^0 = \begin{pmatrix} \tilde{y}_i^f \delta_{ij} & \tilde{y}_{L_i}^f & 0_i \\ \tilde{y}_{R_j}^f & \tilde{\lambda}_f & 0 \\ 0_j & 0 & \lambda'_f \end{pmatrix} = v_H^{-1} \left[\tilde{\mathcal{M}}^f \right]_{ij} \Big|_{M_{F_L} = M_{F_R} = 0}. \quad (\text{B.28})$$

Hence, the Yukawa couplings to SM fermions are diagonal in the mass basis if $\tilde{y}_{L,R}^f$ are neglected. The mixing $U_{f_{L,R}}^2$ induces flavor violating couplings of size

$$\left[(U_{f_R}^1)^\dagger Y_f^h U_{f_L}^0 \right]_{ij} = \tilde{y}_i^f \delta_{ij} + \mathcal{O} \left(\frac{\tilde{y}_{L_i}^f \tilde{y}_{L_j}^f v_H^2}{M_{F_{\text{VL}}}^2}, \frac{\tilde{y}_{R_j}^f \tilde{y}_{R_j}^f v_H^2}{M_{F_{\text{VL}}}^2} \right), \quad (\text{B.29})$$

$$\left[(U_{f_R}^1)^\dagger Y_f^h U_{f_L}^0 \right]_{ib} = \mathcal{O} \left(\tilde{y}_{L_i}^f \right), \quad \left[(U_{f_R}^1)^\dagger Y_f^h U_{f_L}^0 \right]_{aj} = \mathcal{O} \left(\tilde{y}_{R_j}^f \right). \quad (\text{B.30})$$

B.3 Charged Leptons

For charged leptons, let us start in a basis in which the upper-left 3×3 block is diagonal,

$$\mathcal{M}^e = \begin{pmatrix} y_i^e \delta_{ij} v_H & 0_i & \lambda_i^E v_\Phi \\ 0_j & \lambda_e v_H & \lambda_V^E v_\phi \\ \lambda_j^L v_\Phi & \lambda_V^L v_\phi & \lambda_e' v_H \end{pmatrix}, \quad (\text{B.31})$$

such that SM-LFV effects are induced only by $\lambda_i^{L,E}$. We can achieve this form by redefining e_{L_i}, e_{R_i} . Such a redefinition does not change the Z and Z' couplings. The W boson couplings are changed, but this can be absorbed by a redefinition of the neutrinos. The Yukawa couplings to the scalars, namely Higgs boson and χ , are still aligned with the mass matrix. In our analysis, we assume that all parameters in the charged lepton sector are real.

There should be sizable mixing between the muon and VL leptons to explain Δa_μ , while mixing involving e or τ can be small to avoid LFV processes. We introduce mixing parameters involving muon,

$$c_{\mu_L} := \frac{\lambda_V^L v_\phi}{M_{E_L}}, \quad s_{\mu_L} := \frac{\lambda_2^L v_\Phi}{M_{E_L}}, \quad c_{\mu_R} := \frac{\lambda_V^E v_\phi}{M_{E_R}}, \quad s_{\mu_R} := \frac{\lambda_2^E v_\Phi}{M_{E_R}}, \quad (\text{B.32})$$

and those for electron and tau,

$$\epsilon_{e_L} := \frac{\lambda_1^L v_\Phi}{\lambda_V^L v_\phi}, \quad \epsilon_{e_R} := \frac{\lambda_1^E v_\Phi}{\lambda_V^E v_\phi}, \quad \epsilon_{\tau_L} := \frac{\lambda_3^L v_\Phi}{\lambda_V^L v_\phi}, \quad \epsilon_{\tau_R} := \frac{\lambda_3^E v_\Phi}{\lambda_V^E v_\phi}. \quad (\text{B.33})$$

We expect $\epsilon_e, \epsilon_\tau \ll 1$ in order to suppress the LFV processes. With these parameterizations, the leading order unitary matrices are given by

$$U_{e_L}^0 = \begin{pmatrix} 1 & -\epsilon_{e_L} s_{\mu_L} & 0 & \epsilon_{e_L} c_{\mu_L} & 0 \\ 0 & c_{\mu_L} & 0 & s_{\mu_L} & 0 \\ 0 & -\epsilon_{\tau_L} s_{\mu_L} & 1 & \epsilon_{\tau_L} c_{\mu_L} & 0 \\ -\epsilon_{e_L} & -s_{\mu_L} & -\epsilon_{\tau_L} & c_{\mu_L} & 0 \\ 0 & 0 & 0 & 0 & 1 \end{pmatrix}, \quad (\text{B.34})$$

$$U_{e_R}^0 = \begin{pmatrix} 1 & -\epsilon_{e_R} s_{\mu_R} & 0 & -\epsilon_{e_R} c_{\mu_R} & 0 \\ 0 & c_{\mu_R} & 0 & s_{\mu_R} & 0 \\ 0 & -\epsilon_{\tau_R} s_{\mu_R} & 1 & -\epsilon_{\tau_R} c_{\mu_R} & 0 \\ -\epsilon_{e_R} & -s_{\mu_R} & -\epsilon_{\tau_R} & c_{\mu_R} & 0 \\ 0 & 0 & 0 & 0 & 1 \end{pmatrix}. \quad (\text{B.35})$$

The diagonal structure of the upper-left 3×3 block holds as far as $\epsilon_{e_{L,R}}, \epsilon_{\tau_{L,R}} \ll 1$. The large mixing with the muon and VL leptons indicate that $\lambda_e \sim y_2^e \sim m_\mu/v_H$ to explain the muon mass without fine-tuning. The Yukawa couplings in the off-diagonal block are given by

$$\tilde{y}_L^e = \begin{pmatrix} c_{\mu_R}(-\lambda_e \epsilon_{e_L} + y_1^e \epsilon_{e_R}) \\ c_{\mu_L} s_{\mu_R} y_2^e - c_{\mu_R} s_{\mu_L} \lambda_e \\ c_{\mu_R}(-\lambda_e \epsilon_{\tau_L} + y_3^e \epsilon_{\tau_R}) \end{pmatrix}, \quad \tilde{y}_R^e = \begin{pmatrix} c_{\mu_L}(-\lambda_e \epsilon_{e_R} + y_1^e \epsilon_{e_L}) \\ c_{\mu_R} s_{\mu_L} y_2^e - \lambda_e c_{\mu_L} s_{\mu_R} \\ c_{\mu_L}(-\lambda_e \epsilon_{\tau_R} + y_3^e \epsilon_{\tau_L}) \end{pmatrix}. \quad (\text{B.36})$$

Their size is estimated as

$$\tilde{y}_{L_1, R_1}^e \lesssim 1.0 \times 10^{-9} \times \left(\frac{\epsilon_e}{10^{-6}} \right) \left(\frac{\max(\lambda_e, y_1^e)}{10^{-3}} \right), \quad (\text{B.37})$$

$$\tilde{y}_{L_2, R_2}^e \lesssim y_2^e \sim 1.0 \times 10^{-3}, \quad (\text{B.38})$$

$$\tilde{y}_{L_3, R_3}^e \lesssim 1.0 \times 10^{-4} \times \left(\frac{\epsilon_\tau}{10^{-2}} \right) \left(\frac{y_3^e}{m_\tau/v_H} \right). \quad (\text{B.39})$$

Hence, the perturbative corrections to the off-diagonal elements are at most,

$$\begin{aligned} \Delta m_{ij}^e &\sim \frac{\tilde{y}_{L_i}^e \tilde{y}_{R_j}^e \lambda_f'}{M_{E_L} M_{E_R}} v_H^3 \lesssim \epsilon_\tau \frac{m_\mu m_\tau}{M_{E_L} M_{E_R}} \lambda_e' v_H \\ &\sim 1.3 \times 10^{-6} \text{ GeV} \times \left(\frac{\epsilon_\tau}{0.01} \right) \left(\frac{500 \text{ GeV}}{\sqrt{M_{E_L} M_{E_R}}} \right)^2 \left(\frac{\lambda_e'}{1.0} \right). \end{aligned} \quad (\text{B.40})$$

Consequently, the basis defined in Eq. (B.22) is very close to the mass basis and flavor violating couplings of the charged leptons to the SM bosons are strongly suppressed.

Using the above results, the Z' couplings to charged leptons are given by

$$-\hat{g}_{e_L}^{Z'} \sim g' \begin{pmatrix} \epsilon_{e_L}^2 & s_{\mu_L} \epsilon_{e_L} & \epsilon_{e_L} \epsilon_{\tau_L} & -c_{\theta_L} c_{\mu_L} \epsilon_{e_L} & s_{\theta_L} c_{\mu_L} \epsilon_{e_L} \\ s_{\mu_L} \epsilon_{e_L} & s_{\mu_L}^2 & s_{\mu_L} \epsilon_{\tau_L} & -c_{\theta_L} c_{\mu_L} s_{\mu_L} & s_{\theta_L} c_{\mu_L} s_{\mu_L} \\ \epsilon_{\tau_L} \epsilon_{e_L} & s_{\mu_L} \epsilon_{\tau_L} & \epsilon_{\tau_L}^2 & -c_{\theta_L} c_{\mu_L} \epsilon_{\tau_L} & s_{\theta_L} c_{\mu_L} \epsilon_{\tau_L} \\ -c_{\theta_L} c_{\mu_L} \epsilon_{e_L} & -c_{\theta_L} c_{\mu_L} s_{\mu_L} & -c_{\theta_L} c_{\mu_L} \epsilon_{\tau_L} & c_{\theta_L}^2 c_{\mu_L}^2 + s_{\theta_L}^2 & c_{\theta_L} s_{\theta_L} s_{\mu_L}^2 \\ s_{\theta_L} c_{\mu_L} \epsilon_{e_L} & s_{\theta_L} c_{\mu_L} s_{\mu_L} & s_{\theta_L} c_{\mu_L} \epsilon_{\tau_L} & c_{\theta_L} s_{\theta_R} s_{\mu_L}^2 & c_{\theta_L}^2 + c_{\mu_L}^2 s_{\theta_L}^2 \end{pmatrix}, \quad (\text{B.41})$$

$$-\hat{g}_{e_R}^{Z'} \sim g' \begin{pmatrix} \epsilon_{e_R}^2 & s_{\mu_R} \epsilon_{e_R} & \epsilon_{e_R} \epsilon_{\tau_R} & -s_{\theta_R} c_{\mu_R} \epsilon_{e_R} & -c_{\theta_R} c_{\mu_R} \epsilon_{e_R} \\ s_{\mu_R} \epsilon_{e_R} & s_{\mu_R}^2 & s_{\mu_R} \epsilon_{\tau_R} & -s_{\theta_R} c_{\mu_R} s_{\mu_R} & -c_{\theta_R} c_{\mu_R} s_{\mu_R} \\ \epsilon_{\tau_R} \epsilon_{e_R} & s_{\mu_R} \epsilon_{\tau_R} & \epsilon_{\tau_R}^2 & -s_{\theta_R} c_{\mu_R} \epsilon_{\tau_R} & -c_{\theta_R} c_{\mu_R} \epsilon_{\tau_R} \\ -s_{\theta_R} c_{\mu_R} \epsilon_{e_R} & -s_{\theta_R} c_{\mu_R} s_{\mu_R} & -s_{\theta_R} c_{\mu_R} \epsilon_{\tau_R} & c_{\theta_R}^2 + s_{\theta_R}^2 c_{\mu_R}^2 & -c_{\theta_R} s_{\theta_R} s_{\mu_R}^2 \\ -c_{\theta_R} c_{\mu_R} \epsilon_{e_R} & -c_{\theta_R} c_{\mu_R} s_{\mu_R} & -c_{\theta_R} c_{\mu_R} \epsilon_{\tau_R} & -c_{\theta_R} s_{\theta_R} s_{\mu_R}^2 & s_{\theta_R}^2 + c_{\mu_R}^2 c_{\theta_R}^2 \end{pmatrix}. \quad (\text{B.42})$$

The mixing effects from $U_{e_{L,R}}^2$ are neglected. In the same approximation, the off-diagonal Yukawa couplings of χ to VL and SM fermions are given by

$$\left[\hat{Y}_e^\chi \right]_{aj} = \frac{c_{\mu_L} M_{E_L}}{v_\Phi} \begin{pmatrix} c_{\theta_R} \epsilon_{e_L} & c_{\theta_R} s_{\mu_L} & c_{\theta_R} \epsilon_{\tau_L} \\ -s_{\theta_R} \epsilon_{e_L} & -s_{\theta_R} s_{\mu_L} & -s_{\theta_R} \epsilon_{\tau_L} \end{pmatrix}, \quad (\text{B.43})$$

$$\left[\hat{Y}_e^\chi \right]_{ib} = \frac{c_{\mu_R} M_{E_R}}{v_\Phi} \begin{pmatrix} s_{\theta_L} \epsilon_{e_R} & c_{\theta_L} \epsilon_{e_R} \\ s_{\theta_L} s_{\mu_R} & c_{\theta_L} s_{\mu_R} \\ s_{\theta_L} \epsilon_{\tau_R} & c_{\theta_L} \epsilon_{\tau_R} \end{pmatrix}. \quad (\text{B.44})$$

Unlike the Z' boson, χ does not couple to SM fermions unless $U_{e_{L,R}}^2$ is taken into account. The Yukawa couplings to the SM leptons are estimated as

$$\left[\hat{Y}_e^\chi\right]_{ij} \lesssim \frac{1}{M_{E_{VL}}} \begin{pmatrix} \epsilon_e^2 m_e & \epsilon_e m_\mu & \epsilon_e \epsilon_\tau m_\tau \\ \epsilon_e m_\mu & m_\mu & \epsilon_\tau m_\tau \\ \epsilon_e \epsilon_\tau m_\tau & \epsilon_\tau m_\tau & \epsilon_\tau^2 m_\tau \end{pmatrix}, \quad (\text{B.45})$$

where ϵ_e , ϵ_τ and $M_{E_{VL}}$ are typical values of $\epsilon_{e_{L,R}}$, $\epsilon_{\tau_{L,R}}$ and VL lepton masses, respectively. Thus, the χ couplings to two SM fermions have an extra suppression factor $m_\ell/M_{E_{L,R}}$ compared with the Z' couplings, while those to one SM fermion and one VL fermion do not have this suppression. The couplings of σ are similar in structure than those of χ . However the mass of σ is not bounded by v_Φ implying that its effects can be decoupled for large v_ϕ .

Using above results, the leading contribution to Δa_μ from Z' and χ boson can be estimated by Eq. (3.14). Here we want to give more details on the combination of loop functions C_{LR} appearing there. The relevant combination of loop functions is defined as

$$C_{LR} := \frac{\tilde{M}_{E_L}}{\lambda'_e v_H} \left(c_{\theta_L} s_{\theta_R} G_Z(x_L) + s_{\theta_L} c_{\theta_R} \frac{M_{E_L} M_{E_R}}{2m_\chi^2} G_S(y_L) \right) - \frac{\tilde{M}_{E_R}}{\lambda'_e v_H} \left(s_{\theta_L} c_{\theta_R} G_Z(x_R) + c_{\theta_L} s_{\theta_R} \frac{M_{E_L} M_{E_R}}{2m_\chi^2} G_S(y_R) \right), \quad (\text{B.46})$$

where $x_{L,R} := \tilde{M}_{E_{L,R}}^2/m_{Z'}^2$, $y_{L,R} := \tilde{M}_{E_{L,R}}^2/m_\chi^2$. This is straightforwardly obtained from the sum of Eqs. (3.3) and (3.11), while using our approximations above. For large enough mass splitting, $\lambda'_e v_H \ll |\Delta_E|$ we can use Eq. (B.11) to simplify this expression to

$$C_{LR} = \sqrt{x_L x_R} \frac{G_Z(x_L) - G_Z(x_R)}{x_L - x_R} + \frac{1}{2} \sqrt{y_L y_R} \frac{y_L G_S(y_L) - y_R G_S(y_R)}{y_L - y_R} + \mathcal{O}\left(\frac{\lambda'_e v_H}{\Delta_E}\right). \quad (\text{B.47})$$

On the other hand, if the VL mass splitting is small, $|\Delta_E| \ll M_E$, we obtain the following formula by using Eq. (B.15),

$$C_{LR} = x \frac{dG_Z(x)}{dx} + \frac{y}{2} \frac{d(y G_S(y))}{dy} + \mathcal{O}\left(\frac{\mu_E}{M_E}\right), \quad (\text{B.48})$$

where $x := M_E^2/m_{Z'}^2$ and $y := M_E^2/m_\chi^2$ and M_E , Δ_E and μ_E are defined in Eq. (B.14). This expression is identical to the form which is obtained by taking a limit $M_{E_L} \rightarrow M_{E_R}$ or $\Delta_E \rightarrow 0$, in C_{LR} of Eq. (B.47). Hence, C_{LR} in Eq. (B.47) is a good approximation even if $\lambda'_e v_H \sim \Delta_E$. Formulae for $\mu \rightarrow e\gamma$ and $\tau \rightarrow \mu\gamma$, Eq. (3.33) and (3.34), are obtained in an analogous way.

Relatively light VL leptons with large Higgs Yukawa couplings (necessary to explain Δa_μ by chiral enhancement) may contribute significantly to $h \rightarrow \gamma\gamma$. The Higgs couplings

to VL leptons are approximately given by

$$\left[\hat{Y}_e^h\right]_{ab} \sim \lambda'_e \begin{pmatrix} c_{\theta_R} s_{\theta_L} & c_{\theta_R} c_{\theta_L} \\ -s_{\theta_R} s_{\theta_L} & -s_{\theta_R} c_{\theta_L} \end{pmatrix}, \quad (\text{B.49})$$

where λ_e is neglected. The amplitude of $h \rightarrow \gamma\gamma$ from the VL lepton loop is given by

$$\sum_{X=L,R} \frac{y_{E_X} v_H}{\tilde{M}_{E_X}} A_{1/2}^H(\tau_{E_X}) \sim \frac{(\lambda'_e v_H)^2}{\tilde{M}_{E_L}^2 - \tilde{M}_{E_R}^2} (A_{1/2}^H(\tau_{E_L}) - A_{1/2}^H(\tau_{E_R})), \quad (\text{B.50})$$

with $\tau_{E_{L,R}} := m_H^2/4\tilde{M}_{E_{L,R}}^2$. Again, the same result is obtained by using Eq. (B.11) or Eq. (B.15), for small ($|\lambda'_e| v_H \ll |\Delta_E|$) or large ($|\lambda'_e| v_H, |\Delta_E| \ll M_E$) VL mass splitting, respectively.

B.4 Quarks

Before starting the analytical discussion of the quark couplings, let us obtain an estimate for the necessary size of such couplings. Based on above results one finds that

$$\left[\hat{g}_{e_R}^{Z'} + \hat{g}_{e_L}^{Z'}\right]_{22} = g'(s_{\mu_L}^2 + s_{\mu_R}^2) \sim g' \quad (\text{B.51})$$

is required in order to explain Δa_μ . The Z' contribution to C_9^μ can then be estimated as

$$|C_9^\mu| \sim 1.0 \times \left(\frac{0.3}{g'}\right) \left(\frac{1 \text{ TeV}}{v_\Phi}\right)^2 \left(\frac{s_{\mu_L}^2 + s_{\mu_R}^2}{1.0}\right) \left(\frac{[\hat{g}_{d_L}^{Z'}]_{23}}{0.001}\right). \quad (\text{B.52})$$

Thus, the $b \rightarrow sl^+\ell^-$ anomalies can be explained even with the permille Z' couplings to quarks.

Let us start the discussion of quark mass diagonalization in a basis where the upper-left blocks of the quark mass matrices have already been diagonalized,

$$\mathcal{M}^u = \begin{pmatrix} y_i^u \delta_{ij} v_H & 0_i & \lambda_i^U v_\Phi \\ 0_j & \lambda_u v_H & \lambda_V^U v_\phi \\ \lambda_j^Q v_\Phi & \lambda_V^Q v_\phi & \lambda'_u v_H \end{pmatrix}, \quad \mathcal{M}^d = \begin{pmatrix} y_i^d \delta_{ij} v_H & 0_i & \lambda_i^D v_\Phi \\ 0_j & \lambda_d v_H & \lambda_V^D v_\phi \\ \lambda_j^Q v_\Phi & \lambda_V^Q v_\phi & \lambda'_d v_H \end{pmatrix}. \quad (\text{B.53})$$

The quark couplings to the Higgs, Z , and Z' bosons is the same as in the gauge basis, while the W boson couplings (2.29) are changed to

$$\mathcal{L}_W = \frac{g}{\sqrt{2}} W_\mu^+ \bar{u} \gamma^\mu \left[\begin{pmatrix} V_{ij} & 0_i & 0_i \\ 0_j & 1 & 0 \\ 0_j & 0 & 0 \end{pmatrix} P_L + \begin{pmatrix} 0_{ij} & 0_i & 0_i \\ 0_j & 0 & 0 \\ 0_j & 0 & 1 \end{pmatrix} P_R \right] d + \text{h.c.} \quad (\text{B.54})$$

Here, $V_{ij} \sim V_{\text{CKM}}$ is expected because of the small mixings between VL and SM quarks. In general, the mass matrices can be diagonalized exactly in the same way as for the charged leptons in the previous section, but all mixing angles can be taken to be small. We define the small mixing angles,

$$\epsilon_{Q_i} := \frac{v_\Phi \lambda_i^Q}{\lambda_V^Q v_\phi}, \quad \epsilon_{U_i} := \frac{v_\Phi \lambda_i^U}{\lambda_V^U v_\phi}, \quad \epsilon_{D_i} := \frac{v_\Phi \lambda_i^D}{\lambda_V^D v_\phi}. \quad (\text{B.55})$$

With this parametrization, the unitary matrices are

$$U_{u_L}^0 = U_{d_L}^0 = \begin{pmatrix} 1 & 0 & 0 & \epsilon_{Q_1} & 0 \\ 0 & 1 - \epsilon_{Q_2}^2/2 & -\epsilon_{Q_2}\epsilon_{Q_3} & \epsilon_{Q_2} & 0 \\ 0 & 0 & 1 - \epsilon_{Q_3}^2/2 & \epsilon_{Q_3} & 0 \\ -\epsilon_{Q_1} & -\epsilon_{Q_2} & -\epsilon_{Q_3} & 1 - (\epsilon_{Q_2}^2 + \epsilon_{Q_3}^2)/2 & 0 \\ 0 & 0 & 0 & 0 & 1 \end{pmatrix}, \quad (\text{B.56})$$

$$U_{u_R}^0 = \begin{pmatrix} \delta_{ij} & \epsilon_{U_i} & 0_i \\ -\epsilon_{U_j} & 1 & 0 \\ 0_j & 0 & 1 \end{pmatrix}, \quad U_{d_R}^0 = \begin{pmatrix} \delta_{ij} & \epsilon_{D_i} & 0_i \\ -\epsilon_{D_j} & 1 & 0 \\ 0_j & 0 & 1 \end{pmatrix}. \quad (\text{B.57})$$

Here, we keep terms of $\mathcal{O}(\epsilon_{Q_{2,3}}^2)$ and linear for the other angles. The Yukawa couplings in the off-diagonal elements of (B.6) are given by

$$\tilde{y}_{R_i}^u \sim \epsilon_{Q_i} y_i^u, \quad \tilde{y}_{L_i}^u \sim \epsilon_{U_i} y_i^u, \quad \tilde{y}_{R_i}^d \sim \epsilon_{Q_i} y_i^d, \quad \tilde{y}_{L_i}^d \sim \epsilon_{D_i} y_i^d. \quad (\text{B.58})$$

The perturbative correction to the SM up quark mass matrix is

$$\begin{aligned} \Delta m_{ij}^u &\sim -\epsilon_{U_i} \epsilon_{Q_j} y_i^u y_j^u \frac{\lambda'_u v_H^2}{M_{U_L} M_{U_R}} \\ &\sim 1.0 \times 10^{-8} \text{ GeV} \times \left(\frac{\sqrt{\epsilon_{U_i} \epsilon_{Q_j}}}{10^{-2}} \right)^2 \left(\frac{\lambda'_u}{1.0} \right) \left(\frac{\sqrt{m_{u_i} m_{u_j}}}{15 \text{ GeV}} \right)^2 \left(\frac{1.5 \text{ TeV}}{\sqrt{M_{U_L} M_{U_R}}} \right)^2, \end{aligned} \quad (\text{B.59})$$

where the $M_{U_{L(R)}}$ is the left-handed (right-handed) VL quark mass $\sim \lambda_V^{Q(U)} v_\phi$. Hence, the basis defined as in Eq. (B.22) is to a very good approximation the mass basis. Perturbative corrections for the down quarks are even smaller due to their lighter masses.

The Z' boson couplings are estimated as

$$\left[\hat{g}_{u_L}^{Z'} \right]_{ij} = \left[\hat{g}_{d_L}^{Z'} \right]_{ij} \sim g' \epsilon_{Q_i} \epsilon_{Q_j}, \quad \left[\hat{g}_{u_R}^{Z'} \right]_{ij} \sim g' \epsilon_{U_i} \epsilon_{U_j}, \quad \left[\hat{g}_{d_R}^{Z'} \right]_{ij} \sim g' \epsilon_{D_i} \epsilon_{D_j}. \quad (\text{B.60})$$

Thus, the $b \rightarrow sl^+ \ell^-$ anomaly requires $\epsilon_{Q_2} \epsilon_{Q_3} \sim 10^{-3}$.

We now estimate the couplings to Z and Higgs boson. We focus on the up quark sector, where mixing effects are larger due to the heavy top quark. The Higgs Yukawa coupling are estimated as

$$\left[(U_L^u)^\dagger Y_u^h U_R^u \right]_{ij} - y_i^u \delta_{ij} \sim 1.3 \times 10^{-4} \times \left(\frac{\sqrt{\epsilon_{Q_i} \epsilon_{Q_j}}}{0.1} \right)^2 \left(\frac{\sqrt{m_{u_i} m_{u_j}}}{170 \text{ GeV}} \right)^2 \left(\frac{1.5 \text{ TeV}}{M_{U_{\text{VL}}}} \right)^2 \quad (\text{B.61})$$

and the weak-isospin part of the Z boson couplings are

$$\left[(U_L^u)^\dagger P_5 U_L^u \right]_{ij} - \delta_{ij} \sim 1.3 \times 10^{-6} \times \left(\frac{\sqrt{\epsilon_{U_i} \epsilon_{U_j}}}{0.01} \right)^2 \left(\frac{\sqrt{m_{u_i} m_{u_j}}}{170 \text{ GeV}} \right)^2 \left(\frac{1.5 \text{ TeV}}{M_{U_{\text{VL}}}} \right)^2, \quad (\text{B.62})$$

$$\left[(U_R^u)^\dagger P_5 U_R^u \right]_{ij} \sim 1.3 \times 10^{-4} \times \left(\frac{\sqrt{\epsilon_{Q_i} \epsilon_{Q_j}}}{0.1} \right)^2 \left(\frac{\sqrt{m_{u_i} m_{u_j}}}{170 \text{ GeV}} \right)^2 \left(\frac{1.5 \text{ TeV}}{M_{U_{\text{VL}}}} \right)^2, \quad (\text{B.63})$$

where $M_{U_{\text{VL}}}$ is a typical VL up quark mass. Thus, the EW boson couplings to the SM up quarks do not significantly deviated from their SM values. Those for the down quarks are even more suppressed by the smaller down quark masses.

The W boson couplings to the right-handed SM quarks are estimated as

$$\left[(U_R^u)^\dagger P_5 U_R^d \right]_{ij} \sim 1.3 \times 10^{-4} \times \left(\frac{\sqrt{\epsilon_{Q_i} \epsilon_{Q_j}}}{0.1} \right)^2 \left(\frac{\sqrt{m_{u_i} m_{u_j}}}{170 \text{ GeV}} \right)^2 \left(\frac{1.5 \text{ TeV}}{M_{U_{\text{VL}}}} \right)^2. \quad (\text{B.64})$$

An estimation of the non-unitarity of the extended CKM matrix has already been given in Eq. (3.105). In addition, the off-diagonal elements involving the VL quarks are

$$\left[\hat{V}_{\text{CKM}} \right]_{4j} \sim 0, \quad \left[\hat{V}_{\text{CKM}} \right]_{5j} \sim \sum_{k=1,2,3} \frac{\tilde{y}_{L_k}^{u*} v_H}{M_{U_R}} V_{kj} \sim \epsilon_{U_3} \frac{m_t}{M_{U_R}} V_{3j}, \quad (\text{B.65})$$

$$\left[\hat{V}_{\text{CKM}} \right]_{i4} \sim 0, \quad \left[\hat{V}_{\text{CKM}} \right]_{i5} \sim \sum_{k=1,2,3} \frac{\tilde{y}_{L_k}^d v_H}{M_{D_R}} V_{ik} \sim \epsilon_{D_3} \frac{m_b}{M_{D_R}} V_{i3}, \quad (\text{B.66})$$

where we have neglected terms in $U_{u_{L,R}}^1, U_{d_{L,R}}^1$ of $\mathcal{O}(s_{u_{L,R}}, s_{d_{L,R}})$. These effects are much smaller for quarks as compared to charged leptons owing to the heavier VL quark masses.

B.5 Neutrinos

We consider the type-I seesaw mechanism with Majorana masses $M_{\text{Maj}} \sim 10^{14}$ GeV. In this model, there are three left-handed Majorana neutrinos, $m_{\nu_L} \sim v_H^2/M_{\text{Maj}}$, three right-handed Majorana neutrinos, $m_{\nu_R} \sim M_{\text{Maj}}$ and two vector-like Dirac neutrinos, $m_N \sim v_\Phi$. Here we want to show that the mixings among these three types of neutrinos are suppressed by the large Majorana mass terms.

The 10×10 mass matrix in Eq. (2.15) is diagonalized as follows. At first, we rotate only the left-handed neutrinos as

$$\begin{pmatrix} \nu_{L_i} \\ N'_L \\ N_L \end{pmatrix} =: V_L^n \begin{pmatrix} \tilde{\nu}_{L_i} \\ \tilde{N}'_L \\ \tilde{N}_L \end{pmatrix}, \quad (\text{B.67})$$

with a unitary matrix V_L^n which is given by

$$V_L^n = U_{n_L}^0 U_{n_L}^1, \quad U_{n_L}^0 = \begin{pmatrix} \mathbf{1}_{ij} & 0_i & 0_i \\ 0_j & c_N & s_N e^{i\phi_N} \\ 0_j & -s_N e^{-i\phi_N} & c_N \end{pmatrix}, \quad U_{n_L}^1 = \begin{pmatrix} \mathbf{z}_{Nj} & \mathbf{n}_N & \mathbf{0} \\ 0_j & 0 & 1 \end{pmatrix}. \quad (\text{B.68})$$

Here,

$$c_N := \frac{|\lambda_V^N| v_\phi}{\tilde{M}_N}, \quad s_N := \frac{|\lambda_n| v_H}{\tilde{M}_N}, \quad \text{with} \quad \tilde{M}_N := \sqrt{|\lambda_V^N v_\phi|^2 + |\lambda_n v_H|^2}, \quad (\text{B.69})$$

and $\phi_N := \text{Arg}(\lambda_V^N) - \text{Arg}(\lambda_n)$. The four-component vectors $\mathbf{z}_{N_i}, \mathbf{n}_N$ satisfy

$$\mathbf{z}_{N_i}^\dagger \mathbf{z}_{N_j} = \delta_{ij}, \quad \mathbf{z}_{N_i}^\dagger \mathbf{n}_N = 0, \quad \mathbf{n}_N = \tilde{M}_L^{-1} \left(\lambda_j^L v_\phi, \quad c_N \lambda_V^L v_\phi - s_N e^{-i\phi_N} \lambda_n' v_H \right)^\text{T}, \quad (\text{B.70})$$

where \tilde{M}_L is defined as the normalization factor of $\mathbf{n}_N^\dagger \mathbf{n}_N = 1$. The Dirac matrix after this rotation is given by

$$\tilde{\mathcal{M}}^n := \mathcal{M}^n V_L^n =: \begin{pmatrix} \tilde{m}_{ij}^n & \mu_i^n & \mu_i' \\ 0_j & 0 & \tilde{M}_N \\ 0_j & \tilde{M}_L & \tilde{m}_5 \end{pmatrix} =: \begin{pmatrix} \tilde{m}_{ij}^n & \mu_{ib} \\ 0_{aj} & M_{ab}^D \end{pmatrix}, \quad M^D := \begin{pmatrix} 0 & \tilde{M}_N \\ \tilde{M}_L & \tilde{m}_5 \end{pmatrix}, \quad (\text{B.71})$$

where $a, b = 4, 5$. Owing to the first rotation $U_{n_L}^0$, the first three columns in the 4th and 5th rows in $\tilde{\mathcal{M}}^n$ are all zero and there is no mixing between the singlet-like VL neutrinos (\bar{N}_R, \bar{N}'_R) and left-handed light neutrinos $\tilde{\nu}_L$.

Back in the full 10×10 matrix (recall Eqs. (2.15) and (2.16)), we note that only the first three rows couple to ν_{R_i} and they will have $\mathcal{O}(M_{\text{Maj}})$ masses. Therefore, $\tilde{\nu}_{L_i}$ are approximately the light Majorana neutrinos, while $\tilde{N}'_L, \tilde{N}_L$ together with N'_R, N_R form approximately Dirac neutrinos. After integrating out the $\mathcal{O}(M_{\text{Maj}})$ right-handed neutrinos, the effective 7×7 mass matrix is given by

$$\begin{pmatrix} \bar{N}_R & \bar{N}'_R & \tilde{\nu}_L^c & \tilde{N}'_L{}^c & \tilde{N}_L{}^c \end{pmatrix} \begin{pmatrix} 0_{2 \times 2} & 0_{2 \times 3} & M^D \\ 0_{3 \times 2} & m_\nu & \epsilon_{3 \times 2} \\ (M^D)^\text{T} & \epsilon_{2 \times 3} & \epsilon_{2 \times 2} \end{pmatrix} \begin{pmatrix} N_R^c \\ N_R'^c \\ \tilde{\nu}_L \\ \tilde{N}'_L \\ \tilde{N}_L \end{pmatrix}, \quad (\text{B.72})$$

where $\epsilon_{2 \times 3}, \epsilon_{2 \times 2}, \epsilon_{3 \times 2}$ are mass parameters suppressed by the Majorana mass term such as $(\mu^n)^\text{T} M_{\text{Maj}}^{-1} \mu^n$. These terms are at most of $\mathcal{O}(v_\Phi^2/M_{\text{Maj}})$ and, therefore, negligible compared to M^D . The 3×3 effective Majorana mass matrix m_ν for the active neutrinos $\tilde{\nu}_L$ is given by

$$m_\nu = -(\tilde{m}^n)^\text{T} M_{\text{Maj}}^{-1} \tilde{m}^n. \quad (\text{B.73})$$

Altogether, the mass terms for the neutrinos are decomposed as

$$\begin{aligned}\mathcal{L}_{\text{neutrino}} &= \mathcal{L}_R + \mathcal{L}_\nu + \mathcal{L}_D \\ &= \frac{1}{2}\bar{\nu}_R M_{\text{Maj}} \nu_R^c + \frac{1}{2}\bar{\nu}_L^c m_\nu \tilde{\nu}_L + \left[\left(\bar{N}_R \quad \bar{N}'_R \right) M^D \begin{pmatrix} \tilde{N}'_L \\ \tilde{N}_L \end{pmatrix} + \text{h.c.} \right],\end{aligned}\quad (\text{B.74})$$

where the family indices are omitted. The mixing terms among the three types of neutrinos, namely $\tilde{\nu}_L, \nu_R$ and the Dirac neutrinos, are all suppressed by M_{Maj} and not stated.

The remaining mass matrices then are diagonalized as

$$(u_R^N)^\dagger M_D u_L^N = \text{diag}(M_{N_1}, M_{N_2}), \quad (\text{B.75})$$

and

$$(u_R^n)^T M_{\text{Maj}} u_R^n = \text{diag}(M_1, M_2, M_3), \quad (u_L^n)^T m_\nu u_L^n = \text{diag}(m_{\nu_1}, m_{\nu_2}, m_{\nu_3}). \quad (\text{B.76})$$

The mass basis for the active neutrinos $\hat{\nu}_L$, heavy right-handed neutrinos $\hat{\nu}_R$ and Dirac neutrinos $\hat{N}^a := (\hat{N}_L^a, \hat{N}_R^a)$ are given by

$$[\hat{\nu}_L]_i = [(u_L^n)^\dagger]_{ij} [(V_L^n)^\dagger]_{jA} [\nu_L]_A, \quad [\hat{N}_L]_a = [(u_L^N)^\dagger]_{ab} [(V_L^n)^\dagger]_{bA} [\nu_L]_A, \quad (\text{B.77})$$

$$[\hat{\nu}_R]_i = [(u_R^n)^\dagger]_{ij} [\nu_R]_j, \quad [\hat{N}_R]_a = [(u_R^N)^\dagger]_{ab} [\nu_R]_b, \quad (\text{B.78})$$

where $i, j = 1, 2, 3$, $a, b = 4, 5$, and $A = 1, 2, 3, 4, 5$. Altogether, the relation between the mass and gauge basis is

$$n_L = U_L^n \hat{n}_L := V_L^n \begin{pmatrix} u_L^n & 0_{3 \times 2} \\ 0_{2 \times 3} & u_L^N \end{pmatrix} \begin{pmatrix} \hat{\nu}_L \\ \hat{N}_L \end{pmatrix}, \quad n_R = U_R^n \hat{n}_R := \begin{pmatrix} u_R^n & 0_{3 \times 2} \\ 0_{2 \times 3} & u_R^N \end{pmatrix} \begin{pmatrix} \hat{\nu}_R \\ \hat{N}_R \end{pmatrix}. \quad (\text{B.79})$$

The mixing between the left- and right-handed neutrinos is suppressed by the heavy Majorana masses, and therefore negligible.

The W boson coupling to the SM leptons is given by

$$\mathcal{L}_W = \frac{g}{\sqrt{2}} W_\mu^- \bar{e}_i \gamma^\mu P_L [U_{e_L}^\dagger P_{\bar{5}} V_L^n]_{ik} [u_L^n]_{kj} [\hat{\nu}_L]_j + \text{h.c.}, \quad (\text{B.80})$$

where $k = 1, 2, 3$. Therefore, we define flavor neutrino states ν_f and the 3×3 PMNS matrix as

$$\nu_f := V_{\text{PMNS}} \hat{\nu}_L, \quad [V_{\text{PMNS}}]_{ij} := \sum_{k=1,2,3} [U_{e_L}^\dagger P_{\bar{5}} V_L^n]_{ik} [u_L^n]_{kj}. \quad (\text{B.81})$$

The PMNS matrix is not unitary here. The non-unitarity comes from a misalignment between \mathbf{n}_N and \mathbf{n}_L^e (defined in Eqs. (B.70) and (B.3), respectively), and the small mixing $U_{e_L}^2$ defined in Eq. (B.18). The mixing with the $\mathcal{O}(\text{TeV})$ Dirac neutrino can be substantial

if $\lambda_n \sim \mathcal{O}(1)$. This would be an interesting possibility but is beyond the scope of the present paper. We restrict ourselves to the case where λ_n is as small as λ_e and the mixing between active and new Dirac neutrinos is negligible. In this case, the Z' boson couplings to the flavor neutrinos defined in Eq. (B.81) is given by

$$\mathcal{L}_{Z'\nu_f} = g' Z'_\rho \bar{\nu}_i [U_{nL}^\dagger Q'_{nL} U_{nL}]_{ij} \gamma^\rho P_L \hat{\nu}_j = g' Z'_\rho \bar{\nu}_{fi} [U_{eL}^\dagger Q'_{nL} U_{eL}]_{ij} \gamma^\rho P_L \nu_{fj}. \quad (\text{B.82})$$

Hence, the coupling of Z' to muon neutrinos can be estimated as

$$\mathcal{L}_{Z'\nu_\mu} \sim -s_{\mu L}^2 g' Z'_\rho \bar{\nu}_\mu \gamma^\rho P_L \nu_\mu + \mathcal{O}(\epsilon_{eL}, \epsilon_{\tau L}), \quad (\text{B.83})$$

where we have omitted couplings involving the Dirac neutrinos. The electron and tau neutrinos have tiny couplings to Z' due to the tiny mixing angles $\epsilon_{eL}, \epsilon_{\tau L}$.

We can find parameters consistent with the experimental results on neutrino mass differences and PMNS mixing [25]. This can be done by fitting the Yukawa couplings involving the three generations of active neutrinos and the Majorana masses. The explicit values of the neutrino Yukawa couplings at the best fit points are shown in the subsequent section of the appendix. For simplicity, we always assume $\lambda_i^N = 0_i$, $M_{\text{Maj}}^{ij} = M_0 \delta_{ij}$ and take the lightest neutrino to be massless. However, nothing in our analysis really depends on these assumptions. All of our fit points realize the experimental values of the mass differences,

$$\Delta m_{21}^2 = 7.37 \times 10^{-5} \text{ eV}^2, \quad \Delta m_{31}^2 = 2.56 \times 10^{-3} \text{ eV}^2, \quad (\text{B.84})$$

mixing angles

$$\sin^2 \theta_{12} = 0.297, \quad \sin^2 \theta_{23} = 0.425, \quad \sin^2 \theta_{13} = 0.0215, \quad (\text{B.85})$$

and the rephasing invariant

$$J_{\text{CP}} := \text{Im} (V_{\text{PMNS}}^{23} V_{\text{PMNS}}^{13*} V_{\text{PMNS}}^{12} V_{\text{PMNS}}^{22*}) = -0.03, \quad (\text{B.86})$$

within numerical errors. The Majorana mass is set to $M_0 = 10^{14}$ GeV.

C Input Parameters at Best Fit Points

C.1 Best Fit Point A

Values of the inputs parameters for the boson sector are given by

$$m_{Z'} = 277.608, \quad v_\phi = 4079.3, \quad g' = 0.250042, \quad \lambda_\chi = 0.689454, \quad \lambda_\sigma = 0.210518.$$

Values for fermion mass matrices are

$$M_e = \begin{pmatrix} 0.000486575 & 0.000000322078 & -0.0000009971 & 0 & 0.000201232 \\ 0.0000000453521 & 0.159775 & 0.00162206 & 0 & -153.074 \\ -0.0000614248 & -0.00512644 & -1.74616 & 0 & -0.0409467 \\ 0 & 0 & 0 & 0.0000361209 & 448.074 \\ -0.00000237863 & -312.626 & 0.0547758 & 289.432 & -174.104 \end{pmatrix},$$

$$M_n = \begin{pmatrix} 0. & 0. & 0. & 0 & 0 \\ -15.7947 & 28.3788 \cdot e^{-0.0735218i} & 15.4093 \cdot e^{0.107535i} & 0 & 0 \\ 10.4292 \cdot e^{1.19397i} & 67.3777 \cdot e^{0.0000000228655i} & -53.4556 & 0 & 0 \\ 0 & 0 & 0 & 1.54426 & -454.964 \\ -0.00000237863 & -312.626 & 0.0547758 & 289.357 & -21.7762 \end{pmatrix},$$

$$M_u = \begin{pmatrix} 0.000893504 & 0.00562655 & 0.688382 \cdot e^{1.52313i} & 0 & -0.0228009 \\ -0.000172924 & 0.631189 & -0.119538 & 0 & -40.8575 \\ 0.535431 \cdot e^{1.72288i} & 4.4472 & -171.657 & 0 & -8.7671 \\ 0 & 0 & 0 & -0.000301965 & -3596.52 \\ 0.0051151 & 214.302 & -96.8583 & 3445.76 & 5.50646 \end{pmatrix},$$

$$M_d = \begin{pmatrix} 0.0121338 & 0.0527148 & 0.0199472 \cdot e^{-3.08081i} & 0 & -0.0254167 \\ -0.00528222 & -0.0409769 & -2.58755 & 0 & -41.2307 \\ 0.00189847 \cdot e^{-1.62491i} & -0.0198056 & -1.21195 & 0 & 6.1041 \\ 0 & 0 & 0 & -0.122713 & -1571.54 \\ 0.0051151 & 214.302 & -96.8583 & 3445.76 & -1.99223 \end{pmatrix}.$$

C.2 Best Fit point B

Values of the inputs parameters for the boson sector are given by

$$m_{Z'} = 535.334, \quad v_\phi = 3121.37, \quad g' = 0.340407, \quad \lambda_\chi = 0.0062973, \quad \lambda_\sigma = 0.00109477.$$

The fermion mass matrices are

$$M_e = \begin{pmatrix} 0.000486573 & 0.00000134295 & -0.0000688018 & 0 & 0.0000061799 \\ -0.000000884741 & 0.174184 & 0.00486889 & 0 & 684.361 \\ -0.00000034416 & 0.00029932 & 1.74617 & 0 & -0.0829304 \\ 0 & 0 & 0 & 0.0000177937 & 1115.66 \\ 0.000428239 & 926.678 & 0.0199536 & 887.77 & -174.061 \end{pmatrix},$$

$$M_n = \begin{pmatrix} 0. & 0. & 0. & 0 & 0 \\ -15.7951 & 27.8222 \cdot e^{3.06781i} & 15.4457 \cdot e^{-3.03449i} & 0 & 0 \\ 10.43 \cdot e^{1.19378i} & -66.2876 & 53.3662 \cdot e^{0.0000000376777i} & 0 & 0 \\ 0 & 0 & 0 & -1.21561 & -1069.88 \\ 0.000428239 & 926.678 & 0.0199536 & 887.769 & 0.540635 \end{pmatrix},$$

$$M_u = \begin{pmatrix} -0.00312202 & -0.0252024 & 0.0072623 \cdot e^{-1.88131i} & 0 & -0.649726 \\ 0.17765 & -5.43688 & 167.589 & 0 & -1.65829 \\ 0.0045274 \cdot e^{-1.07337i} & 2.00559 & -41.9368 & 0 & -8.95522 \\ 0 & 0 & 0 & -0.00177389 & -1852.98 \\ 0.0376789 & 93.9529 & -311.597 & 2728.52 & -0.157394 \end{pmatrix},$$

$$M_d = \begin{pmatrix} -0.00346891 & -0.000644624 & 2.63889 \cdot e^{-1.76496i} & 0 & 0.00777153 \\ 0.00266115 & 0.00621731 & -0.0159 & 0 & 34.7376 \\ 0.0116163 \cdot e^{1.39463i} & 0.0575321 & 1.13518 & 0 & -5.3196 \\ 0 & 0 & 0 & -0.00422283 & 2130.63 \\ 0.0376789 & 93.9529 & -311.597 & 2728.52 & 0.0672149 \end{pmatrix}.$$

C.3 Best Fit point C

Values of the inputs parameters for the boson sector are given by

$$m_{Z'} = 486.709, \quad v_\phi = 4980.22, \quad g' = 0.322661, \quad \lambda_\chi = 1., \quad \lambda_\sigma = 0.674008.$$

Values for fermion mass matrices are

$$M_e = \begin{pmatrix} -0.000486574 & -0.000000218258 & 0.0000503735 & 0 & 0.00061118 \\ 0.00000012205 & 0.367187 & -0.000101055 & 0 & -305.194 \\ -0.00000174729 & -0.000547026 & 1.74617 & 0 & 0.0455051 \\ 0 & 0 & 0 & 0.00551033 & 406.321 \\ -0.000421884 & -500.988 & 0.00636737 & -193.583 & -174.104 \end{pmatrix},$$

$$M_n = \begin{pmatrix} 0. & 0. & 0. & 0 & 0 \\ 15.7952 \cdot e^{-0.0000000265697i} & 53.3929 \cdot e^{3.06779i} & 15.4488 \cdot e^{0.107064i} & 0 & 0 \\ 10.4299 \cdot e^{-1.94779i} & -127.249 & -53.3586 & 0 & 0 \\ 0 & 0 & 0 & 0.362325 & -4980.22 \\ -0.000421884 & -500.988 & 0.00636737 & -193.583 & -0.0644098 \end{pmatrix},$$

$$M_u = \begin{pmatrix} 0.00527096 & 0.251612 & 0.000517685 \cdot e^{-1.90963i} & 0 & -0.00571705 \\ 0.0154127 & 0.567102 & -0.200693 & 0 & -90.1228 \\ 0.151639 \cdot e^{1.15375i} & -7.16893 & -172.466 & 0 & -0.116493 \\ 0 & 0 & 0 & -0.000772971 & -4980.22 \\ 0.019648 & 100.573 & 338.918 & 3708.84 & -0.271052 \end{pmatrix},$$

$$M_d = \begin{pmatrix} 0.00985885 & -0.0404963 & 0.0721585 \cdot e^{1.99027i} & 0 & -1.03475 \\ 0.00481504 & -0.0343246 & 0.0324285 & 0 & -0.48716 \\ 0.00766034 \cdot e^{1.63225i} & 0.000571412 & 2.86587 & 0 & -13.2473 \\ 0 & 0 & 0 & -0.000462012 & 4803.69 \\ 0.019648 & 100.573 & 338.918 & 3708.84 & 0.873924 \end{pmatrix}.$$

C.4 Best Fit point D

Values of the inputs parameters for the boson sector are given by

$$m_{Z'} = 758.743, \quad v_\phi = 4820.94, \quad g' = 0.348599, \quad \lambda_\chi = 0.00892191, \quad \lambda_\sigma = 0.999999.$$

Values for fermion mass matrices are

$$M_e =$$

$$\begin{pmatrix} 0.000486575 & -0.00000000602545 & 0.00000019239 & 0 & -0.0000102812 \\ 0.00000112006 & 0.146358 & -0.0000795331 & 0 & -407.638 \\ -0.00000448652 & -0.0000111978 & -1.74616 & 0 & 0.0247399 \\ 0 & 0 & 0 & -0.0735254 & 635.847 \\ -0.00010118 & -488.24 & 0.0995171 & -337.63 & -173.973 \end{pmatrix},$$

$$M_n =$$

$$\begin{pmatrix} 0. & 0. & 0. & 0 & 0 \\ -15.7954 & 33.8318 \cdot e^{3.06777i} & 15.455 \cdot e^{0.106991i} & 0 & 0 \\ 10.4297 \cdot e^{1.19386i} & -80.6485 & -53.3437 & 0 & 0 \\ 0 & 0 & 0 & -0.358095 & -4820.94 \\ -0.00010118 & -488.24 & 0.0995171 & -337.63 & -0.575107 \end{pmatrix},$$

$$M_u =$$

$$\begin{pmatrix} -0.00226803 & -0.00526038 & 0.00673866 \cdot e^{2.97063i} & 0 & -0.00737306 \\ 0.119732 & 0.618476 & -0.00585875 & 0 & -315.604 \\ 0.00911865 \cdot e^{0.802338i} & 0.0270238 & -172.537 & 0 & 1.13048 \\ 0 & 0 & 0 & 0.295538 & 4498.79 \\ -0.15859 & 223.445 & 430.866 & 4039.17 & 110.941 \end{pmatrix},$$

$$M_d =$$

$$\begin{pmatrix} -0.000626484 & -0.0522184 & 0.124081 \cdot e^{0.546067i} & 0 & 0.00126174 \\ -0.00330599 & 0.0273122 & 0.00102239 & 0 & -0.107688 \\ 0.0214224 \cdot e^{2.66418i} & -0.115298 & 2.86442 & 0 & 2.97535 \\ 0 & 0 & 0 & 0.577941 & -2442.58 \\ -0.15859 & 223.445 & 430.866 & 4039.17 & -1.82777 \end{pmatrix}.$$

D Full List of Observables at Best Fit Points

The CKM matrices at the best fit points are as follows:

$$\hat{V}_{\text{CKM}}^A = \tag{D.1}$$

$$\begin{pmatrix} 0.974468 & 0.224499 & 0.003595 \cdot e^{-1.227622i} & 0.000000 & 0.000000 \\ 0.224355 \cdot e^{-3.140947i} & 0.973615 & 0.041688 & 0.000003 \cdot e^{1.366139i} & 0.000000 \\ 0.008820 \cdot e^{-0.382954i} & 0.040903 \cdot e^{-3.122994i} & 0.999124 & 0.000042 \cdot e^{-1.775654i} & 0.000074 \cdot e^{1.418692i} \\ 0.000001 & 0.000003 \cdot e^{-1.560707i} & 0.000076 \cdot e^{1.562550i} & 0.000707 \cdot e^{2.928496i} & 0.999823 \cdot e^{-0.160351i} \\ 0.000001 \cdot e^{-0.344253i} & 0.000007 \cdot e^{3.077755i} & 0.000116 \cdot e^{-0.076994i} & 0.000013 \cdot e^{-1.852631i} & 0.018809 \cdot e^{1.341708i} \end{pmatrix}$$

$$\hat{V}_{\text{CKM}}^B = \tag{D.2}$$

$$\begin{pmatrix} 0.974466 & 0.224508 & 0.003584 \cdot e^{-1.226648i} & 0.000000 & 0.000000 \\ 0.224366 \cdot e^{-3.140954i} & 0.973626 & 0.041369 & 0.000000 & 0.000000 \\ 0.008750 \cdot e^{-0.384851i} & 0.040591 \cdot e^{-3.122912i} & 0.999137 & 0.000002 \cdot e^{2.471251i} & 0.000452 \cdot e^{3.135974i} \\ 0.000001 & 0.000003 \cdot e^{0.131789i} & 0.000028 \cdot e^{-3.020122i} & 0.000000 & 0.000107 \cdot e^{0.115817i} \\ 0.000004 \cdot e^{-0.379008i} & 0.000018 \cdot e^{-3.117107i} & 0.000451 \cdot e^{0.005807i} & 0.000059 \cdot e^{-0.661943i} & 1.000000 \cdot e^{0.000188i} \end{pmatrix}$$

$$\hat{V}_{\text{CKM}}^C = \tag{D.3}$$

$$\begin{pmatrix} 0.974464 & 0.224515 & 0.003607 \cdot e^{-1.228436i} & 0.000000 & 0.000000 \\ 0.224372 \cdot e^{-3.140948i} & 0.973621 & 0.041465 & 0.000000 & 0.000000 \\ 0.008778 \cdot e^{-0.386411i} & 0.040686 \cdot e^{-3.122824i} & 0.999133 & 0.000197 \cdot e^{-1.153121i} & 0.000002 \cdot e^{-2.377782i} \\ 0.000002 \cdot e^{-2.344296i} & 0.000008 \cdot e^{1.202460i} & 0.000197 \cdot e^{-1.957901i} & 1.000000 \cdot e^{0.030571i} & 0.000353 \cdot e^{-1.192357i} \\ 0.000000 & 0.000002 \cdot e^{1.151528i} & 0.000002 \cdot e^{1.142344i} & 0.000092 \cdot e^{-0.011322i} & 0.000000 \end{pmatrix}$$

$$\hat{V}_{\text{CKM}}^D = \tag{D.4}$$

$$\begin{pmatrix} 0.974469 & 0.224495 & 0.003583 \cdot e^{-1.226283i} & 0.000002 \cdot e^{2.166735i} & 0.000000 \\ 0.224353 \cdot e^{-3.140955i} & 0.973629 & 0.041373 & 0.000013 \cdot e^{2.159161i} & 0.000000 \\ 0.008749 \cdot e^{-0.384634i} & 0.040596 \cdot e^{-3.122928i} & 0.999137 & 0.000026 \cdot e^{-0.956519i} & 0.000190 \cdot e^{2.280798i} \\ 0.000002 \cdot e^{-2.598386i} & 0.000010 \cdot e^{0.880650i} & 0.000191 \cdot e^{-2.281000i} & 0.000829 \cdot e^{3.045676i} & 0.993172 \cdot e^{3.141399i} \\ 0.000002 \cdot e^{-2.249810i} & 0.000013 \cdot e^{0.886543i} & 0.000002 \cdot e^{0.865773i} & 0.000097 \cdot e^{-0.095778i} & 0.116659 \cdot e^{-0.000055i} \end{pmatrix}$$

Table 13: Observables for charged leptons at the benchmark points.

Name	Point (A)	Point (B)	Point (C)	Point (D)	Data	Unc.
$m_e(m_Z)$ [GeV] $\times 10^4$	4.8658	4.8658	4.8658	4.8658	4.8658	0.00049
$m_\mu(m_Z)$ [GeV]	0.102719	0.102719	0.102719	0.102719	0.102719	0.000010
$m_\tau(m_Z)$ [GeV]	1.7462	1.7462	1.7462	1.7462	1.7462	0.00017
$\text{Br}(\mu \rightarrow e\nu\bar{\nu})$	0.999965	0.999970	0.999971	0.999971	0.999971	0.000100
$\text{Br}(\mu \rightarrow e\gamma) \times 10^{13}$	0.147	1.597	6.1×10^{-2}	0.822	0	2.6
$\text{Br}(\mu^- \rightarrow e^- e^+ e^-) \times 10^{13}$	0.000	0.000	0.000	0.000	0	6.1
$\text{Br}(\tau \rightarrow e\nu\bar{\nu})$	0.178510	0.178510	0.178510	0.178510	0.178510	0.000018
$\text{Br}(\tau \rightarrow \mu\nu\bar{\nu})$	0.173611	0.173612	0.173612	0.173612	0.173612	0.000017
$\text{Br}(\tau \rightarrow e\gamma) \times 10^8$	0.000	0.000	0.000	0.000	0	2.0
$\text{Br}(\tau \rightarrow \mu\gamma) \times 10^8$	3.3×10^{-4}	3.6×10^{-4}	3.3×10^{-6}	8.5×10^{-7}	0	2.7
$\text{Br}(\tau^- \rightarrow e^- e^+ e^-) \times 10^8$	0.000	0.000	0.000	0.000	0	1.6
$\text{Br}(\tau^- \rightarrow e^- \mu^+ \mu^-) \times 10^8$	0.000	0.000	0.000	0.000	0	1.6
$\text{Br}(\tau^- \rightarrow \mu^- e^+ \mu^-) \times 10^8$	0.000	0.000	0.000	0.000	0	1.0
$\text{Br}(\tau^- \rightarrow \mu^- e^+ e^-) \times 10^8$	0.000	0.000	0.000	0.000	0	1.1
$\text{Br}(\tau^- \rightarrow \mu^- e^+ \mu^-) \times 10^8$	0.000	0.000	0.000	0.000	0	1.0
$\text{Br}(\tau^- \rightarrow \mu^- \mu^+ \mu^-) \times 10^8$	7.0×10^{-3}	4.8×10^{-4}	6.6×10^{-5}	4.4×10^{-6}	0	1.3
$\Delta a_e \times 10^{13}$	0.000	-8.8×10^{-9}	0.000	0.000	-8.700	3.6
$\Delta a_\mu \times 10^9$	2.62	2.52	2.52	2.45	2.68	0.76

Table 14: Observables for SM bosons at the benchmark points.

Name	Point (A)	Point (B)	Point (C)	Point (D)	Data	Unc.
$\text{Br}(W^+ \rightarrow e^+\nu)$	0.10862	0.10862	0.10862	0.10862	0.10862	0.00011
$\text{Br}(W^+ \rightarrow \mu^+\nu)$	0.10862	0.10862	0.10862	0.10862	0.10862	0.00011
$\text{Br}(W^+ \rightarrow \tau^+\nu)$	0.10855	0.10855	0.10855	0.10855	0.10855	0.00011
$\text{Br}(W \rightarrow \text{had})$	0.652	0.652	0.652	0.652	0.666	0.025
$\text{Br}(W^+ \rightarrow c\bar{s})$	0.309	0.309	0.309	0.309	0.324	0.032
$\text{Br}(Z \rightarrow e^+e^-) \times 10^2$	3.333	3.333	3.333	3.333	3.333	0.0062
$\text{Br}(Z \rightarrow \mu^+\mu^-) \times 10^2$	3.333	3.333	3.333	3.333	3.333	0.0062
$\text{Br}(Z \rightarrow \tau^+\tau^-) \times 10^2$	3.326	3.326	3.326	3.326	3.326	0.0062
$\text{Br}(Z \rightarrow \text{had})$	0.676	0.676	0.676	0.676	0.677	0.025
$\text{Br}(Z \rightarrow u\bar{u} + c\bar{c})/2$	0.1157	0.1157	0.1157	0.1157	0.1157	0.0043
$\text{Br}(Z \rightarrow d\bar{d} + s\bar{s} + b\bar{b})/3$	0.1483	0.1483	0.1483	0.1483	0.1483	0.0056
$\text{Br}(Z \rightarrow c\bar{c})$	0.1157	0.1157	0.1157	0.1157	0.1157	0.0043
$\text{Br}(Z \rightarrow b\bar{b})$	0.1479	0.1479	0.1479	0.1479	0.1479	0.0056
$\text{Br}(Z \rightarrow e\mu) \times 10^7$	0.000	0.000	0.000	0.000	0	3.8
$\text{Br}(Z \rightarrow e\tau) \times 10^6$	0.000	0.000	0.000	0.000	0	5.0
$\text{Br}(Z \rightarrow \mu\tau) \times 10^6$	0.000	0.000	0.000	0.000	0	6.1
A_e	0.1469	0.1469	0.1469	0.1469	0.1469	0.0015
A_μ	0.147	0.147	0.147	0.147	0.147	0.015
A_τ	0.1469	0.1469	0.1469	0.1469	0.1469	0.0015
A_s	0.941	0.941	0.941	0.941	0.941	0.094
A_c	0.6949	0.6949	0.6949	0.6949	0.6949	0.0069
A_b	0.9406	0.9406	0.9406	0.9406	0.9406	0.0094
$\mu_{\mu\mu}$	0.977	0.977	0.976	0.977	0	1.3
$\mu_{\tau\tau}$	0.981	0.981	0.981	0.981	1.12	0.23
μ_{bb}	0.843	0.842	0.843	0.842	0.950	0.22
$\mu_{\gamma\gamma}$	1.00	1.00	1.00	1.00	1.16	0.18
$\text{Br}(h \rightarrow e^+e^-) \times 10^4$	4.8×10^{-5}	4.8×10^{-5}	4.8×10^{-5}	4.8×10^{-5}	0	9.7
$\text{Br}(h \rightarrow e\mu) \times 10^4$	0.000	0.000	0.000	0.000	0	1.8
$\text{Br}(h \rightarrow e\tau) \times 10^3$	0.000	0.000	0.000	0.000	0	3.1
$\text{Br}(h \rightarrow \mu\tau) \times 10^3$	0.000	0.000	0.000	0.000	0	1.3

Table 15: SM quark masses and CKM matrix at the benchmark points.

Name	Point (A)	Point (B)	Point (C)	Point (D)	Data	Unc.
$m_u(m_Z)$ [GeV] $\times 10^3$	1.27	1.29	1.32	1.22	1.29	0.39
$m_c(m_Z)$ [GeV]	0.627	0.627	0.627	0.626	0.627	0.019
$m_t(m_Z)$ [GeV]	171.64	171.71	171.88	171.57	171.68	1.5
$m_d(m_Z)$ [GeV] $\times 10^3$	2.76	2.76	2.76	2.72	2.75	0.29
$m_s(m_Z)$ [GeV] $\times 10^3$	54.30	54.47	54.14	55.11	54.32	2.9
$m_b(m_Z)$ [GeV]	2.86	2.85	2.86	2.85	2.85	0.026
$ V_{ud} $	0.97447	0.97447	0.97446	0.97447	0.97420	0.00021
$ V_{us} $	0.22450	0.22451	0.22451	0.22450	0.22430	0.00050
$ V_{ub} \times 10^3$	3.60	3.58	3.61	3.58	3.94	0.36
$ V_{cd} $	0.2244	0.2244	0.2244	0.2244	0.2180	0.0040
$ V_{cs} $	0.974	0.974	0.974	0.974	0.997	0.017
$ V_{cb} \times 10^2$	4.17	4.14	4.15	4.14	4.22	0.080
$ V_{td} \times 10^3$	8.82	8.75	8.78	8.75	8.10	0.50
$ V_{ts} \times 10^2$	4.09	4.06	4.07	4.06	3.94	0.23
$ V_{tb} $	0.999	0.999	0.999	0.999	1.02	0.025
α	1.53	1.53	1.53	1.53	1.47	0.097
$\sin 2\beta$	0.694	0.697	0.699	0.697	0.691	0.017
γ	1.23	1.23	1.23	1.23	1.28	0.081

Table 16: Observables for quarks at the benchmark points.

Name	Point (A)	Point (B)	Point (C)	Point (D)	Data	Unc.
ΔM_K [ps $^{-1}$] $\times 10^3$	6.886	5.012	4.633	4.622	5.293	2.2
$\epsilon_K \times 10^3$	2.23	2.23	2.17	2.22	2.23	0.21
ΔM_{B_d} [ps $^{-1}$]	0.561	0.610	0.598	0.590	0.506	0.081
$S_{\psi K_s}$	0.697	0.696	0.692	0.695	0.695	0.019
ΔM_{B_s} [ps $^{-1}$]	19.61	19.75	19.44	19.95	17.76	2.5
$S_{\psi\phi} \times 10^2$	3.659	3.742	3.730	3.791	2.100	3.1
$ x_{12}^D \times 10^3$	1.7×10^{-3}	5.4×10^{-3}	0.195	0.285	0	5.0
$R_K^{\nu\nu}$	1.046	1.053	1.060	1.057	1.000	2.6
$R_{K^*}^{\nu\nu}$	1.046	1.053	1.060	1.057	1.000	2.7
$R_{B_d \rightarrow \mu\mu}$	0.985	0.888	0.867	0.971	1.509	1.4
$R_{B_s \rightarrow \mu\mu}$	0.841	0.890	0.850	0.861	0.750	0.16
Γ_t	1.49	1.49	1.49	1.49	1.41	0.17
$\text{Br}(t \rightarrow Zq) \times 10^4$	0.000	0.000	0.000	0.000	0	2.6
$\text{Br}(t \rightarrow Zu) \times 10^4$	0.000	0.000	0.000	0.000	0	9.7
$\text{Br}(t \rightarrow Zc) \times 10^4$	0.000	0.000	0.000	0.000	0	8.2

Table 17: Wilson coefficients relevant to $b \rightarrow s\ell\ell$ processes and $\text{BR}(B \rightarrow K\tau^+\tau^-)$ at the benchmark points.

Name	Point (A)	Point (B)	Point (C)	Point (D)	Data	Unc.
$\text{Re}C_9^e$	0.000	0.000	0.000	0.000	0	0.10
$\text{Im}C_9^e$	0.000	0.000	0.000	0.000	0	0.10
$\text{Re}C_{10}^e$	0.000	0.000	0.000	0.000	0	0.10
$\text{Im}C_{10}^e$	0.000	0.000	0.000	0.000	0	0.10
$\text{Re}C_9^{\prime e}$	0.000	0.000	0.000	0.000	0	0.10
$\text{Im}C_9^{\prime e}$	0.000	0.000	0.000	0.000	0	0.10
$\text{Re}C_{10}^{\prime e}$	0.000	0.000	0.000	0.000	0	0.10
$\text{Im}C_{10}^{\prime e}$	0.000	0.000	0.000	0.000	0	0.10
$\text{Re}C_9^\mu$	-0.548	-0.806	-0.838	-0.808	-0.700	0.30
$\text{Im}C_9^\mu$	-1.0×10^{-2}	6.2×10^{-4}	-6.8×10^{-3}	5.4×10^{-3}	0	0.10
$\text{Re}C_{10}^\mu$	0.370	0.252	0.347	0.322	0.400	0.20
$\text{Im}C_{10}^\mu$	6.9×10^{-3}	-1.9×10^{-4}	2.8×10^{-3}	-2.1×10^{-3}	0	0.10
$\text{Re}C_9^{\prime \mu}$	1.0×10^{-3}	8.9×10^{-5}	2.2×10^{-4}	-2.6×10^{-6}	0	0.10
$\text{Im}C_9^{\prime \mu}$	8.5×10^{-4}	-4.1×10^{-5}	-4.4×10^{-5}	-4.1×10^{-6}	0	0.10
$\text{Re}C_{10}^{\prime \mu}$	-7.1×10^{-4}	-2.8×10^{-5}	-9.2×10^{-5}	1.1×10^{-6}	0	0.10
$\text{Im}C_{10}^{\prime \mu}$	-5.8×10^{-4}	1.3×10^{-5}	1.8×10^{-5}	1.6×10^{-6}	0	0.10
$\text{Br}(B \rightarrow K\tau^+\tau^-) \times 10^3$	1.2×10^{-4}	1.2×10^{-4}	1.2×10^{-4}	1.2×10^{-4}	0	1.4

Table 18: Masses, total widths, and branching fractions (BR) at point (A). Decay 1(2) denote the (next to) dominant decay mode.

	Mass [GeV]	Width [GeV]	Decay 1	BR	Decay 2	BR
Z'	277.6	0.1361	$\mu\mu$	0.5091	$\nu\nu$	0.4907
χ	651.9	0.669538	$E_1\mu$	0.4391	$N_1\nu$	0.4227
σ	1871.7	0.9049	N_2N_2	0.2988	E_2E_2	0.1473
E_1	367.9	0.0354639	$Z'\mu$	1.	$h\mu$	0.
N_1	422.2	0.0817534	$Z'\nu$	0.9995	$W\mu$	0.0003
N_2	459.	0.113389	WE_1	0.8792	$Z'\nu$	0.1179
E_2	548.3	4.07452	WN_1	0.4799	ZE_1	0.4415
D_1	1572.1	0.0371	$Z'b$	0.4117	χb	0.2831
U_1	3453.7	3.0221	$Z'c$	0.4117	χc	0.3829
D_2	3453.8	3.0228	$Z's$	0.4063	χs	0.3779
U_2	3596.8	0.1085	$Z'c$	0.4504	χc	0.4213

Table 19: Masses, total widths, and branching fractions (BR) at point (B). Decay 1(2) denote the (next to) dominant decay mode.

	Mass [GeV]	Width [GeV]	Decay 1	BR	Decay 2	BR
Z'	535.3	0.5097	$\mu\mu$	0.5595	$\nu\nu$	0.4388
χ	88.2	1.6×10^{-8}	$\mu\mu$	0.6045	bb	0.36
σ	103.3	2.3×10^{-9}	$\mu\mu$	0.6041	bb	0.3604
N_1	1069.9	0.000572547	$W\mu$	0.4724	$Z\nu$	0.2362
E_1	1211.1	3.27601	$\chi\mu$	0.5235	$Z'\mu$	0.4765
N_2	1283.3	4.05237	$\chi\nu$	0.5185	$Z'\nu$	0.4814
E_2	1386.9	8.53551	ZE_1	0.2959	$\chi\mu$	0.2563
U_1	1853.	0.0013	χc	0.4647	$Z'c$	0.4576
D_1	2130.9	0.0223	χd	0.4696	$Z'd$	0.4659
D_2	2747.9	2.8004	χb	0.3747	$Z'b$	0.3739
U_2	2747.9	2.8081	χt	0.3827	$Z't$	0.3818

Table 20: Masses, total widths, and branching fractions (BR) at best fit point C. Decay 1(2) denote the (next to) dominant decay mode.

	Mass [GeV]	Width [GeV]	Decay 1	BR	Decay 2	BR
Z'	486.7	1.1178	$\mu\mu$	0.5335	$\nu\nu$	0.4552
χ	1066.6	1.587	$E_1\mu$	0.3284	$E_2\mu$	0.2668
σ	4088.7	0.8017	$E_2\mu$	0.2006	E_1E_1	0.1768
E_1	441.7	6.613×10^{-6}	$h\mu$	0.6816	$Z\mu$	0.2172
N_1	537.1	0.851545	WE_1	0.9924	$Z'\nu$	0.0076
E_2	618.	2.17089	ZE_1	0.8738	WN_1	0.0772
N_2	4980.2	0.000430776	$W\mu$	0.4334	$Z\nu$	0.2167
D_1	3725.6	4.0242	$Z'b$	0.46	χb	0.3881
U_1	3725.7	4.0254	$Z't$	0.4705	χt	0.3967
D_2	4803.7	0.0086	$Z'b$	0.4274	χb	0.3864
U_2	4981.	0.3388	$Z'c$	0.4381	χc	0.3989

Table 21: Masses, total widths, and branching fractions (BR) at best fit point D. Decay 1(2) denote the (next to) dominant decay mode.

	Mass [GeV]	Width [GeV]	Decay 1	BR	Decay 2	BR
Z'	758.7	1.481	$\mu\mu$	0.448	$\nu\nu$	0.3779
χ	145.4	6.0×10^{-9}	bb	0.5551	$\mu\mu$	0.2299
σ	4820.9	2.8529	E_2E_2	0.2771	$E_2\mu$	0.1646
E_1	561.3	0.0765212	$\chi\mu$	1.	$h\mu$	0.
N_1	593.6	0.0849371	$\chi\nu$	1.	$W\mu$	0.
E_2	798.8	8.70794	WN_1	0.526	ZE_1	0.3138
N_2	4820.9	0.00162908	WE_1	0.3378	ZN_1	0.2083
D_1	2442.6	0.0001	χb	0.46	$Z'b$	0.4511
U_1	4061.7	4.3534	χt	0.3504	$Z't$	0.3501
D_2	4068.2	4.4075	χb	0.3372	$Z'b$	0.3368
U_2	4517.1	14.0401	WD_2	0.4354	ZU_1	0.2226

References

- [1] J. Kawamura, S. Raby, and A. Trautner, *Complete vectorlike fourth family and new $U(1)'$ for muon anomalies*, *Phys. Rev.* **D100** (2019), no. 5 055030, [[arXiv:1906.11297](#)].
- [2] A. Czarnecki and W. J. Marciano, *The Muon anomalous magnetic moment: A Harbinger for 'new physics'*, *Phys. Rev.* **D64** (2001) 013014, [[hep-ph/0102122](#)].
- [3] K. Kannike, M. Raidal, D. M. Straub, and A. Strumia, *Anthropic solution to the magnetic muon anomaly: the charged see-saw*, *JHEP* **02** (2012) 106, [[arXiv:1111.2551](#)]. [Erratum: *JHEP*10,136(2012)].
- [4] R. Dermisek and A. Raval, *Explanation of the Muon $g-2$ Anomaly with Vectorlike Leptons and its Implications for Higgs Decays*, *Phys. Rev.* **D88** (2013) 013017, [[arXiv:1305.3522](#)].
- [5] M. Lindner, M. Platscher, and F. S. Queiroz, *A Call for New Physics : The Muon Anomalous Magnetic Moment and Lepton Flavor Violation*, *Phys. Rept.* **731** (2018) 1–82, [[arXiv:1610.06587](#)].
- [6] W. Altmannshofer, S. Gori, M. Pospelov, and I. Yavin, *Quark flavor transitions in $L_\mu - L_\tau$ models*, *Phys. Rev.* **D89** (2014) 095033, [[arXiv:1403.1269](#)].
- [7] A. Crivellin, G. D'Ambrosio, and J. Heeck, *Explaining $h \rightarrow \mu^\pm \tau^\mp$, $B \rightarrow K^* \mu^+ \mu^-$ and $B \rightarrow K \mu^+ \mu^- / B \rightarrow K e^+ e^-$ in a two-Higgs-doublet model with gauged $L_\mu - L_\tau$* , *Phys. Rev. Lett.* **114** (2015) 151801, [[arXiv:1501.00993](#)].
- [8] S. F. King, *Flavourful Z' models for $R_{K^{(*)}}$* , *JHEP* **08** (2017) 019, [[arXiv:1706.06100](#)].
- [9] A. Falkowski, S. F. King, E. Perdomo, and M. Pierre, *Flavourful Z' portal for vector-like neutrino Dark Matter and $R_{K^{(*)}}$* , *JHEP* **08** (2018) 061, [[arXiv:1803.04430](#)].
- [10] B. Gripaios, M. Nardecchia, and S. A. Renner, *Linear flavour violation and anomalies in B physics*, *JHEP* **06** (2016) 083, [[arXiv:1509.05020](#)].
- [11] P. Arnan, L. Hofer, F. Mescia, and A. Crivellin, *Loop effects of heavy new scalars and fermions in $b \rightarrow s \mu^+ \mu^-$* , *JHEP* **04** (2017) 043, [[arXiv:1608.07832](#)].
- [12] B. Grinstein, S. Pokorski, and G. G. Ross, *Lepton non-universality in B decays and fermion mass structure*, *JHEP* **12** (2018) 079, [[arXiv:1809.01766](#)].
- [13] P. Arnan, A. Crivellin, M. Fedele, and F. Mescia, *Generic Loop Effects of New Scalars and Fermions in $b \rightarrow s \ell^+ \ell^-$ and a Vector-like 4th Generation*, [[arXiv:1904.05890](#)].
- [14] C.-W. Chiang and H. Okada, *A simple model for explaining muon-related anomalies and dark matter*, [[arXiv:1711.07365](#)].
- [15] J. M. Cline and J. M. Cornell, *$R(K^{(*)})$ from dark matter exchange*, *Phys. Lett.* **B782** (2018) 232–237, [[arXiv:1711.10770](#)].
- [16] J. Kawamura, S. Okawa, and Y. Omura, *Interplay between the $b \rightarrow s \ell \ell$ anomalies and dark matter physics*, *Phys. Rev.* **D96** (2017), no. 7 075041, [[arXiv:1706.04344](#)].

- [17] B. Barman, D. Borah, L. Mukherjee, and S. Nandi, *Correlating the anomalous results in $b \rightarrow s$ decays with inert Higgs doublet dark matter and muon $(g - 2)$* , [arXiv:1808.06639](#).
- [18] D. G. Cerdeño, A. Cheek, P. Martín-Ramiro, and J. M. Moreno, *B anomalies and dark matter: a complex connection*, [arXiv:1902.01789](#).
- [19] B. Allanach, F. S. Queiroz, A. Strumia, and S. Sun, *Z' models for the LHCb and $g - 2$ muon anomalies*, *Phys. Rev.* **D93** (2016), no. 5 055045, [[arXiv:1511.07447](#)]. [Erratum: *Phys. Rev.*D95,no.11,119902(2017)].
- [20] W. Altmannshofer, M. Carena, and A. Crivellin, *$L_\mu - L_\tau$ theory of Higgs flavor violation and $(g - 2)_\mu$* , *Phys. Rev.* **D94** (2016), no. 9 095026, [[arXiv:1604.08221](#)].
- [21] E. Megias, M. Quiros, and L. Salas, *$g_\mu - 2$ from Vector-Like Leptons in Warped Space*, *JHEP* **05** (2017) 016, [[arXiv:1701.05072](#)].
- [22] S. Raby and A. Trautner, *Vectorlike chiral fourth family to explain muon anomalies*, *Phys. Rev.* **D97** (2018), no. 9 095006, [[arXiv:1712.09360](#)].
- [23] L. Darmé, K. Kowalska, L. Roszkowski, and E. M. Sessolo, *Flavor anomalies and dark matter in SUSY with an extra $U(1)$* , *JHEP* **10** (2018) 052, [[arXiv:1806.06036](#)].
- [24] S. Antusch and V. Maurer, *Running quark and lepton parameters at various scales*, *JHEP* **11** (2013) 115, [[arXiv:1306.6879](#)].
- [25] **Particle Data Group** Collaboration, M. Tanabashi et al., *Review of Particle Physics*, *Phys. Rev.* **D98** (2018), no. 3 030001.
- [26] H. Davoudiasl and W. J. Marciano, *Tale of two anomalies*, *Phys. Rev.* **D98** (2018), no. 7 075011, [[arXiv:1806.10252](#)].
- [27] G. F. Giudice, P. Paradisi, and M. Passera, *Testing new physics with the electron $g-2$* , *JHEP* **11** (2012) 113, [[arXiv:1208.6583](#)].
- [28] A. Crivellin, M. Hoferichter, and P. Schmidt-Wellenburg, *Combined explanations of $(g - 2)_{\mu,e}$ and implications for a large muon EDM*, *Phys. Rev.* **D98** (2018), no. 11 113002, [[arXiv:1807.11484](#)].
- [29] J. Liu, C. E. M. Wagner, and X.-P. Wang, *A light complex scalar for the electron and muon anomalous magnetic moments*, *JHEP* **03** (2019) 008, [[arXiv:1810.11028](#)].
- [30] B. Dutta and Y. Mimura, *Electron $g - 2$ with flavor violation in MSSM*, *Phys. Lett.* **B790** (2019) 563–567, [[arXiv:1811.10209](#)].
- [31] R. H. Parker, C. Yu, W. Zhong, B. Estey, and H. Müller, *Measurement of the fine-structure constant as a test of the Standard Model*, [arXiv:1812.04130](#).
- [32] X.-F. Han, T. Li, L. Wang, and Y. Zhang, *Simple interpretations of lepton anomalies in the lepton-specific inert two-Higgs-doublet model*, *Phys. Rev.* **D99** (2019), no. 9 095034, [[arXiv:1812.02449](#)].

- [33] M. Endo and W. Yin, *Explaining electron and muon $g - 2$ anomaly in SUSY without lepton-flavor mixings*, [arXiv:1906.08768](#).
- [34] M. Bauer, M. Neubert, S. Renner, M. Schnubel, and A. Thamm, *Axion-like particles, lepton-flavor violation and a new explanation of a_μ and a_e* , [arXiv:1908.00008](#).
- [35] M. Badziak and K. Sakurai, *Explanation of electron and muon $g - 2$ anomalies in the MSSM*, *JHEP* **10** (2019) 024, [[arXiv:1908.03607](#)].
- [36] A. E. Cárcamo Hernández, S. F. King, H. Lee, and S. J. Rowley, *Is it possible to explain the muon and electron $g - 2$ in a Z' model?*, [arXiv:1910.10734](#).
- [37] F. Jegerlehner and A. Nyffeler, *The Muon $g-2$* , *Phys. Rept.* **477** (2009) 1–110, [[arXiv:0902.3360](#)].
- [38] L. Lavoura, *General formulae for $f(1) \rightarrow f(2)\gamma$* , *Eur. Phys. J.* **C29** (2003) 191–195, [[hep-ph/0302221](#)].
- [39] Y. Kuno and Y. Okada, *Muon decay and physics beyond the standard model*, *Rev. Mod. Phys.* **73** (2001) 151–202, [[hep-ph/9909265](#)].
- [40] Y. Okada, K.-i. Okumura, and Y. Shimizu, *Mu to e gamma and mu to 3 e processes with polarized muons and supersymmetric grand unified theories*, *Phys. Rev.* **D61** (2000) 094001, [[hep-ph/9906446](#)].
- [41] A. Brignole and A. Rossi, *Anatomy and phenomenology of mu-tau lepton flavor violation in the MSSM*, *Nucl. Phys.* **B701** (2004) 3–53, [[hep-ph/0404211](#)].
- [42] Z. Poh and S. Raby, *Vectorlike leptons: Muon $g-2$ anomaly, lepton flavor violation, Higgs boson decays, and lepton nonuniversality*, *Phys. Rev.* **D96** (2017), no. 1 015032, [[arXiv:1705.07007](#)].
- [43] A. Djouadi, *The Anatomy of electro-weak symmetry breaking. I: The Higgs boson in the standard model*, *Phys. Rept.* **457** (2008) 1–216, [[hep-ph/0503172](#)].
- [44] **HFLAV** Collaboration, Y. Amhis et al., *Averages of b -hadron, c -hadron, and τ -lepton properties as of summer 2016*, *Eur. Phys. J.* **C77** (2017), no. 12 895, [[arXiv:1612.07233](#)].
- [45] **BaBar** Collaboration, J. P. Lees et al., *Search for $B \rightarrow K^{(*)}\nu\bar{\nu}$ and invisible quarkonium decays*, *Phys. Rev.* **D87** (2013), no. 11 112005, [[arXiv:1303.7465](#)].
- [46] **Belle** Collaboration, O. Lutz et al., *Search for $B \rightarrow h^{(*)}\nu\bar{\nu}$ with the full Belle $\Upsilon(4S)$ data sample*, *Phys. Rev.* **D87** (2013), no. 11 111103, [[arXiv:1303.3719](#)].
- [47] C. Bobeth, M. Gorbahn, T. Hermann, M. Misiak, E. Stamou, and M. Steinhauser, *$B_{s,d} \rightarrow l^+l^-$ in the Standard Model with Reduced Theoretical Uncertainty*, *Phys. Rev. Lett.* **112** (2014) 101801, [[arXiv:1311.0903](#)].
- [48] W. Altmannshofer, C. Niehoff, and D. M. Straub, *$B_s \rightarrow \mu^+\mu^-$ as current and future probe of new physics*, *JHEP* **05** (2017) 076, [[arXiv:1702.05498](#)].

- [49] **BaBar** Collaboration, J. P. Lees et al., *Search for $B^+ \rightarrow K^+\tau^+\tau^-$ at the BaBar experiment*, *Phys. Rev. Lett.* **118** (2017), no. 3 031802, [[arXiv:1605.09637](#)].
- [50] A. J. Buras and M. Munz, *Effective Hamiltonian for $B \rightarrow X(s)e^+e^-$ beyond leading logarithms in the NDR and HV schemes*, *Phys. Rev.* **D52** (1995) 186–195, [[hep-ph/9501281](#)].
- [51] C. Bobeth, M. Misiak, and J. Urban, *Photonic penguins at two loops and m_t dependence of $BR[B \rightarrow X_sl^+l^-]$* , *Nucl. Phys.* **B574** (2000) 291–330, [[hep-ph/9910220](#)].
- [52] J. Aebischer, W. Altmannshofer, D. Guadagnoli, M. Reboud, P. Stangl, and D. M. Straub, *B-decay discrepancies after Moriond 2019*, [arXiv:1903.10434](#).
- [53] W. Altmannshofer, C. Niehoff, P. Stangl, and D. M. Straub, *Status of the $B \rightarrow K^*\mu^+\mu^-$ anomaly after Moriond 2017*, *Eur. Phys. J.* **C77** (2017), no. 6 377, [[arXiv:1703.09189](#)].
- [54] W. Altmannshofer, P. Stangl, and D. M. Straub, *Interpreting Hints for Lepton Flavor Universality Violation*, *Phys. Rev.* **D96** (2017), no. 5 055008, [[arXiv:1704.05435](#)].
- [55] A. K. Alok, B. Bhattacharya, A. Datta, D. Kumar, J. Kumar, and D. London, *New Physics in $b \rightarrow s\mu^+\mu^-$ after the Measurement of R_{K^*}* , *Phys. Rev.* **D96** (2017), no. 9 095009, [[arXiv:1704.07397](#)].
- [56] B. Capdevila, A. Crivellin, S. Descotes-Genon, J. Matias, and J. Virto, *Patterns of New Physics in $b \rightarrow sl^+\ell^-$ transitions in the light of recent data*, *JHEP* **01** (2018) 093, [[arXiv:1704.05340](#)].
- [57] M. Ciuchini, A. M. Coutinho, M. Fedele, E. Franco, A. Paul, L. Silvestrini, and M. Valli, *On Flavourful Easter eggs for New Physics hunger and Lepton Flavour Universality violation*, *Eur. Phys. J.* **C77** (2017), no. 10 688, [[arXiv:1704.05447](#)].
- [58] G. D’Amico, M. Nardecchia, P. Panci, F. Sannino, A. Strumia, R. Torre, and A. Urbano, *Flavour anomalies after the R_{K^*} measurement*, *JHEP* **09** (2017) 010, [[arXiv:1704.05438](#)].
- [59] L.-S. Geng, B. Grinstein, S. Jäger, J. Martin Camalich, X.-L. Ren, and R.-X. Shi, *Towards the discovery of new physics with lepton-universality ratios of $b \rightarrow s\ell\ell$ decays*, *Phys. Rev.* **D96** (2017), no. 9 093006, [[arXiv:1704.05446](#)].
- [60] D. Ghosh, *Explaining the R_K and R_{K^*} anomalies*, *Eur. Phys. J.* **C77** (2017), no. 10 694, [[arXiv:1704.06240](#)].
- [61] A. Arbey, T. Hurth, F. Mahmoudi, and S. Neshatpour, *Hadronic and New Physics Contributions to $b \rightarrow s$ Transitions*, *Phys. Rev.* **D98** (2018), no. 9 095027, [[arXiv:1806.02791](#)].
- [62] M. Algueró, B. Capdevila, A. Crivellin, S. Descotes-Genon, P. Masjuan, J. Matias, and J. Virto, *Addendum: "Patterns of New Physics in $b \rightarrow sl^+\ell^-$ transitions in the light of recent data" and "Are we overlooking Lepton Flavour Universal New Physics in $b \rightarrow s\ell\ell$?"*, [arXiv:1903.09578](#).

- [63] A. K. Alok, A. Dighe, S. Gangal, and D. Kumar, *Continuing search for new physics in $b \rightarrow s\mu\mu$ decays: two operators at a time*, [arXiv:1903.09617](#).
- [64] M. Ciuchini, A. M. Coutinho, M. Fedele, E. Franco, A. Paul, L. Silvestrini, and M. Valli, *New Physics in $b \rightarrow s\ell^+\ell^-$ confronts new data on Lepton Universality*, [arXiv:1903.09632](#).
- [65] A. Datta, J. Kumar, and D. London, *The B Anomalies and New Physics in $b \rightarrow se^+e^-$* , [arXiv:1903.10086](#).
- [66] K. Kowalska, D. Kumar, and E. M. Sessolo, *Implications for New Physics in $b \rightarrow s\mu\mu$ transitions after recent measurements by Belle and LHCb*, [arXiv:1903.10932](#).
- [67] A. Arbey, T. Hurth, F. Mahmoudi, D. Martinez Santos, and S. Neshatpour, *Update on the $b \rightarrow s$ anomalies*, [arXiv:1904.08399](#).
- [68] D. Kumar, K. Kowalska, and E. M. Sessolo, *Global Bayesian Analysis of new physics in $b \rightarrow s\mu\mu$ transitions after Moriond-2019*, 2019. [arXiv:1906.08596](#).
- [69] B. Capdevila, A. Crivellin, S. Descotes-Genon, L. Hofer, and J. Matias, *Searching for New Physics with $b \rightarrow s\tau^+\tau^-$ processes*, *Phys. Rev. Lett.* **120** (2018), no. 18 181802, [[arXiv:1712.01919](#)].
- [70] G. Buchalla, A. J. Buras, and M. E. Lautenbacher, *Weak decays beyond leading logarithms*, *Rev. Mod. Phys.* **68** (1996) 1125–1144, [[hep-ph/9512380](#)].
- [71] A. J. Buras and R. Fleischer, *Quark mixing, CP violation and rare decays after the top quark discovery*, *Adv. Ser. Direct. High Energy Phys.* **15** (1998) 65–238, [[hep-ph/9704376](#)]. [,65(1997)].
- [72] A. J. Buras, *Weak Hamiltonian, CP violation and rare decays*, in *Probing the standard model of particle interactions. Proceedings, Summer School in Theoretical Physics, NATO Advanced Study Institute, 68th session, Les Houches, France, July 28-September 5, 1997. Pt. 1, 2*, pp. 281–539, 1998. [hep-ph/9806471](#).
- [73] A. J. Buras, F. De Fazio, and J. Girrbach, *The Anatomy of Z' and Z with Flavour Changing Neutral Currents in the Flavour Precision Era*, *JHEP* **02** (2013) 116, [[arXiv:1211.1896](#)].
- [74] A. J. Buras, F. De Fazio, J. Girrbach, R. Knegjens, and M. Nagai, *The Anatomy of Neutral Scalars with FCNCs in the Flavour Precision Era*, *JHEP* **06** (2013) 111, [[arXiv:1303.3723](#)].
- [75] L. Di Luzio, M. Kirk, and A. Lenz, *Updated B_s -mixing constraints on new physics models for $b \rightarrow s\ell^+\ell^-$ anomalies*, *Phys. Rev.* **D97** (2018), no. 9 095035, [[arXiv:1712.06572](#)].
- [76] A. J. Buras and J. Girrbach, *Complete NLO QCD Corrections for Tree Level $\Delta F = 2$ FCNC Processes*, *JHEP* **03** (2012) 052, [[arXiv:1201.1302](#)].
- [77] **Flavour Lattice Averaging Group** Collaboration, S. Aoki et al., *FLAG Review 2019*, [arXiv:1902.08191](#).

- [78] **ETM Collaboration**, N. Carrasco et al., *B-physics from $N_f = 2$ tmQCD: the Standard Model and beyond*, *JHEP* **03** (2014) 016, [[arXiv:1308.1851](#)].
- [79] **Fermilab Lattice, MILC Collaboration**, A. Bazavov et al., *$B_{(s)}^0$ -mixing matrix elements from lattice QCD for the Standard Model and beyond*, *Phys. Rev.* **D93** (2016), no. 11 113016, [[arXiv:1602.03560](#)].
- [80] N. Carrasco et al., *$D^0 - \bar{D}^0$ mixing in the standard model and beyond from $N_f = 2$ twisted mass QCD*, *Phys. Rev.* **D90** (2014), no. 1 014502, [[arXiv:1403.7302](#)].
- [81] A. J. Buras, S. Jager, and J. Urban, *Master formulae for Delta F=2 NLO QCD factors in the standard model and beyond*, *Nucl. Phys.* **B605** (2001) 600–624, [[hep-ph/0102316](#)].
- [82] S. Aoki et al., *Review of lattice results concerning low-energy particle physics*, *Eur. Phys. J.* **C74** (2014) 2890, [[arXiv:1310.8555](#)].
- [83] J. Brod and M. Gorbahn, *Next-to-Next-to-Leading-Order Charm-Quark Contribution to the CP Violation Parameter ϵ_K and ΔM_K* , *Phys. Rev. Lett.* **108** (2012) 121801, [[arXiv:1108.2036](#)].
- [84] A. J. Buras, M. Jamin, and P. H. Weisz, *Leading and Next-to-leading QCD Corrections to ϵ Parameter and $B^0 - \bar{B}^0$ Mixing in the Presence of a Heavy Top Quark*, *Nucl. Phys.* **B347** (1990) 491–536.
- [85] J. Brod and M. Gorbahn, *ϵ_K at Next-to-Next-to-Leading Order: The Charm-Top-Quark Contribution*, *Phys. Rev.* **D82** (2010) 094026, [[arXiv:1007.0684](#)].
- [86] A. J. Buras and D. Guadagnoli, *Correlations among new CP violating effects in $\Delta F = 2$ observables*, *Phys. Rev.* **D78** (2008) 033005, [[arXiv:0805.3887](#)].
- [87] A. J. Buras, D. Guadagnoli, and G. Isidori, *On ϵ_K Beyond Lowest Order in the Operator Product Expansion*, *Phys. Lett.* **B688** (2010) 309–313, [[arXiv:1002.3612](#)].
- [88] J. Urban, F. Krauss, U. Jentschura, and G. Soff, *Next-to-leading order QCD corrections for the $B0$ anti- $B0$ mixing with an extended Higgs sector*, *Nucl. Phys.* **B523** (1998) 40–58, [[hep-ph/9710245](#)].
- [89] P. Marquard, A. V. Smirnov, V. A. Smirnov, and M. Steinhauser, *Quark Mass Relations to Four-Loop Order in Perturbative QCD*, *Phys. Rev. Lett.* **114** (2015), no. 14 142002, [[arXiv:1502.01030](#)].
- [90] D. King, A. Lenz, and T. Rauh, *B_s mixing observables and $-V_{td}/V_{ts}$ from sum rules*, *JHEP* **05** (2019) 034, [[arXiv:1904.00940](#)].
- [91] G. Buchalla and A. J. Buras, *The rare decays $K \rightarrow \pi \nu \bar{\nu}$, $B \rightarrow X \nu \bar{\nu}$ and $B \rightarrow l^+ l^-$: An Update*, *Nucl. Phys.* **B548** (1999) 309–327, [[hep-ph/9901288](#)].
- [92] M. Misiak and J. Urban, *QCD corrections to FCNC decays mediated by Z penguins and W boxes*, *Phys. Lett.* **B451** (1999) 161–169, [[hep-ph/9901278](#)].

- [93] K. De Bruyn, R. Fleischer, R. Kneijens, P. Koppenburg, M. Merk, and N. Tuning, *Branching Ratio Measurements of B_s Decays*, *Phys. Rev.* **D86** (2012) 014027, [[arXiv:1204.1735](#)].
- [94] K. De Bruyn, R. Fleischer, R. Kneijens, P. Koppenburg, M. Merk, A. Pellegrino, and N. Tuning, *Probing New Physics via the $B_s^0 \rightarrow \mu^+ \mu^-$ Effective Lifetime*, *Phys. Rev. Lett.* **109** (2012) 041801, [[arXiv:1204.1737](#)].
- [95] A. J. Buras, R. Fleischer, J. Girrbach, and R. Kneijens, *Probing New Physics with the $B_s \rightarrow \mu^+ \mu^-$ Time-Dependent Rate*, *JHEP* **07** (2013) 77, [[arXiv:1303.3820](#)].
- [96] R. Fleischer, *Flavour Physics and CP Violation: Expecting the LHC*, in *High-energy physics. Proceedings, 4th Latin American CERN-CLAF School, Vina del Mar, Chile, February 18-March 3, 2007*, pp. 105–157, 2008. [arXiv:0802.2882](#).
- [97] A. J. Buras, J. Girrbach-Noe, C. Niehoff, and D. M. Straub, *$B \rightarrow K^{(*)} \nu \bar{\nu}$ decays in the Standard Model and beyond*, *JHEP* **02** (2015) 184, [[arXiv:1409.4557](#)].
- [98] W. Altmannshofer, A. J. Buras, D. M. Straub, and M. Wick, *New strategies for New Physics search in $B \rightarrow K^* \nu \bar{\nu}$, $B \rightarrow K \nu \bar{\nu}$ and $B \rightarrow X_s \nu \bar{\nu}$ decays*, *JHEP* **04** (2009) 022, [[arXiv:0902.0160](#)].
- [99] L. Calibbi, A. Crivellin, and T. Ota, *Effective Field Theory Approach to $b \rightarrow s \ell \ell'$, $B \rightarrow K^{(*)} \nu \bar{\nu}$ and $B \rightarrow D^{(*)} \tau \nu$ with Third Generation Couplings*, *Phys. Rev. Lett.* **115** (2015) 181801, [[arXiv:1506.02661](#)].
- [100] M. Kohda, T. Modak, and A. Soffer, *Identifying a Z' behind $b \rightarrow s \ell \ell$ anomalies at the LHC*, *Phys. Rev.* **D97** (2018), no. 11 115019, [[arXiv:1803.07492](#)].
- [101] B. C. Allanach, J. M. Butterworth, and T. Corbett, *Collider Constraints on Z' Models for Neutral Current B -Anomalies*, [arXiv:1904.10954](#).
- [102] **ATLAS** Collaboration, G. Aad et al., *Search for high-mass dilepton resonances using 139 fb^{-1} of pp collision data collected at $\sqrt{s} = 13 \text{ TeV}$ with the ATLAS detector*, [arXiv:1903.06248](#).
- [103] J. Alwall, R. Frederix, S. Frixione, V. Hirschi, F. Maltoni, O. Mattelaer, H. S. Shao, T. Stelzer, P. Torrielli, and M. Zaro, *The automated computation of tree-level and next-to-leading order differential cross sections, and their matching to parton shower simulations*, *JHEP* **07** (2014) 079, [[arXiv:1405.0301](#)].
- [104] C. Degrande, C. Duhr, B. Fuks, D. Grellscheid, O. Mattelaer, and T. Reiter, *UFO - The Universal FeynRules Output*, *Comput. Phys. Commun.* **183** (2012) 1201–1214, [[arXiv:1108.2040](#)].
- [105] N. D. Christensen and C. Duhr, *FeynRules - Feynman rules made easy*, *Comput. Phys. Commun.* **180** (2009) 1614–1641, [[arXiv:0806.4194](#)].
- [106] A. Hook, E. Izaguirre, and J. G. Wacker, *Model Independent Bounds on Kinetic Mixing*, *Adv. High Energy Phys.* **2011** (2011) 859762, [[arXiv:1006.0973](#)].

- [107] W. Altmannshofer, S. Gori, M. Pospelov, and I. Yavin, *Neutrino Trident Production: A Powerful Probe of New Physics with Neutrino Beams*, *Phys. Rev. Lett.* **113** (2014) 091801, [[arXiv:1406.2332](#)].
- [108] G. Magill and R. Plestid, *Neutrino Trident Production at the Intensity Frontier*, *Phys. Rev.* **D95** (2017), no. 7 073004, [[arXiv:1612.05642](#)].
- [109] S.-F. Ge, M. Lindner, and W. Rodejohann, *Atmospheric Trident Production for Probing New Physics*, *Phys. Lett.* **B772** (2017) 164–168, [[arXiv:1702.02617](#)].
- [110] P. Ballett, M. Hostert, S. Pascoli, Y. F. Perez-Gonzalez, Z. Tabrizi, and R. Zukanovich Funchal, *Neutrino Trident Scattering at Near Detectors*, *JHEP* **01** (2019) 119, [[arXiv:1807.10973](#)].
- [111] W. Altmannshofer, S. Gori, J. Martín-Albo, A. Sousa, and M. Wallbank, *Neutrino Tridents at DUNE*, [arXiv:1902.06765](#).
- [112] B. Zhou and J. F. Beacom, *Neutrino-nucleus cross sections for W-boson and trident production*, [arXiv:1910.08090](#).
- [113] **MEG II** Collaboration, A. M. Baldini et al., *The design of the MEG II experiment*, *Eur. Phys. J.* **C78** (2018), no. 5 380, [[arXiv:1801.04688](#)].
- [114] **Belle-II** Collaboration, W. Altmannshofer et al., *The Belle II Physics Book*, [arXiv:1808.10567](#).
- [115] P. N. Bhattiprolu and S. P. Martin, *Prospects for vectorlike leptons at future proton-proton colliders*, [arXiv:1905.00498](#).
- [116] **ATLAS** Collaboration, G. Aad et al., *Search for heavy lepton resonances decaying to a Z boson and a lepton in pp collisions at $\sqrt{s} = 8$ TeV with the ATLAS detector*, *JHEP* **09** (2015) 108, [[arXiv:1506.01291](#)].
- [117] R. Dermisek, J. P. Hall, E. Lunghi, and S. Shin, *Limits on Vectorlike Leptons from Searches for Anomalous Production of Multi-Lepton Events*, *JHEP* **12** (2014) 013, [[arXiv:1408.3123](#)].
- [118] **CMS** Collaboration, A. M. Sirunyan et al., *Search for vector-like leptons in multilepton final states in proton-proton collisions at $\sqrt{s} = 13$ TeV*, [arXiv:1905.10853](#).
- [119] N. Kumar and S. P. Martin, *Vectorlike Leptons at the Large Hadron Collider*, *Phys. Rev.* **D92** (2015), no. 11 115018, [[arXiv:1510.03456](#)].
- [120] A. Falkowski, D. M. Straub, and A. Vicente, *Vector-like leptons: Higgs decays and collider phenomenology*, *JHEP* **05** (2014) 092, [[arXiv:1312.5329](#)].
- [121] S. A. R. Ellis, R. M. Godbole, S. Gopalakrishna, and J. D. Wells, *Survey of vector-like fermion extensions of the Standard Model and their phenomenological implications*, *JHEP* **09** (2014) 130, [[arXiv:1404.4398](#)].